Titre: Title:	The boundary contour method for two-dimensional linear elasticity : applications in stress analysis and shape optimization
Auteur: Author:	Anh-Vu Phan
Date:	1997
Type:	Mémoire ou thèse / Dissertation or Thesis
Référence: Citation:	Phan, A.-V. (1997). The boundary contour method for two-dimensional linear elasticity : applications in stress analysis and shape optimization [Ph.D. thesis, École Polytechnique de Montréal]. PolyPublie. https://publications.polymtl.ca/6828/

UNIVERSITÉ DE MONTRÉAL

THE BOUNDARY CONTOUR METHOD FOR TWO-DIMENSIONAL LINEAR ELASTICITY - APPLICATIONS IN STRESS ANALYSIS AND SHAPE OPTIMIZATION

ANH-VŨ PHAN
DÉPARTEMENT DE GÉNIE MÉCANIQUE
ÉCOLE POLYTECHNIQUE DE MONTRÉAL

THÈSE PRÉSENTÉE EN VUE DE L'OBTENTION
DU DIPLÔME DE PHILOSOPHIAE DOCTOR (Ph.D.)
(GÉNIE MÉCANIQUE)
SEPTEMBRE 1997

UNIVERSITÉ DE MONTRÉAL

ÉCOLE POLYTECHNIQUE DE MONTRÉAL

Cette thèse intitulée:

THE BOUNDARY CONTOUR METHOD FOR TWO-DIMENSIONAL LINEAR ELASTICITY – APPLICATIONS IN STRESS ANALYSIS AND SHAPE OPTIMIZATION

présentée par: **PHAN Anh-Vũ**
en vue de l'obtention du diplôme de: **Philosophiae Doctor**
a été dûment acceptée par le jury d'examen constitué de:

M. **SHIRAZI-ADL Aboulfazl**, Ph.D., président
M. **MAYER René**, Ph.D., membre et directeur de recherche
M. **MUKHERJEE Subrata**, Ph.D., membre et codirecteur de recherche
M. **TROCHU François**, Ph.D., membre
M. **HONGOH Masamichi**, Ph.D., membre

DEDICATION

To my parents, *Phan Van Tinh* and *Ly Thi Hao*, for bringing me up during the most difficult days of the Vietnam war and post-war periods; and to my wife, *Phan Trân-Nam*, for all her love and support throughout my graduate study.

ACKNOWLEDGEMENTS

First of all, I gratefully acknowledge the Quebec Ministry of Education for having awarded me and my wife a scholarship through the "Programme québécois de bourses d'excellence" to pursue our graduate study at University of Montreal. Je tiens à remercier Madame Lucie Duranceau et Madame Ginette Angers pour l'aide qu'elles nous ont apportée dans le cadre de ce programme.

I would like to thank my supervisors, Professor René Mayer and Professor Subrata Mukherjee, for their guidance, valuable advice and helpful support. Their kindness and openness are strongly appreciated. René's great viewpoint has helped me to find out the research topic that my educational background seems to match the most, and to work as a really senior graduate student. The final stage of my study was partly funded by him.

I would particularly like to thank Professor Subrata Mukherjee for having offered me the opportunity to work in his research group during the '96 summer at the Departement of Theoretical and Applied Mechanics (TAM), Cornell University. This visit marked a great turning-point in my academic career. By the way, I must thank today's computer achievements because during the course of the research at École Polytechnique de Montréal, I have mostly been working with Subrata through emails and FTP.

Thanks also go to my fellow graduate students at the Departement of Mechanical Engineering (École Polytechnique), my officemates and computer roommates at TAM department, for their assistance. I am indebted to Govind Menon for his useful discussions while I was being at Cornell.

Finally and most importantly, I would like to express my sincere gratitude to my wife, Trân-Nam, for sharing everything with me in our life. Without her unfailing love and moral support, this would not have been possible.

RÉSUMÉ

Cette thèse, constituée de quatre articles, vise à développer de nouvelles variantes de la *méthode des éléments de frontière* (MEFr) en élasticité linéaire bidimemsionnelle (2-D). Ces variantes sont nommées génériquement *méthode des contours de frontière* (MCF) et *méthode des contours de frontière hypersingulière* (MCFH). Un développement ultérieur de la MCF 2-D est réalisé tandis qu'une théorie générale de la MCFH 2-D est introduite dans la bibliographie pour la première fois. Les applications de ces méthodes à l'analyse des contraintes et à l'optimisation de forme sont les objectifs principaux de cette étude. Plusieurs exemples numériques ayant des solutions analytiques connues sont résolus afin d'illustrer les avantages de ces méthodes dans ces types d'applications.

La MEFr est une méthode polyvalente qui utilise *l'équation intégrale de frontière* (EIF) (voir une dérivation de cette équation à la section 4.1 du chapitre IV) pour solutionner des problèmes aux limites. L'idée centrale des nouvelles méthodes (MCF et MCFH) consistent à employer des fonctions d'interpolation spéciales du champ de déplacement et de contrainte. Ces fonctions sont celles de domaine et satisfont les équations d'équilibre et constitutives. Par conséquent, la divergence de l'expression vectorielle sousintégrale de l'EIF et celle de *l'équation intégrale de frontière hypersingulière* (EIFH) (voir une dérivation de cette équation à la section 4.8 du chapitre IV) sont nulles et alors, la dimension des intégrales usuelles dans ces équations peut être réduite par un. En d'autres mots, des intégrales de surface pour des problèmes tridimensionnels (3-D) et celles curvilignes pour des problèmes 2-D peuvent être transformées respectivement en des intégrales curvilignes et l'évaluation de fonctions analytiques aux noeuds de frontière.

Cette réduction en dimension offerte par la MCF et la MCFH, et le fait que ces méthodes utilisent des fonctions d'interpolation spéciales, permettent à ces deux méthodes d'être très compétitives avec la *méthode des éléments finis* (MEF) et la MEFr dans certains domaines d'application de la mécanique appliquée. Due à ces caractéristiques, et en particilier à l'absence des intégrations numériques dans la

MCF et la MCFH pour des cas 2-D, les résultats numériques de l'analyse des contraintes sont très précis en général. Cela est montré via les exemples numériques présentés dans les articles.

Les sensibilités de design sont des coefficients requis pour solutionner numériquement un problème d'optimisation. C'est pourquoi la précision de ces quantités joue un rôle important en optimisation de forme. Comme dans l'analyse des contraintes, la précision des résultats numériques de l'analyse des sensibilités peut être bien assurée par la MCF. Cet avantage et le fait que la MCF ne requiert que des maillages aux rives (comme dans la MEFr) lui permettent de devenir une méthode très appropriée en optimisation de forme.

Les avantages mentionnés plus haut offerts par la MCF et la MCFH sont remarquables. Ils sont bien demontrés à travers les articles et en particulier, via les résultats numériques des exemples illustrés. La recherche menée dans cette thèse vise à introduire au monde du calcul numérique et de la mécanique appliquée, la MCF et la MCFH en linéaire élasticité 2-D ainsi qu'un nouveau succès dans la solution numérique des problèmes d'optimisation de forme.

ABSTRACT

This dissertation, based on four papers, is involved with novel variants of the conventional *boundary element method* (BEM), called the *boundary contour method* (BCM) and *hypersingular boundary contour method* (HBCM), for two-dimensional (2-D) linear elasticity. A further development of the 2-D BCM is carried out whereas a general theory of the 2-D HBCM is introduced to the literature for the first time. Applications of these methods to stress analysis and structural shape optimization are the main objectives of this study. Several numerical examples having known analytical solutions are solved in order to show the advantages of both methods in these kinds of applications.

The BEM is a general purpose approach which starts from the *boundary integral equation* (BIE) (see a derivation of this equation in section 4.1 of chapter IV) in order to solve a given boundary value problem. The key idea of the new methods consists of using special displacement and stress shape functions in the domain of a body that satisfy the equilibrium and constitutive equations. As a result, the integrand vectors of the BIE and regularized *hypersingular boundary integral equation* (HBIE) (see a derivation of this equation in section 4.8 of chapter IV) are divergent-free, and thus the dimension of the usual integrals in the above equations can be reduced by one. In other words, surface integrals for three-dimensional (3-D) problems and line integrals in 2-D cases can be converted respectively into line integrals and the evaluation of analytical functions at boundary nodes.

This reduction in dimensionality offered by the BCM and HBCM, as well as the fact that these methods use special shape functions, are expected to make them competitive with the *finite element method* (FEM) and the BEM for some applications in computational mechanics. Due to these above features and especially, the absence of numerical integrations in the BCM and HBCM for 2-D problems, numerical results obtained for stress analysis are very accurate as it can be seen from the numerical examples presented in the papers.

Design sensitivities are coefficients required for numerically solving an optimiza-

tion problem. Hence, the accuracy of these quantities plays a crucial role in shape optimization. As for stress analysis, the accuracy of numerical results for design sensitivity analysis can be well ensured by the BCM. This advantage and the fact that, as for the BEM, the BCM only needs boundary meshing, as opposed to domain meshing required by the FEM, make the BCM a very attractive method in shape optimal design.

The aforementioned advantages offered by the BCM and HBCM are remarkable. They are clearly shown through the papers and especially, from numerical results of the illustrative examples. The research presented in this dissertation aims to introduce the BCM and HBCM for 2-D linear elasticity, as well as a new successful approach for numerically solving shape optimization problems, into the world of computational and applied mechanics.

CONDENSÉ EN FRANÇAIS

Depuis plus d'une trentaine d'années, la MEF est considérée comme un outil très performant et une technique bien établie dans le calcul numérique en mécanique. Le maillage requis par cette méthode consiste à discrétiser le domaine à analyser en un nombre fini de sous domaines (éléments) (voir Figure 1.1) sur lesquels sont effectuées des intégrations de domaine (intégrales doubles et triples pour des problèmes 2-D et 3-D, respectivement). Bien qu'il n'y ait pas de difficultés importantes pour les maillages 2-D, on est d'accord en général que le maillage 3-D des objets complexes demeure un grand défi pour la MEF. C'est pourquoi des efforts considérables sont déployés en vue de proposer de nouvelles méthodes numériques dans lesquelles la tâche de maillage peut être simplifiée par rapport à la MEF.

Récemment, la MEFr est apparue comme une méthode alternative de la MEF en mécanique (e.g. Banerjee et Butterfield, 1981; Brebbia et al., 1984; Hall, 1994; Mukherjee, 1982). La MEFr réduit la dimension d'analyse d'un problème par un, c.à.d. qu'elle génère des équations d'intégrales curvilignes unidimensionnelles (1-D) pour des problèmes 2-D et des équations d'intégrales de surface 2-D dans des cas 3-D. Par conséquent, la MEFr discrétise la frontière seulement (voir Figure 1.2). La création des maillages devient alors beaucoup plus simple et moins coûteuse que celle dans la MEF. Cet avantage, ainsi que le fait que la MEFr produit souvent des réponses physiques aux rives (déplacements, tractions, contraintes) plus précises que celles données par la MEF, permettent à la MEFr de devenir une méthode très prometteuse dans le domaine du calcul numérique en mécanique.

Comme mentionné précédemment, la MEFr conventionnelle en élasticité linéaire exige l'évaluation numérique des intégrales curvilignes pour des problèmes 2-D et des intégrales de surface dans des cas 3-D (voir, par exemple, Hall, 1994). Il y a quelques années, Nagarajan, Lutz et Mukherjee ont proposé la MCF qui atteint une réduction plus loin de la dimension d'analyse. En fait, ces auteurs ont employés des fonctions d'interpolation spéciales du champ de déplacement et de contrainte pour que la divergence de l'expression vectorielle sousintégrale de l'EIF soit nulle. La

propriété de divergence nulle permet, pour des problèmes 3-D, d'utiliser la formule de Stokes afin de transformer des intégrales de surface sur les éléments de frontière en des intégrales curvilignes sur les contours bornant ces éléments. Pour des problèmes 2-D, une transformation similaire, employant l'idée de l'indépendance de l'intégrale curviligne du chemin d'intégration, élimine complètement l'intégration numérique. Alors, la MCF réduit la dimension d'analyse des problèmes par deux: la méthode n'exige que l'évaluation numérique des intégrales curvilignes 1-D pour des problèmes 3-D et tout simplement, l'évaluation de fonctions analytiques (appelées fonctions potentielles) aux extrémités des éléments de frontière dans les cas 2-D. Cette idée est aussi valable pour d'autres problèmes linéaires tels que la théorie potentielle.

Cette thèse est reliée à un développement ultérieur de la MCF et une étude complète de la MCFH en élasticité linéaire 2-D. Il s'agit également de l'application de ces méthodes à l'analyse des contraintes et particulièrement, de l'optimisation de forme par la MCF.

La plupart des concepteurs employent des processus itératifs pour améliorer leur design jusqu'à ce que des critères donnés soient rencontrés. Le processus traditionnel de conception est basé sur une technique appelée "essai et erreur" avec laquelle, les ingénieurs utilisent l'expérience et l'intuition pour modifier leur design vers la "meilleure" solution. L'avantage principal de cette méthode heuristique est que la connaissance des ingénieurs peut être employée directement dans leur design. Jusqu'à présent cette approche a dominé le processus de conception. Néanmoins, plus les problèmes de conception sont complexes, plus leur amélioration devient difficile, et donc plus on a besoin d'un nouvel outil permettant de guider l'amélioration du design ou d'optimiser le processus de conception. Par ailleurs, l'intérêt actuel en optimisation de forme est aussi extrêmement motivé par le besoin d'une conception très compétitive au niveau des coûts partout dans le secteur industriel y compris l'aérospatiale, l'automobile, la marine, l'industrie des génératrices, la conception des machines et autres domaines d'ingénierie. Il faut noter que le terme "optimisation de forme" utilisé dans ce travail implique la conception optimale de la forme d'un objet tandis que le terme "optimisation de structures" signifie l'optimisation d'ossatures.

Un processus de conception optimale est un outil qui utilise des techniques d'optimisation mathématique afin de répondre au défi mentionné précédemment. Ici, le problème de conception est transformé en un modèle mathématique de telle manière qu'une technique d'optimisation puisse être appliquée pour améliorer le modèle vers la solution optimale de façon automatique ou semi-automatique.

La théorie fondamentale des approches d'optimisation est apparue aux 17^e et 18^e siècles. Cependant, l'optimisation de nature purement mathématique ne peut pas être appliquée à la plupart des problèmes en pratique car ces problèmes sont impossibles à résoudre analytiquement. C'est pour cette raison que des méthodes numériques ont été développées. Avec le développement de la MEF, Schmith (1960) fut l'un des premiers à mettre sur pied une classe de techniques d'optimisation de structures. Puis, l'introduction des méthodes de programmation mathématique couplée avec la MEF est devenu un événement marquant la mise au monde d'un outil ayant le plus de succès dans la solution des problèmes d'optimisation de structures en pratique. Dans le cadre de l'optimisation de forme utilisant la MEF, une des premières approches a été présentée par Zienkiewics et Campbell (1973) dans laquelle des noeuds de frontière ont été choisis comme les variables de design et la solution optimale numérique est obtenue par la programmation linéaire séquentielle.

Malgré le succès de la MEF dans l'optimisation de structures où le maillage des structures est simple car elles sont modélisées par des éléments 1-D tels que des barres ou des poutres, il reste encore un désavantage important. Le re-maillage, durant le processus d'optimisation où la forme de l'objet change avec les itérations successives de conception, est très coûteux, en particulier dans des cas 3-D. Aussi, ce re-maillage provoque souvent des distorsions des éléments près de la frontière à optimiser.

Grâce à l'avantage de maillage offert par la MEFr, depuis les années 80, plusieurs chercheurs ont contribué des efforts considérables afin de développer des techniques efficaces pour l'optimisation de forme utilisant la MEFr et des succès remarquables ont été atteints. La plupart de ces contributions sont concentrées sur le calcul des sensibilités de design qui sont des coefficients requis par les méthodes de program-

mation mathématique. L'efficacité (précision et vitesse) du calcul des sensibilités joue un rôle décisif dans la réussite de l'optimisation de forme.

La MCF possède le même avantage de maillage que la MEFr conventionnelle. D'ailleurs, comme mentionné plus haut, la première offre une réduction additionnelle de la dimension d'analyse. Par conséquent, la MCF s'avère très prometteuse dans le domaine d'analyse des contraintes ainsi que d'optimisation de forme des structures mécaniques. Cette idée a motivé l'étude présentée par cette thèse.

La thèse est associée aux quatre articles suivants:

1. The boundary contour method for two-dimensional linear elasticity with quadratic boundary elements.

2. The hypersingular boundary contour method for two-dimensional linear elasticity.

3. A boundary contour formulation for design sensitivity analysis in two-dimensional linear elasticity.

4. Stresses, stress sensitivities and shape optimization in two-dimensional linear elasticity by the boundary contour method.

Ces articles sont inclus en Annexes. Comme l'indique leur titre, les deux premiers articles introduisent la MCF et la MCFH avec l'application à l'analyse des contraintes. Le troisième emploie la MCF pour développer une analyse des sensibilités de design nécessaires à l'optimisation de forme. Finalement, la première partie du dernier article présente de nouvelles formules concernant le calcul des contraintes et leurs sensibilités de design tandis que la deuxième partie s'attaque à l'application de la MCF à l'optimisation de forme.

Bien que ce soit une thèse par articles, il existe un lien raisonnable entre les quatre articles utilisés. Le premier article présente un développement ultérieur de la MCF dans l'analyse des contraintes en élasticité linéaire 2-D. Dans ce travail, une implémentation numérique avec des éléments quadratiques est effectuée en

vue d'améliorer la précision des résultats numériques obtenus par l'utilisation des éléments linéaires comme elle a été faite dans l'étude précédente (voir Nagarajan et al., 1994). En dehors de l'analyse primaire où les quantités physiques aux rives telles que des déplacements, des tractions et des contraintes sont calculées, cet article adresse également l'analyse ultérieure où on évalue des contraintes à l'intérieur du domaine. En étape ultérieure, une propriété remarquable a été découverte: l'expression formulée pour calculer des contraintes à l'intérieur du domaine peut aussi être employée pour évaluer des contraintes à la frontière (sauf aux noeuds d'extrémité) sans avoir recours à aucun moyen particulier pour traiter des singularités comme dans la MEFr conventionnelle.

Il faut noter que les valeurs numériques des contraintes, données par la MCF, aux extrémités des éléments sont discontinues même si, à ces endroits, les contraintes sont continues d'une manière physique. Bien que ce soit un désavantage mineur, la modélisation aux coins d'un domaine 2-D devient triviale dans ce cas. Ces discontinuités numériques à travers des éléments de frontière peuvent être bien améliorées en utilisant la MCFH présentée dans le deuxième article, pourvu qu'il n'y ait aucune discontinuité de contrainte dans le problème à traiter. La différence entre la MCF et la MCFH est que, au point de départ, la première utilise l'EIF tandis que la dernière emploie une équation intégrale de frontière hypersingulière déjà régularisée. Donc, pour des problèmes 2-D, chaque méthode est caractérisée par ses propres fonctions potentielles. Comme dans le premier article, les deux analyses primaire et ultérieure sont adressées et implémentées avec des éléments quadratiques dans l'article sur la MCFH 2-D. Via les exemples numériques dans ces articles, on s'aperçoit que les deux méthodes peuvent produire des résultats numériques de grande précision, en particulier ceux en étape ultérieure. Finalement, comme dans la MEFr conventionnelle, en dehors de l'application à l'analyse des contraintes, la MCFH peut aussi être développée pour solutionner des problèmes en mécanique de la rupture.

Avec les avantages sur le maillage à la frontière, sur la précision des résultats obtenus et sur le temps de calcul, la MCF est évidemment une méthode numérique très appropriée à l'optimisation de forme. Ce type d'application requiert l'étude d'analyse des sensibilités de design employant la MCF et cette étude est le sujet

du troisième article. Dans ce travail, afin d'obtenir des coefficients de sensibilité de design (sensibilités de déplacement, de traction et de contrainte), les équations de la MCF sont différenciées analytiquement par rapport aux variables de design. Ici, on traite les équations de la MCF des analyses primaire et ultérieure, donc cet article adresse non seulement les coefficients de sensibilité aux rives mais aussi ceux à l'intérieur du domaine. Encore une fois, la MCF produit des résultats numériques précis pour les exemples traités et surtout, cette précision est uniforme. La précision des coefficients de sensibilité obtenus est cruciale parce qu'elle détermine le succès de la solution des problèmes d'optimisation de forme. Finalement, cette étude montre deux avantages additionnels de la MCF par rapport à la MEFr conventionnelle: (a) dû à l'utilisation des fonctions d'interpolation globales, après avoir résolu les équations primaires, la récupération des sensibilités de contrainte aux noeuds est très simple et (b) il n'est pas requis d'employer de traitements particuliers pour régulariser des singularités dans le calcul des sensibilités de déplacement et de contrainte en étape ultérieure.

Il y a deux approches pour évaluer les contraintes et leurs sensibilités en étape ultérieure. La première approche utilise les fonctions potentielles de la MCF comme présentée dans les premier et troisième articles tandis que la deuxième approche emploie les fonctions potentielles de la MCFH comme présentée dans la première partie du quatrième article. Bien que les deux approches produisent les mêmes résultats numériques pour un problème donné, le temps de calcul requis par la deuxième approche est inférieur car sa formulation est plus simple que celle de la première approche.

Avec les réussites mentionnées précédemment de la MCF 2-D en analyse des contraintes et des sensibilités, il est approprié d'appliquer cette méthode à l'optimisation de forme. Ce type d'application est effectué dans la deuxième partie du quatrième article. En fait, deux exemples bien connus sont solutionnés en employant l'analyse des sensibilités de design par la MCF developpée dans le troisième article. Les résultats sont comparés avec ceux obtenus par des chercheurs qui ont utilisé la MEFr. Finalement, ces résultats sont excellents ce qui justifie l'avantage de la MCF par rapport aux autres méthodes numériques en optimisation de forme.

Tout comme le deuxième article sur la MCFH 2-D, les troisième et quatrième articles présentent les premières contributions à la bibliographie en ce qui concerne un développement de l'analyse des sensibilités employant la MCF 2-D et une application de cette méthode à l'optimisation de forme. Pour conclure, on peut dire que la MCF présente des avantages potentiels par rapport à d'autres méthodes numériques dans le domaine d'optimisation de forme. Par conséquent, l'étude menée dans cette thèse devrait motiver de futures recherches sur ce type d'application en 3-D.

TABLE OF CONTENTS

LIST OF FIGURES

LIST OF ABBREVIATIONS

EIF: Équation Intégrale de Frontière.

EIFH: Équation Intégrale de Frontière Hypersingulière.

MCF: Méthode des Contours de Frontière.

MCFH: Méthode des Contours de Frontière Hypersingulière.

MEF: Méthode des Éléments Finis.

MEFr: Méthode des Éléments de Frontière.

ASA: Adjoint Structure Approach.

BCM: Boundary Contour Method.

BEM: Boundary Element Method.

BIE: Boundary Integral Equation.

CPV: Cauchy Principal Values.

DDA: Direct Differentiation Approach.

DSCs: Design Sensitivity Coefficients.

FDA: Finite Difference Approach.

FEM: Finite Element Method.

HBCM: Hypersingular Boundary Contour Method.

HBIE: Hypersingular Boundary Integral Equation.

SLP: Successive Linear Programming.

SQP: Successive Quadratic Programming.

LIST OF APPENDICES

CHAPTER I
INTRODUCTION

Over the last three decades, the FEM has been considered to be a powerful tool and a well-established numerical technique in computational mechanics. The meshing required by this method involves discretizing the total domain into a finite number of subdomains (elements) (see Figure 1.1) on which domain integrations (2-D and 3-D integrals for 2-D and 3-D problems, respectively) are performed. Although there are no serious difficulties for 2-D meshing, it is generally recognized that 3-D mesh generation of a complex body remains a big challenge for the FEM. Therefore, considerable effort has been devoted in proposing numerical analysis methods in which the meshing task can be simplified.

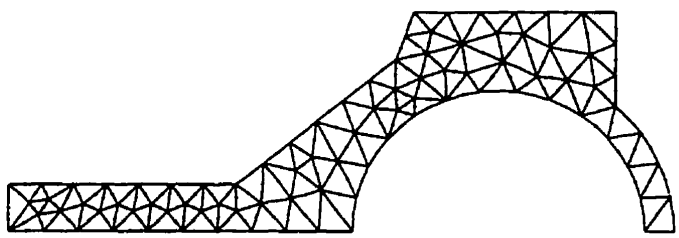

Figure 1.1: FEM meshing of a connecting rod.

Recently, the BEM has been widely acknowledged as an alternative numerical method for engineering analysis (e.g. Banerjee and Butterfield, 1981; Brebbia et al., 1984; Hall, 1994; Mukherjee, 1982). The BEM reduces the dimensionality of analysis problems by one, i.e. it generates one-dimensional (1-D) line integral equations for 2-D problems and 2-D surface integral equations in 3-D cases. As a consequence, the BEM discretizes the boundary only (see Figure 1.2), so the mesh generation becomes much more straightforward and inexpensive compared to the FEM. This advantage, as well as the fact that the BEM usually provides boundary physical responses (displacements, tractions, stresses) more precisely than the FEM, makes

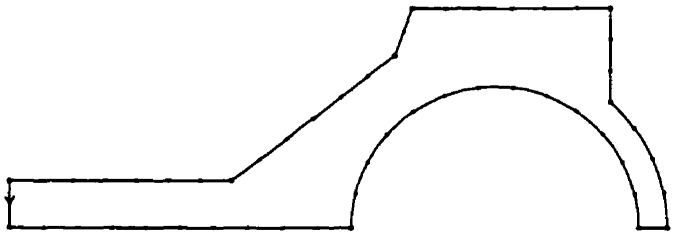

Figure 1.2: BEM meshing of a connecting rod.

the BEM a very attractive numerical method in computational mechanics.

As mentioned above, the conventional BEM for linear elasticity requires the numerical evaluation of line integrals for 2-D problems and surface integrals for 3-D ones (see, for example, Hall, 1994). By observing that the integrand vector of the usual linear elasticity BEM equation without body forces is divergence free, a few years ago, Nagarajan, Lutz and Mukherjee proposed a novel approach, termed generically the *boundary contour method* (BCM), that achieves a further reduction in dimension. The divergence free property allows, for 3-D problems, the use of Stokes' theorem to transform surface integrals on the usual boundary elements into line integrals on the bounding contours of these elements. For 2-D problems, a similar transformation, using the simple idea of path-independent integrals, eliminates numerical integration altogether. The above transformations are quite general and apply to boundary elements of arbitrary shape. Thus, the BCM reduces the dimensionality of analysis problems by two: the method only requires numerical evaluation of 1-D line integrals for 3-D problems and simply the evaluation of functions (called potential functions) at endpoint nodes on the boundary of a body for 2-D cases. The above idea also works for other linear problems such as potential theory.

The present dissertation deals with a further development of the BCM and a full study of its variant, called the hypersingular BCM, for 2-D linear elasticity. Application of these novel methods in stress analysis and in particular, application of the BCM in shape optimization are also included. It should be noted that the term shape optimization used in this work refers to the optimal design of the shape

boundary of structural components.

Most engineering designers use iterative processes to improve their design until it meets some given criteria. The traditional design process is based on the so called "trial and error" technique, in which design engineers use their experience and intuition to modify the design process towards the goal. The main advantage of this heuristic based design method is that the designers' knowledge can be used directly in their design, and up to now this approach still dominates the design process. But as design problems become more complex, design improvement becomes more difficult and hence, the need for new tools to guide the design improvement, or to optimize the design process, becomes greater. Furthermore, current interest in structural shape optimization is also largely motivated by demands for more cost-competitive design throughout the industrial sector including aerospace, automotive, marine, power generation, machine design and other engineering areas.

An optimal design process is a tool which uses mathematical optimization techniques to meet the aforementioned challenge. Here, the design problem is transformed into a mathematical model so that an optimization technique can be applied to improve the model towards the optimum solution in a full- or semi-automated manner.

The basic theory for optimization approaches was set forth long ago (17^{th} and 18^{th} centuries). However, pure mathematical optimization can rarely be applied in practical design because most design problems cannot be solved analytically. Therefore, numerical methods have been developed for this purpose. Over the last three decades, the FEM has been considered to be a powerful tool for structural analysis. With the development of the FEM, a class of techniques for structural optimization problems was pioneered by Schmith (1960). Then, the introduction of the mathematical programming methods coupled with the FEM was a milestone in solving pratical structural optimization problems, which proved to be the most successful tool for optimum structural design. In the context of shape optimization using the FEM, one of the first approaches was presented by Zienkiewics and Campbell (1973), in which boundary nodes are chosen as the design variables and

the numerical optimization solution is obtained by sequential linear programming.

Despite the success of the FEM in structural optimization where the meshing of structures is straightforward since they are modeled by 1-D elements such as bars or beams, there still remains one main shortcoming. The remeshing during the optimization process, where the shape of the body changes during successive design iterations, is very expensive, especially in 3-D cases. This remeshing also often causes element distortion near the design boundary.

Due to the meshing advantage of the BEM, from the 1980s several researchers have contributed considerable efforts to develop efficient techniques for shape optimization using the BEM and remarkable successes have been achieved.

Besides having the same advantage in mesh generation as in the conventional BEM, as mentioned above, the BCM offers a further reduction in dimension of analysis problems. Therefore, the generation of the BCM promises a new successful approach for stress analysis as well as for optimal shape design and the above idea has motivated the study presented in this dissertation.

The dissertation is associated with the four following papers:

1. The boundary contour method for two-dimensional linear elasticity with quadratic boundary elements.

2. The hypersingular boundary contour method for two-dimensional linear elasticity.

3. A boundary contour formulation for design sensitivity analysis in two-dimensional linear elasticity.

4. Stresses, stress sensitivities and shape optimization in two-dimensional linear elasticity by the boundary contour method.

which are enclosed in the Appendices. As described by the titles, the first two papers present the BCM and HBCM with their application in stress analysis for 2-D linear elasticity, whereas the last two papers deal with an application of the 2-D BCM in shape optimization.

CHAPTER II
LITERATURE REVIEW

2.1 The BCM for linear elasticity

The BCM has been presented in the literature for 2-D (see Nagarajan et al., 1994) and for 3-D (see Nagarajan et al., 1996 and Mukherjee et al., 1997) linear elasticity problems. In the 2-D paper, however, only the primary BCM analysis, i.e. the determination of boundary tractions and displacements (see Figure 2.1), is addressed. Also, the idea of rigid body modes, to regularize Cauchy singular integrals, is not employed in the Nagarajan et al. papers in an explicit manner. In addition, the numerical implementation carried out with linear boundary elements is not quite accurate enough for engineering analysis, and especially, for design sensitivity analysis which is required for shape optimization.

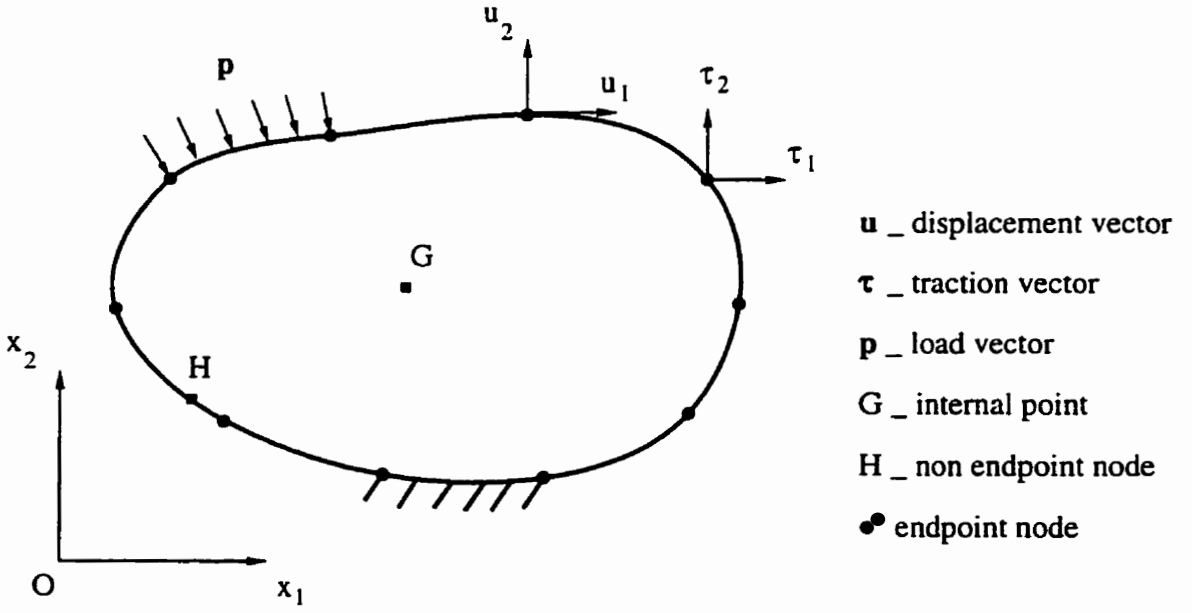

Figure 2.1: 2-D elastic body.

The above shortcomings led to the need for a further development for the 2-D

BCM in linear elasticity. This study is the topic of the first paper presented in Appendix I. In this paper, a numerical implementation is set up with quadratic boundary elements and the rigid body motion technique is employed in an explicit manner. Also, the secondary BCM analysis, namely the calculation of stresses both at internal points and non-endpoint nodes on the boundary (see Figure 2.1), as well as the primary BCM analysis, are addressed in this work.

2.2 Regularized hypersingular boundary integral equations and the hypersingular BCM

Regularized HBIEs have several important applications in engineering, such as, in computation of boundary stresses (e.g. Guiggiani et al., 1992), in wave scattering by thin screens (e.g. Krishnasamy et al., 1990), in fracture mechanics (e.g. Gray et al., 1990; Lutz et al., 1992; Paulino, 1995; Gray and Paulino, 1997-a), in obtaining symmetric Galerkin boundary element formulations (e.g. Gray et al., 1995; Bonnet, 1995-a; Gray and Paulino, 1997-b), and in adaptative analysis (e.g. Paulino et al., 1996; Menon, 1996 and Menon et al., 1997).

Again, since the integrand vector of the regularized HBIE under consideration is divergent-free, these equations can be converted into a boundary contour version, here called the hypersingular boundary contour method (HBCM), in order to achieve a reduction in dimensionality as in the BCM. The first study on the HBCM has been pioneered by Mukherjee and Mukherjee (1997-a and -b). In their work, a general theory for converting a regularized HBIE into the HBCM for 3-D linear elasticity is presented. These papers, however, do not contain any general numerical examples in order to show the validity of the HBCM in such cases.

With the purpose of completing the HBCM for linear elasticity, an investigation of the method for 2-D problems is the topic of the second paper enclosed in Appendix II. This is a full study because, as in the first paper on the usual BCM, both primary and secondary analyses as well as general numerical examples are presented.

2.3 Design sensitivity analysis using the BEM

Most shape optimization problems use gradient based mathematical programming algorithms where design sensitivity coefficients (DSCs), which are defined as the rates of change of physical quantities with respect to changes in the design variables, are required for the determination of the optimum shape of a body. Therefore, the evaluation of design sensitivities has become an important research topic for the last two decades. In practice, the success of mathematical programming methods for solving shape optimization problems often depends on the way the design sensitivities are computed, i.e. the approach, its accuracy and efficiency. In the context of the FEM as well as the BEM, there are three methods for design sensitivity calculation, namely, the finite difference approach (FDA), the adjoint structure approach (ASA) and the direct differentiation approach (DDA).

Before the research leading to this dissertation, no paper had been published on the topic of design sensitivity analysis using the BCM. However, since the BCM is a variant of the conventional BEM, it is useful to review the literature on design sensitivity analysis using the BEM.

In elastostatics using the BEM, the FDA has been presented by Wu (1986), and Kane and Prasad (1993) for 2-D and 3-D problems; the ASA has been introduced by Choi and Kwak (1988), and Aithal and Saigal (1990) for 2-D problems, by Lee (1996) for axisymmetric analysis, by Zhao (1993) for 3-D solids; and the DDA has been given by Barone and Yang (1988), Kane and Saigal (1988), and Zhang and Mukherjee (1991) and Mellings and Aliabadi (1995) for 2-D problems, by Saigal *et al.* (1989), Rice and Mukherjee (1990), and also Lee (1996) for axisymmetric problems, by Aithal *et al.* (1991), Kane *et al.* (1992) and Bonnet (1995-b) for 3-D bodies, and by Mukherjee and Chandra (1989, 1991) for 2-D non linear problems.

In most of the above papers, the authors limited their illustration at the design sensitivity analysis on the boundary nodes of the body. Since the BIE is associated with boundary displacements and tractions, but not boundary stresses, it follows that a stress recovery process had to be developed in the above papers in order to compute boundary stress sensitivities. This stress recovery process is not simple

because the shape functions are described in a local curvilinear coordinate system whereas the displacement-strain relationship and Hooke's law are described in the global Cartesian coordinate system. By using a 2-D linear elastic BIE formulated in terms of tangential gradient of displacements ("derivative BIE"), the stress recovery presented by Zhang and Mukherjee (1991) seems to be easier but since this BIE formulation is associated with the tangential gradient of displacements, it does not provide displacements directly and thus, their sensitivities.

Conceptually, the FDA is the simplest method for the determination of DSCs. Typically, the current design is analyzed and the response quantities are evaluated. Then the design variables are perturbed in succession. For each perturbation, the design responses are reevaluated, and the DSCs are obtained by the finite difference formula which is the ratio of the differences of design responses and the corresponding perturbation intervals. The main drawback of the FDA is its sensitivity to the choice of perturbation intervals: truncation errors can be substantial if the perturbation magnitude is too large and round-off errors (condition errors) can be significant if this magnitude is too small. In addition, this method is very computer time consuming due to the requirement of forming new BEM system matrices. That's why even though Wu (1986) was able to show convergence of the numerical results considered in his work using the FDA, the effect of selecting perturbation step sizes on convergence in more general applications is still in question.

The DDA uses analytical methods instead of the finite difference formula to yield exact expressions for the sensitivities. Studies on the subject using the DDA originated with the work of Kane and Saigal (1988), and Barone and Yang (1988). A difficulty with the DDA lies in the singular feature of the governing BIE. Kane and Saigal (1988) generated the desired sensitivities by differentiating the resulting BEM system matrix analytically. In these formulations, the source point must be placed outside the region to avoid singular integrations. But, as noted by Barone and Yang (1988), besides being somewhat arbitrary, this strategic adjustment appears to introduce unwarranted complications. Barone and Yang (1988) carried out the opposite process to the one employed by Kane and Saigal (1988) by differentiating the BIE to obtain the sensitivities analytically before numerical implementation.

Here, the rigid body motion technique is used to treat singular integral terms in the calculation of displacement sensitivities, but the integration of strongly singular kernels is required for computing stress sensitivities by a direct formulation. Besides an easier stress recovery process discussed so far, the derivative BIE formulation used by Zhang and Mukherjee (1991) is only involved in a weakly singular feature, thus its differentiated kernels are completely regular for 2-D design sensitivity problems. With the same effort to avoid strongly singular integrals involved in the design sensitivity analysis, Bonnet (1995) applied the material derivative concept to the regularized displacement boundary integral equation.

The DDA is advantageous for optimal shape problems with few design variables and a large number of constraints because the differentiation is taken with respect to one design variable at a time, so the computing time depends mainly on the number of design variables, not the number of constraints.

The ASA is an exact approach for evaluating DSCs and does not involve finite differences. In this method, an adjoint system must be prescribed in addition to the physical system. One auxiliary system is defined for each constraint, rather than for each design variable. Hence, for problems with many design variables and fewer constraints, the ASA is more suitable. However, as noted by Barone and Yang (1988), although the ASA is conceptually a straightforward technique, major computational difficulties are involved in evaluating displacement and stress sensitivities at discrete points. This is because the adjoint solutions for these two cases correspond to a concentrated force and moment, respectively, and these solutions using the BEM give rise to unbounded integrals. This problem was circumvented by Choi and Kwak (1988) for stress sensitivity analysis by representing the von Mises stress over an element (or over an area) in an average value using an averaging characteristic function m_p. Therefore, only an averaged stress sensitivity for the element is obtained and the procedure still does not provide the sensitivity informations at discrete nodal points.

An improved formulation using the ASA has been presented by Aithal and Saigal (1990) in which the adjoint problem is established starting from the elasticity

equations of equilibrium and then, the BEM is employed to solve both the primitive and the adjoint problems. Here, stress sensitivities are determined by the implicit differentiation of the boundary stress recovery expression and thus, this procedure enables the stress sensitivity calculation at discrete points.

Based on the above review, it can be seen that the topic of shape design sensitivity analysis plays a crucial role in the numerical optimization techniques. In the context of the BEM, the DDA is a preferred method because of the consistency due to its analytical nature and since it facilitates the design sensitivity calculation at any discrete point. Therefore, a study on design sensitivities using the DDA and by the BCM for 2-D linear elasticity is obviously necessary for the application of this method in shape optimization. Details of the work are presented in the third paper shown in Appendix III.

2.4 Shape optimization using the BEM

Theories for shape optimization using the BEM can be found in Zhao (1991) or Chandra and Mukherjee (1997).

The application of the BEM in optimal shape design started from the 1980's. One of the earliest studies was published by Barone and Caulk (1982) in which the position, the size and the surface temperature of circular holes inside a 2-D heat conductor are optimized.

Choi and Kwak (1988) applied the ASA for computing DSCs in their shape optimization work where an algorithm for optimum structural design without line search is employed and the design shape is represented by cubic splines.

The use of the generalized reduced gradient method in BEM shape optimization has been developed by Sandgren and Wu (1988) in which substructuring is employed to isolate the portion of the structure undergoing geometric change. B-spline curves and surfaces whose control points are chosen as the design variables are introduced to describe the shape in 2-D and 3-D design problems. Design sensitivity coefficients are computed using the FDA. The optimal shape design of a hook is selected as an

application example in which the nominal stress needs to be minimized. But as mentioned by the authors, additional time savings could be achieved by applying an analytical approach for sensitivity informations (such as the DDA) instead of the FDA used in this work.

A modular approach for shape optimization used in the finite element context was adapted to the BEM by Yang (1990) to optimize an infinite plate with an elliptical hole and an fillet problem. In this study, the feasible direction algorithm is employed as the optimization technique. The displacement sensitivity formulation given by Barone and Yang (1988) and a stress sensitivity formulation obtained by differentiating the shape function in each boundary element, are used. Despite the simplicity of this stress sensitivity calculation, the errors in such computation can be substantial due to the approximate nature of the shape functions.

By using a formulation for design sensitivity analysis presented by Kane and Saigal (1988), the same authors (Saigal and Kane, 1990) have proposed a model for optimizing structural components such as a rod to half-space attachment or a slotted ring in an aircraft gas turbine engine. Here, the mesh generation and remeshing are done using a parametric and auxiliary geometry concept. The above informations are then coupled with the general purpose numerical optimization code ADS to solve the given problems.

Optimal shape design of solids undergoing small-strain, small rotation and elasto-viscoplastic deformation was investigated by Wei et al. (1994). In this work, shape optimization is performed by coupling the standard BIE and the DDA sensitivity analyses with an optimizer using sequential quadratic programming. The approach is then applied to shape optimization of cutouts in plates undergoing purely elastic and elasto-viscoplastic deformation.

Yamazaki et al. (1994) determined optimum shapes of minimum weight subjected to stress constraints and a connecting rod in which the design sensitivity calculation is based on the DDA of the discrete BIE.

Tafreshi and Fenner (1995) have presented a general purpose computer program, named STRESOPT, for optimal shape design of 2-D structures in order to smooth

stress peaks, i.e. to reduce stress concentration effects. In this work, the design sensitivity analysis is carried out by using both the FDA and DDA for discretized BEM formulations. The numerical optimization technique used in the program is the extended penalty function approach, together with the golden section method for the one-dimensional search. The shape is represented by hermitian cubic splines so that complex geometries can be described by a small number of design variables. The optimum shape design of fillets and holes in plates as well as bars were shown as illustrative examples.

Recently, it can be seen that papers on the topic of shape optimization by the BEM have not presented new important contributions in this field. They usually tackle the application of known formulations for design sensitivities to new problems or the numerical implementation of known theories into a new optimization package.

The above studies have shown encouraging successes for optimal shape design by the BEM. Hence, a new success of the BCM in this kind of application is very challenging. In order to meet this challenge, shape optimization by the BCM must demonstrate its performance and efficiency in resulting accuracy as well as in computational time. This demonstration is one of the topics of the fourth paper enclosed in Appendix IV.

CHAPTER III
PAPER SYNTHESIS

Even though this is a dissertation composed from papers, there is a reasonable link between the four papers used. The first paper presents a further development of the BCM for stress analysis in 2-D linear elasticity. In this work, a numerical implementation with quadratic boundary elements as opposed to linear ones in the previous study (see Nagarajan et al., 1994) is performed for the purpose of increasing the accuracy of numerical results. Besides the usual primary analysis where boundary physical quantities of a body such as displacements, tractions and stresses are calculated, the post-processing analysis is also addressed for computing stresses inside the body under consideration. In the post-processing stage, a remarkable issue is realized: the boundary contour formulation for computing the stress at an internal point can also be employed to evaluate stresses at regular points on the boundary except at endpoint nodes. This can be achieved without any special singularity treatment as must be done in the conventional BEM.

It should be mentioned that since traction nodes are not placed at the endpoints of boundary elements (see Figure 1 in Appendix I), traction continuities can not be numerically enforced at endpoint nodes where tractions are physically continuous. As a result, stresses across boundary elements provided by the BCM are numerically discontinuous even if they are physically continuous there. Although this is a minor drawback, it makes the corner modeling trivial because one does not have to model each corner (corners are always endpoint nodes) with two traction nodes as in the conventional BEM. The numerical discontinuities across boundary elements in problems without stress jumps on the boundary can be much improved by using the HBCM presented in the second paper. The difference between the BCM and HBCM is that, for the primary analysis, the former uses the BIE whereas the latter uses a regularized HBIE as the starting point. Hence, for 2-D problems, each method is characterized by its own potential functions. As in the first paper, both the primary and post-processing analyses are addressed and implemented with quadratic domain

shape functions in the 2-D HBCM paper. Via the numerical examples in the above papers, it is shown that both methods can provide highly accurate results and especially those given from the post-processing stage. Finally, as in the conventional BEM, besides the application in stress analysis, the HBCM can also be extended to solve fracture mechanics problems. However, this has not been done yet.

With the advantages in boundary meshing, accuracy and computational times, the BCM is obviously an appropriate numerical method for shape optimization. This kind of application requires the evaluation of DSCs. Therefore, a study on shape design sensitivity analysis using the BCM is necessary and this is the subject of the third paper. In this work, in order to obtain DSCs (sensitivities of displacements, tractions and stresses), the BCM equations are analytically differentiated with respect to the design variables. Here, the BCM equations of both the primary and post-processing analyses are treated, therefore not only the DSCs on the boundary but also those inside the body under consideration are addressed. Once again, the BCM provides high and uniform precisions for numerical results of DSCs on the boundary as well as within the domain for the illustrative examples. The accuracy of the obtained DSCs is very crucial because it decides the success in using gradient based mathematical programming algorithm to solve optimal shape design problems. Through this study, two more advantages of the BCM over the BEM are derived: (a) due to the use of global displacement and stress shape functions, the recovery of boundary stress sensitivities after solving the primary equations is straightforward, and (b) no special singularity treatment has to be carried out for computing displacement and stress sensitivities in the post-processing stage.

There are two approaches for evaluating stresses and stress sensitivities by the BCM as post-processing steps. The first approach starts from the BCM version of the standard BIE written for the displacement at an internal point whereas the second approach starts directly from this equation. As a result, the first approach uses the BCM potential functions as shown in the first and third papers while the second approach uses the HBCM potential functions as presented in the first part of the fourth paper. Since both approaches start from the same equation (BIE), they provide the same numerical results for a given problem. However, computational

times required by the second approach are less because its formulation is simpler than that in the first approach.

With the above achievement of the 2-D BCM in stress and design sensitivity analyses, an application of this method in shape optimization is obviously appropriate. This kind of application is carried out in the second part of the fourth paper. Here, the development and execution of a shape optimization algorithm with DCSs calculated from the BCM is contributed into the literature for the first time. In fact, the BCM and design sensitivity codes are coupled with the successive (sequential) quadratic programming algorithm (here, the C function "`f_min_con_nonlin`" from the commercial IMSL library is employed) to solve shape optimization problems. Two well-known examples in optimal shape design are solved using the design sensitivity analysis by the BCM developed in the third paper. The results are compared with those obtained by researchers using the BEM. These results are excellent and this confirms great potential advantages of the BCM in shape optimization.

CHAPTER IV
MATHEMATICAL DETAILS SUPPLEMENTING THE PAPERS

This chapter provides further mathematical details needed for comprehending the four papers presented in the Appendices. Therefore, the reading of these papers before referring to this chapter is recommended.

Regarding the referencing of equations, it is noted that the referencing prefixed by a roman number is referred to equations in the paper indicated by this roman number. For example, (III.12) means Eq. (12) in the third paper.

4.1 Derivation of the BIE (Eq. (I.1))

4.1.1 Review of basic equations in linear elasticity

- Differential equations of equilibrium without body forces

$$\frac{\partial \sigma_{ij}}{\partial x_j} = 0 \quad \text{or} \quad \sigma_{ij,j} = 0 \tag{4.1}$$

where σ_{ij}, x_j are the stress tensor and coordinate vector. For 2-D problems, $i = 1, 2$ and $j = 1, 2$. The comma denotes partial derivative.

- Compatibility equations

$$\epsilon_{ij} = \frac{1}{2}(u_{i,j} + u_{j,i}) \tag{4.2}$$

where ϵ_{ij}, u_i are the strain tensor and displacement vector.

- Hooke's law (constitutive relationships)

$$\sigma_{ij} = \lambda \delta_{ij} \epsilon_{kk} + 2\mu \epsilon_{ij} \tag{4.3}$$

where λ and μ are Lamé constants of the material, and δ_{ij} is the Kronecker delta ($\equiv 1$ for $i = j$ and $\equiv 0$ for $i \neq j$).

- The Navier-Cauchy equations

  By substituting (4.3) and (4.2) into (4.1), the results are the equilibrium equations in terms of displacements or the Navier-Cauchy equations:

$$\left(\frac{1}{1-2\nu}\right) u_{j,ji} + u_{i,jj} = 0 \tag{4.4}$$

  where ν is Poisson's ratio.

4.1.2 Kelvin solution

A particular solution of the Navier-Cauchy equations (4.4), called Kelvin solution, is obtained when a unit point load is applied at a point P (source point) in the direction of the unit vector e_k, producing displacements and stresses at any point Q in the domain (field points), given by:

$$\left.\begin{aligned} \mathring{u}_i\,(Q) &= U_{ik}(P,Q)e_k(P) \\ \mathring{\sigma}_{ij}\,(Q) &= \Sigma_{ijk}(P,Q)e_k(P) \end{aligned}\right\} \tag{4.5}$$

In (4.5), U_{ik} and Σ_{ijk} are called Kelvin kernel tensors and their expressions are given by (I-2).

4.1.3 Symmetry of the elasticity tensor

Hooke's law (4.3) can be applied to a second stress $\mathring{\sigma}_{ij}$ and strain $\mathring{\epsilon}_{ij}$, i.e.

$$\mathring{\sigma}_{ij} = \lambda\delta_{ij}\,\mathring{\epsilon}_{kk} + 2\mu\,\mathring{\epsilon}_{ij} \tag{4.6}$$

Multiplying Eq. (4.3) by $\mathring{u}_{i,j}$ yields

$$\sigma_{ij}\,\mathring{u}_{i,j} = \lambda\delta_{ij}\epsilon_{ii}\,\mathring{u}_{j,j} + 2\mu\epsilon_{ij}\,\mathring{u}_{i,j} \tag{4.7}$$

and Eq. (4.6) by $u_{i,j}$ yields

$$\mathring{\sigma}_{ij}\,u_{i,j} = \lambda\delta_{ij}\,\mathring{\epsilon}_{ii}\,u_{j,j} + 2\mu\,\mathring{\epsilon}_{ij}\,u_{i,j} \tag{4.8}$$

Subtracting Eqs. (4.7) and (4.8) gives the following expression which describes the symmetry of the elasticity tensor

$$\sigma_{ij}\,\mathring{u}_{i,j} - \mathring{\sigma}_{ij}\,u_{i,j} = 0 \tag{4.9}$$

4.1.4 Boundary integral formulation

Equilibrium equations (4.1) for both stress states give

$$\sigma_{ij,j} = \mathring{\sigma}_{ij,j} = 0 \tag{4.10}$$

Thus, it follows from Eqs. (4.9) and (4.10) that

$$\left(\sigma_{ij}\,\mathring{u}_i - \mathring{\sigma}_{ij}\,u_i\right)_{,j} = 0 \tag{4.11}$$

First, expression (4.11) is integrated over the whole domain B and then transformed to the following boundary integral using Gauss' divergence theorem

$$\int_{\partial B}\left(\sigma_{ij}\,\mathring{u}_i - \mathring{\sigma}_{ij}\,u_i\right)\mathbf{e}_j \cdot d\mathbf{S} = 0 \tag{4.12}$$

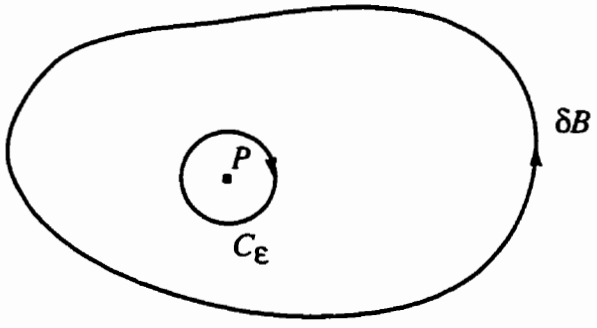

Figure 4.1: Exclusion of the singular point P in the elastic domain.

Substituting the Kelvin solution (4.5) into (4.12) leads to

$$\left[\int_{\partial B \bigcup C_\epsilon}\left(\sigma_{ij}U_{ik} - \Sigma_{ijk}u_i\right)\mathbf{e}_j \cdot d\mathbf{S}\right] e_k = 0 \tag{4.13}$$

where the singular point P is excluded by a small circle C_ϵ. In Eq. (4.13), the unit base vectors e_k are constant and can have any value. Hence,

$$\int_{\partial B \bigcup C_\epsilon}\left(\sigma_{ij}U_{ik} - \Sigma_{ijk}u_i\right)\mathbf{e}_j \cdot d\mathbf{S} = 0 \tag{4.14}$$

By the exclusion of the singular point P using a small circle C_ϵ of radius ϵ, it can be shown that

$$\left.\begin{aligned} \lim_{\epsilon\to 0}\left[\int_{C_\epsilon} \sigma_{ij}U_{ik}\mathbf{e}_j \cdot d\mathbf{S}\right] &= 0 \\ \lim_{\epsilon\to 0}\left[\int_{C_\epsilon} \Sigma_{ijk}u_i\mathbf{e}_j \cdot d\mathbf{S}\right] &= u_k(P) \end{aligned}\right\} \tag{4.15}$$

Use of Eqs. (4.14) and (4.15) gives the BIE for an internal source point P

$$u_k(P) = \int_{\partial B} \left[U_{ik}\sigma_{ij}(Q) - \Sigma_{ijk}u_i(Q)\right]\mathbf{e}_j \cdot d\mathbf{S} \tag{4.16}$$

A limiting process must be taken for Eq. (4.16), as an internal source point P approaches the boundary ∂B, to produce the following general BIE

$$c_{ik}(P)u_i(P) = \int_{\partial B} \left[U_{ik}\sigma_{ij}(Q) - \Sigma_{ijk}u_i(Q)\right]\mathbf{e}_j \cdot d\mathbf{S} \tag{4.17}$$

where the corner tensor $c_{ik} = \frac{1}{2}\delta_{ik}$ if the boundary is locally smooth at P. Otherwise, c_{ik} can be computed in closed form for 2-D problems, but direct evaluation of c_{ik} in 3-D cases is difficult. Fortunately, explicit calculations of this value can be avoided by using the rigid body motion technique as shown in the first paper.

4.2 Proof of $\nabla_Q \cdot \mathbf{F}_k = 0$ (Eq. (I.4))

By denoting

$$\mathbf{F}_k = \left[U_{ik}(P,Q)\sigma_{ij}(Q) - \Sigma_{ijk}(P,Q)u_i(Q)\right]\mathbf{e}_j = F_{kj}\mathbf{e}_j \tag{4.18}$$

the divergence of $\mathbf{F}_k$ at a field point Q is written as

$$\nabla_Q \cdot \mathbf{F}_k = F_{kj,j} = \sigma_{ij}U_{ik,j} - \Sigma_{ijk}u_{i,j} + \sigma_{ij,j}U_{ik} - \Sigma_{ijk,j}u_i \tag{4.19}$$

Let us determine each term in the right hand side of Eq. (4.19). Due to the symmetry of the elasticity tensor (4.9), we have

$$\sigma_{ij}U_{ik,j} - \Sigma_{ijk}u_{i,j} = 0 \tag{4.20}$$

Since body forces b_i are absent in the BCM, the equilibrium equations for linear elastostatics in this case are

$$\sigma_{ij,j} + b_i = \sigma_{ij,j} = 0 \tag{4.21}$$

Finally, knowing that Σ_{ijk} is the point load at the source point P, so at every field point Q which does not coincide with P, one gets

$$\Sigma_{ijk,j} = 0 \tag{4.22}$$

Substitution of (4.20), (4.21) and (4.22) into (4.19) yields

$$\nabla_Q \cdot \mathbf{F}_k = 0 \tag{4.23}$$

everywhere except at the source point P.

Equation (4.23) shows the existence of a function Φ_k such that

$$\mathbf{F}_k = \frac{\partial \Phi_k}{\partial y}\mathbf{e}_1 - \frac{\partial \Phi_k}{\partial x}\mathbf{e}_2 \tag{4.24}$$

because (4.24) ensures the identity (4.23).

4.3 Matrix [T(x, y)] (Eq. (I.22))

In Eq. (I.19), one has

$$[T_u(x,y)] = \begin{bmatrix} 1 & x & y & 0 & 0 & 0 & x^2 & y^2 & k_1xy & k_2xy \\ 0 & 0 & 0 & 1 & x & y & k_2xy & k_1xy & x^2 & y^2 \end{bmatrix} \tag{4.25}$$

where $k_1 = -2(1-2\nu)$, $k_2 = -4(1-\nu)$ and ν is the Poisson's ratio.

By using Eqs. (I.18) and (I.21), the traction vector can be written in matrix form as

$$\begin{Bmatrix} \tau_1 \\ \tau_2 \end{Bmatrix} = [T_\tau(x,y)]\,\{\beta\} \tag{4.26}$$

where

$$[T_\tau(x,y)] = \begin{bmatrix} 0 & k_3 n_1 & \mu n_2 & 0 & \mu n_2 & \lambda n_1 & k_4(n_1 x - n_2 y) \\ 0 & \lambda n_2 & \mu n_1 & 0 & \mu n_1 & k_3 n_2 & k_6 n_2 x - k_4 n_1 y \\ & k_5(n_1 x - n_2 y) & & -k_4 n_1 y - k_5 n_2 x & & & k_6 n_1 y - k_4 n_2 x \\ & -k_4 n_2 x - k_5 n_1 y & & k_5(n_2 y - n_1 x) & & & k_4(n_2 y - n_1 x) \end{bmatrix} \tag{4.27}$$

In Eq. (4.27), $k_3 = \lambda + 2\mu$, $k_4 = 4\mu(1-\nu)$, $k_5 = -4\mu\nu$, $k_6 = -4\mu(2-\nu)$ and λ and μ are Lamé constants of the material.

Therefore, in Eq. (I.22), the matrix $\left[T^{(\ell)}(x,y)\right]$ for element (ℓ) is given by

$$\left[T^{(\ell)}(x,y)\right] = \begin{bmatrix} \left[T_u^{(2\ell-1)}(x,y)\right] \\ \left[T_\tau^{(2\ell-1)}(x,y)\right] \\ \left[T_u^{(2\ell)}(x,y)\right] \\ \left[T_\tau^{(2\ell)}(x,y)\right] \\ \left[T_u^{(2\ell+1)}(x,y)\right] \end{bmatrix} \tag{4.28}$$

4.4 Matrix [B_j] (Eq. (I.26))

Substituting (I.24) into (I.19) yields

$$\begin{Bmatrix} u_1 \\ u_2 \end{Bmatrix} = \begin{bmatrix} 1 & \xi & \eta & 0 & 0 & 0 & \xi^2 & \eta^2 & k_1\xi\eta & k_2\xi\eta \\ 0 & 0 & 0 & 1 & \xi & \eta & k_2\xi\eta & k_1\xi\eta & \xi^2 & \eta^2 \end{bmatrix} [B_j]\{\beta\} \tag{4.29}$$

By comparing the matrix in (4.29) with (4.25) and letting $[B_j]\{\beta\} = \{\hat{\beta}\}$, one gets Eq. (I.25). The matrix $[B_j]$, giving the relationship between the vectors of the artificial variables $\{\beta\}$ and $\{\hat{\beta}\}$ in the global (x,y) and a (ξ,η) coordinate system

centered at the source point $P(x_j, y_j)$, respectively, is easily found as

$$[B_j] = \begin{bmatrix} 1 & x_j & y_j & 0 & 0 & 0 & x_j^2 & y_j^2 & k_1 x_j y_j & k_2 x_j y_j \\ 0 & 1 & 0 & 0 & 0 & 0 & 2x_j & 0 & k_1 y_j & k_2 y_j \\ 0 & 0 & 1 & 0 & 0 & 0 & 0 & 2y_j & k_1 x_j & k_2 x_j \\ 0 & 0 & 0 & 1 & x_j & y_j & k_2 x_j y_j & k_1 x_j y_j & x_j^2 & y_j^2 \\ 0 & 0 & 0 & 0 & 1 & 0 & k_2 y_j & k_1 y_j & 2x_j & 0 \\ 0 & 0 & 0 & 0 & 0 & 1 & k_2 x_j & k_1 x_j & 0 & 2y_j \\ 0 & 0 & 0 & 0 & 0 & 0 & 1 & 0 & 0 & 0 \\ 0 & 0 & 0 & 0 & 0 & 0 & 0 & 1 & 0 & 0 \\ 0 & 0 & 0 & 0 & 0 & 0 & 0 & 0 & 1 & 0 \\ 0 & 0 & 0 & 0 & 0 & 0 & 0 & 0 & 0 & 1 \end{bmatrix} \tag{4.30}$$

4.5 Displacement field $[u_i(Q) - u_i(P)]$ (Eq. (I.12))

In a (ξ, η) coordinate system centered at a source point P, the displacement shape functions are described by Eq. (I.25), i.e.

$$\begin{Bmatrix} u_1(Q) \\ u_2(Q) \end{Bmatrix} = \hat{\beta}_1 \begin{Bmatrix} 1 \\ 0 \end{Bmatrix} + \hat{\beta}_2 \begin{Bmatrix} \xi \\ 0 \end{Bmatrix} + \hat{\beta}_3 \begin{Bmatrix} \eta \\ 0 \end{Bmatrix} + \hat{\beta}_4 \begin{Bmatrix} 0 \\ 1 \end{Bmatrix} + \hat{\beta}_5 \begin{Bmatrix} 0 \\ \xi \end{Bmatrix}$$
$$+\hat{\beta}_6 \begin{Bmatrix} 0 \\ \eta \end{Bmatrix} + \hat{\beta}_7 \begin{Bmatrix} \xi^2 \\ k_2 \xi\eta \end{Bmatrix} + \hat{\beta}_8 \begin{Bmatrix} \eta^2 \\ k_1 \xi\eta \end{Bmatrix} + \hat{\beta}_9 \begin{Bmatrix} k_1 \xi\eta \\ \xi^2 \end{Bmatrix} + \hat{\beta}_{10} \begin{Bmatrix} k_2 \xi\eta \\ \eta^2 \end{Bmatrix} \tag{4.31}$$

where it can be seen from the matrix in (4.30) that $\hat{\beta}_h = \beta_h$ for $h = 7, \ldots, 10$.

Since the coordinates of P are $(0, 0)$, one gets

$$\begin{Bmatrix} u_1(P) \\ u_2(P) \end{Bmatrix} = \hat{\beta}_1^{(q)} \begin{Bmatrix} 1 \\ 0 \end{Bmatrix} + \hat{\beta}_4^{(q)} \begin{Bmatrix} 0 \\ 1 \end{Bmatrix} \tag{4.32}$$

where (q) is the element (if P is placed at a midpoint node) or either of the elements (if P is placed at a endpoint node) containing P.

Finally, for element (ℓ)

$$\begin{Bmatrix} u_1(Q) - u_1(P) \\ u_2(Q) - u_2(P) \end{Bmatrix}^{(\ell)} = \tilde{\beta}_1^{(\ell)} \begin{Bmatrix} 1 \\ 0 \end{Bmatrix} + \tilde{\beta}_2^{(\ell)} \begin{Bmatrix} \xi \\ 0 \end{Bmatrix} + \tilde{\beta}_3^{(\ell)} \begin{Bmatrix} \eta \\ 0 \end{Bmatrix} + \tilde{\beta}_4^{(\ell)} \begin{Bmatrix} 0 \\ 1 \end{Bmatrix}$$

$$+\tilde{\beta}_5^{(\ell)}\begin{Bmatrix}0\\ \xi\end{Bmatrix}+\tilde{\beta}_6^{(\ell)}\begin{Bmatrix}0\\ \eta\end{Bmatrix}+\tilde{\beta}_7^{(\ell)}\begin{Bmatrix}\xi^2\\ k_2\xi\eta\end{Bmatrix}$$
$$+\tilde{\beta}_8^{(\ell)}\begin{Bmatrix}\eta^2\\ k_1\xi\eta\end{Bmatrix}+\tilde{\beta}_9^{(\ell)}\begin{Bmatrix}k_1\xi\eta\\ \xi^2\end{Bmatrix}+\tilde{\beta}_{10}^{(\ell)}\begin{Bmatrix}k_2\xi\eta\\ \eta^2\end{Bmatrix} \quad (4.33)$$

in which

$$\left.\begin{aligned}\tilde{\beta}_h^{(\ell)} &= \hat{\beta}_h^{(\ell)} - \hat{\beta}_h^{(q)} \qquad \text{if} \quad h = 1,4\\ \tilde{\beta}_h^{(\ell)} &= \beta_h^{(\ell)} \qquad \text{if} \quad h = 7,\ldots,10\\ \tilde{\beta}_h^{(\ell)} &= \hat{\beta}_h^{(\ell)} \qquad \text{otherwise}\end{aligned}\right\} \quad (4.34)$$

4.6 Determination of the potential functions ϕ_z (Eq. (I.12))

In a (ξ,η) coordinate system, the displacement shape functions described by Eq. (I.25) can also be written as

$$\begin{Bmatrix}u_1(\xi,\eta)\\ u_2(\xi,\eta)\end{Bmatrix}^{(\ell)} = \sum_{h=1}^{10}\hat{\beta}_h^{(\ell)}\begin{Bmatrix}\overline{u}_{1h}(\xi,\eta)\\ \overline{u}_{2h}(\xi,\eta)\end{Bmatrix}^{(\ell)} \quad (4.35)$$

Hence, by applying Hooke's law (I.17) to (4.35), stress shape functions are found as

$$\begin{Bmatrix}\sigma_{11}(\xi,\eta)\\ \sigma_{22}(\xi,\eta)\\ \sigma_{12}(\xi,\eta)\end{Bmatrix}^{(\ell)} = \sum_{h=1}^{10}\hat{\beta}_h^{(\ell)}\begin{Bmatrix}\overline{\sigma}_{11h}(\xi,\eta)\\ \overline{\sigma}_{22h}(\xi,\eta)\\ \overline{\sigma}_{12h}(\xi,\eta)\end{Bmatrix}^{(\ell)} \quad (4.36)$$

Use of (4.35) and (4.36) in the integrand (4.18) of the BIE on an non-singular element (ℓ) gives

$$\mathbf{F}_k = \sum_{h=1}^{10}\hat{\beta}_h^{(\ell)}\left[U_{ik}\overline{\sigma}_{ijh}(\xi,\eta) - \Sigma_{ijk}\overline{u}_{ih}(\xi,\eta)\right]\mathbf{e}_j \quad (4.37)$$

Expression (4.24) in this case takes the following form

$$\mathbf{F}_k = \sum_{h=1}^{10}\hat{\beta}_h^{(\ell)}\left[\frac{\partial\phi_z}{\partial\eta}\mathbf{e}_1 - \frac{\partial\phi_z}{\partial\xi}\mathbf{e}_2\right] \quad (4.38)$$

Identification of (4.37) and (4.38) leads to the following system of equations that enables the determination of the potential functions ϕ_z

$$\left.\begin{aligned} \frac{\partial \phi_z}{\partial \eta} &= U_{ik}\overline{\sigma}_{i1h}(\xi,\eta) - \Sigma_{i1k}\overline{u}_{ih}(\xi,\eta) \\ \frac{\partial \phi_z}{\partial \xi} &= -U_{ik}\overline{\sigma}_{i2h}(\xi,\eta) + \Sigma_{i2k}\overline{u}_{ih}(\xi,\eta) \end{aligned}\right\} \tag{4.39}$$

It should be noted that since

$$\left\{ \begin{array}{c} u_1(Q) - u_1(P) \\ u_2(Q) - u_2(P) \end{array} \right\}^{(\ell)} = \sum_{h=1}^{10} \tilde{\beta}_h^{(\ell)} \left\{ \begin{array}{c} \overline{u}_{1h}(\xi,\eta) \\ \overline{u}_{2h}(\xi,\eta) \end{array} \right\}^{(\ell)} \tag{4.40}$$

by comparing (4.40) with (4.35), the expressions of the forms (4.37) and (4.38) for $\mathbf{G}_k$ can easily be derived from the last equations by replacing $\hat{\beta}_h^{(\ell)}$ with $\tilde{\beta}_h^{(\ell)}$. Thus $\mathbf{F}_k$ and $\mathbf{G}_k$ have the same potential functions ϕ_z.

For example, system (4.39) in case of $k = 1$ and $h = 7$ (i.e. $z = 7$) is

$$\left.\begin{aligned} \frac{\partial \phi_7}{\partial \eta} &= U_{11}\overline{\sigma}_{117}(\xi,\eta) + U_{21}\overline{\sigma}_{217}(\xi,\eta) - \Sigma_{111}\overline{u}_{17}(\xi,\eta) - \Sigma_{211}\overline{u}_{27}(\xi,\eta) \\ \frac{\partial \phi_7}{\partial \xi} &= -U_{11}\overline{\sigma}_{127}(\xi,\eta) - U_{21}\overline{\sigma}_{227}(\xi,\eta) + \Sigma_{121}\overline{u}_{17}(\xi,\eta) + \Sigma_{221}\overline{u}_{27}(\xi,\eta) \end{aligned}\right\} \tag{4.41}$$

where the expressions for the Kelvin kernel tensors are given by Eq. (I.2) and,

$$\left\{ \begin{array}{c} \overline{u}_{17}(\xi,\eta) \\ \overline{u}_{27}(\xi,\eta) \end{array} \right\} = \left\{ \begin{array}{c} \xi^2 \\ k_2\xi\eta \end{array} \right\} \tag{4.42}$$

$$\left\{ \begin{array}{c} \overline{\sigma}_{117}(\xi,\eta) \\ \overline{\sigma}_{227}(\xi,\eta) \\ \overline{\sigma}_{127}(\xi,\eta) \end{array} \right\} = \frac{2E}{1+\nu} \left\{ \begin{array}{c} \xi(1-\nu) \\ \xi(\nu-2) \\ \eta(\nu-1) \end{array} \right\} \tag{4.43}$$

Finally, the solution of system (4.41) is

$$\phi_7(\xi,\eta) = \frac{\xi\eta}{4\pi(1-\nu)} \left[(5-4\nu)\frac{\xi^2}{r^2} - (8\nu^2 - 14\nu + 6)\ln(r) \right] \tag{4.44}$$

The above method for determining ϕ_z is general and thus, can also be employed to derive other potential functions required by a boundary contour version for 2-D problems.

4.7 Plane stress problems

The formulas for the Kelvin kernel tensors (I.2), for Hooke's law (I.17) and thus, for the derived potential functions ϕ_z, are built for a plane strain state. However, these formulas can also be employed to solve plane stress problems provided that the appropriate material data are used.

In fact, by observing the relationship between the constitutive law of plane strain and plane stress states, for plane stress problems, one only needs to substitute ν by $\overline{\nu} = \nu/(1+\nu)$ and E by $\overline{E} = E(1-\overline{\nu}^2)$ in the appropriate formulas presented in all of the four papers.

4.8 Derivation of the regularized HBIE (Eq. (II.28))

Taking the partial derivative of Eq. (4.16) (written for an internal source point P) with respect to P yields

$$u_{k,M}(P) = \int_{\partial B} [U_{ik,M}(P,Q)\sigma_{ij}(Q) - \Sigma_{ijk,M}(P,Q)u_i(Q)]\,\mathbf{e}_j \cdot d\mathbf{S} \tag{4.45}$$

By using the identity $r_{,m} = -r_{,M}$ (see (I-2)) where $_{,m}$ denotes partial derivative with respect to a field point Q, Eq. (4.45) becomes

$$u_{k,m}(P) = -\int_{\partial B} [U_{ik,m}(P,Q)\sigma_{ij}(Q) - \Sigma_{ijk,m}(P,Q)u_i(Q)]\,\mathbf{e}_j \cdot d\mathbf{S} \tag{4.46}$$

Now, modes are used in order to regularize (4.46).

First, use of the following linear mode

$$u_i(Q) = u_{i,s}(P)\,[x_s(Q) - x_s(P)] \tag{4.47}$$

gives

$$u_{i,j}(Q) = u_{i,j}(P) \tag{4.48}$$

and thus, the following constant stress field (see Eqs. (4.2) and (4.3))

$$\sigma_{ij}(Q) = \sigma_{ij}(P) \tag{4.49}$$

By applying the fields (4.47) and (4.49) to Eq. (4.46), one gets

$$u_{k,m}(P) = -\int_{\partial B} \{U_{ik,m}(P,Q)\sigma_{ij}(P) - \Sigma_{ijk,m}(P,Q)u_{i,s}(P)\,[x_s(Q) - x_s(P)]\}\,\mathbf{e}_j \cdot d\mathbf{S} \tag{4.50}$$

Next, using a rigid body mode $u_i(Q) = u_i(P)$ in Eq. (4.46) immediately gives

$$0 = u_i(P)\int_{\partial B} \Sigma_{ijk,m}(P,Q)\mathbf{e}_j \cdot d\mathbf{S} \tag{4.51}$$

Subtracting (4.46) from (4.50) yields

$$\begin{aligned} 0 \;=\; & \int_{\partial B} \{U_{ik,m}(P,Q)\,[\sigma_{ij}(Q) - \sigma_{ij}(P)] \\ & -\Sigma_{ijk,m}(P,Q)\,[u_i(Q) - u_{i,s}(P)\,[x_s(Q) - x_s(P)]]\}\,\mathbf{e}_j \cdot d\mathbf{S} \end{aligned} \tag{4.52}$$

Use of (4.51) in (4.52) leads to the following regularized expression at an internal source point

$$0 = \int_{\partial B} \left\{U_{ik,m}(P,Q)\,[\sigma_{ij}(Q) - \sigma_{ij}(P)] - \Sigma_{ijk,m}(P,Q)\left[u_i(Q) - u_i^{(L)}\right]\right\}\mathbf{e}_j \cdot d\mathbf{S} \tag{4.53}$$

where $u_i^{(L)} = u_i(P) + u_{i,s}(P)\,[x_s(Q) - x_s(P)]$

Finally, by taking a limiting process of (4.53) as an internal source point approaches the boundary ∂B, one gets the regularized HBIE under consideration.

4.9 Displacement field $[\mathbf{u_i(Q) - u_i^{(L)}}]$ (Eq. (II.28))

The displacement field used in the regularized HBIE (II.28) is

$$u_i(Q) - u_i^{(L)} = u_i(Q) - u_i(P) - u_{i,s}(P)\,[x_s(Q) - x_s(P)] \tag{4.54}$$

where $s = 1, 2$; $x_1 \equiv x$ and $x_2 \equiv y$. In a (ξ, η) coordinate system, by using (I.24) Eq. (4.54) becomes

$$u_i(Q) - u_i^{(L)} = u_i(Q) - u_i(P) - u_{i,1}(P)\xi - u_{i,2}(P)\eta \tag{4.55}$$

- **For the HBCM primary analysis (Eq. (II.39))**

The displacement gradient field $u_{i,s}(Q)$ can easily be found from (4.31) as

$$\left\{ \begin{array}{c} u_{1,1}(Q) \\ u_{2,1}(Q) \end{array} \right\} = \hat{\beta}_2 \left\{ \begin{array}{c} 1 \\ 0 \end{array} \right\} + \hat{\beta}_5 \left\{ \begin{array}{c} 0 \\ 1 \end{array} \right\} + \hat{\beta}_7 \left\{ \begin{array}{c} 2\xi \\ k_2\eta \end{array} \right\} + \hat{\beta}_8 \left\{ \begin{array}{c} 0 \\ k_1\eta \end{array} \right\} + \hat{\beta}_9 \left\{ \begin{array}{c} k_1\eta \\ 2\xi \end{array} \right\} + \hat{\beta}_{10} \left\{ \begin{array}{c} k_2\eta \\ 0 \end{array} \right\} \tag{4.56}$$

$$\left\{ \begin{array}{c} u_{1,2}(Q) \\ u_{2,2}(Q) \end{array} \right\} = \hat{\beta}_3 \left\{ \begin{array}{c} 1 \\ 0 \end{array} \right\} + \hat{\beta}_6 \left\{ \begin{array}{c} 0 \\ 1 \end{array} \right\} + \hat{\beta}_7 \left\{ \begin{array}{c} 0 \\ k_2\xi \end{array} \right\} + \hat{\beta}_8 \left\{ \begin{array}{c} 2\eta \\ k_1\xi \end{array} \right\} + \hat{\beta}_9 \left\{ \begin{array}{c} k_1\xi \\ 0 \end{array} \right\} + \hat{\beta}_{10} \left\{ \begin{array}{c} k_2\xi \\ 2\eta \end{array} \right\} \tag{4.57}$$

In the primary analysis, the source points are only placed at endpoint nodes on the boundary. Hence, in Eq. (4.55), $u_{i,s}(P)$ at a source point P can be determined from the displacement gradient field $u_{i,s}(Q)$ of either of the elements (q) containing this source point. Since the coordinates of P are $(0,0)$, we have

$$\left\{ \begin{array}{c} u_{1,1}(P) \\ u_{2,1}(P) \end{array} \right\} = \hat{\beta}_2^{(q)} \left\{ \begin{array}{c} 1 \\ 0 \end{array} \right\} + \hat{\beta}_5^{(q)} \left\{ \begin{array}{c} 0 \\ 1 \end{array} \right\} \tag{4.58}$$

$$\left\{ \begin{array}{c} u_{1,2}(P) \\ u_{2,2}(P) \end{array} \right\} = \hat{\beta}_3^{(q)} \left\{ \begin{array}{c} 1 \\ 0 \end{array} \right\} + \hat{\beta}_6^{(q)} \left\{ \begin{array}{c} 0 \\ 1 \end{array} \right\} \tag{4.59}$$

Finally, for element (ℓ), use of (4.58), (4.59) and (4.33) in (4.55) leads to

$$\left\{ \begin{array}{c} u_1(Q) - u_1^{(L)} \\ u_2(Q) - u_2^{(L)} \end{array} \right\}^{(\ell)} = \check{\beta}_1^{(\ell)} \left\{ \begin{array}{c} 1 \\ 0 \end{array} \right\} + \check{\beta}_2^{(\ell)} \left\{ \begin{array}{c} \xi \\ 0 \end{array} \right\} + \check{\beta}_3^{(\ell)} \left\{ \begin{array}{c} \eta \\ 0 \end{array} \right\} + \check{\beta}_4^{(\ell)} \left\{ \begin{array}{c} 0 \\ 1 \end{array} \right\} + \check{\beta}_5^{(\ell)} \left\{ \begin{array}{c} 0 \\ \xi \end{array} \right\} + \check{\beta}_6^{(\ell)} \left\{ \begin{array}{c} 0 \\ \eta \end{array} \right\} + \check{\beta}_7^{(\ell)} \left\{ \begin{array}{c} \xi^2 \\ k_2\xi\eta \end{array} \right\} + \check{\beta}_8^{(\ell)} \left\{ \begin{array}{c} \eta^2 \\ k_1\xi\eta \end{array} \right\} + \check{\beta}_9^{(\ell)} \left\{ \begin{array}{c} k_1\xi\eta \\ \xi^2 \end{array} \right\} + \check{\beta}_{10}^{(\ell)} \left\{ \begin{array}{c} k_2\xi\eta \\ \eta^2 \end{array} \right\} \tag{4.60}$$

where

$$\left. \begin{array}{ll} \check{\beta}_h^{(\ell)} = \hat{\beta}_h^{(\ell)} - \hat{\beta}_h^{(q)} & \text{if} \quad h = 1, \ldots, 6 \\ \check{\beta}_h^{(\ell)} = \beta_h^{(\ell)} & \text{if} \quad h = 7, \ldots, 10 \end{array} \right\} \tag{4.61}$$

- **For the HBCM post-processing analysis (Eq. (II.51))**

As mentioned in the second paper, only source points in the domain B^* need to be considered in the post-processing stage. Since these source points do not lie at endpoint nodes as in the primary analysis, $u_i(P)$ and $u_{i,s}(P)$ in (4.55) can not be calculated from the displacement field (4.31) and displacement gradient field (4.56), (4.57) in which $\hat{\beta}_h^{(\ell)}$ $(h = 1, 2, \ldots, 10)$ for all boundary elements (ℓ) are known from the primary analysis.

Use of Eq. (4.31) in (4.55) also gives expression (4.60), but now the coefficients $\check{\beta}_h^{(\ell)}$ for $h = 1, \ldots, 6$ are given by

$$\left.\begin{array}{lll} \check{\beta}_1^{(\ell)} = \hat{\beta}_1^{(\ell)} - u_1(P)\ ; & \check{\beta}_2^{(\ell)} = \hat{\beta}_2^{(\ell)} - u_{1,1}(P)\ ; & \check{\beta}_3^{(\ell)} = \hat{\beta}_3^{(\ell)} - u_{1,2}(P) \\ \check{\beta}_4^{(\ell)} = \hat{\beta}_4^{(\ell)} - u_2(P)\ ; & \check{\beta}_5^{(\ell)} = \hat{\beta}_5^{(\ell)} - u_{2,1}(P)\ ; & \check{\beta}_6^{(\ell)} = \hat{\beta}_6^{(\ell)} - u_{2,2}(P) \end{array}\right\} \tag{4.62}$$

The post-processing analysis consists of solving systems of equations with the unknowns $u_i(P)$ and $u_{i,s}(P)$ in (4.62). This enables the determination of displacements and stresses in the domain B^*.

4.10 Determination of the potential functions λ_w (Eq. (II.42))

By anology with (4.35) and (4.36), the displacement field (4.60) and its stress field can be written in a (ξ, η) coordinate system as

$$\left\{\begin{array}{l} u_1(Q) - u_1^{(L)} \\ u_2(Q) - u_2^{(L)} \end{array}\right\}^{(\ell)} = \sum_{h=1}^{10} \check{\beta}_h^{(\ell)} \left\{\begin{array}{l} \overline{u}_{1h}(\xi, \eta) \\ \overline{u}_{2h}(\xi, \eta) \end{array}\right\}^{(\ell)} \tag{4.63}$$

$$\left\{\begin{array}{l} \sigma_{11}(Q) - \sigma_{11}(P) \\ \sigma_{22}(Q) - \sigma_{22}(P) \\ \sigma_{12}(Q) - \sigma_{12}(P) \end{array}\right\}^{(\ell)} = \sum_{h=1}^{10} \check{\beta}_h^{(\ell)} \left\{\begin{array}{l} \overline{\sigma}_{11h}(\xi, \eta) \\ \overline{\sigma}_{22h}(\xi, \eta) \\ \overline{\sigma}_{12h}(\xi, \eta) \end{array}\right\}^{(\ell)} \tag{4.64}$$

Substitution of (4.63) and (4.64) into the integrand (II.32) of the regularized HBIE yields

$$\mathbf{J}_{km} = \sum_{h=1}^{10} \check{\beta}_h^{(\ell)} \left[U_{ik,m} \overline{\sigma}_{ijh}(\xi, \eta) - \Sigma_{ijk,m} \overline{u}_{ih}(\xi, \eta)\right] \mathbf{e}_j \tag{4.65}$$

Expression (II.38) in this case takes the following form

$$\mathbf{J}_{km} = \sum_{h=1}^{10} \check{\beta}_h^{(\ell)} \left[\frac{\partial \lambda_w}{\partial \eta} \mathbf{e}_1 - \frac{\partial \lambda_w}{\partial \xi} \mathbf{e}_2 \right] \tag{4.66}$$

It is noted that by using (4.35) and (4.36), the integrand vector (IV.30) on a non-singular element (ℓ) is written as

$$\mathbf{H}_{km} = \sum_{h=1}^{10} \hat{\beta}_h^{(\ell)} \left[U_{ik,m} \overline{\sigma}_{ijh}(\xi,\eta) - \Sigma_{ijk,m} \overline{u}_{ih}(\xi,\eta) \right] \mathbf{e}_j \tag{4.67}$$

Hence the potential functions associated with $\mathbf{J}_{km}$ and $\mathbf{H}_{km}$ are the same and they are called λ_w.

Equations (4.65) and (4.66) lead to the following system of equations that enables the determination of λ_w

$$\left.\begin{aligned} \frac{\partial \lambda_w}{\partial \eta} &= U_{ik,m} \overline{\sigma}_{i1h}(\xi,\eta) - \Sigma_{i1k,m} \overline{u}_{ih}(\xi,\eta) \\ \frac{\partial \lambda_w}{\partial \xi} &= -U_{ik,m} \overline{\sigma}_{i2h}(\xi,\eta) + \Sigma_{i2k,m} \overline{u}_{ih}(\xi,\eta) \end{aligned}\right\} \tag{4.68}$$

For example, system (4.68) in case of $k = 1$, $m = 2$ and $h = 4$ (i.e. $w = 24$) is

$$\left.\begin{aligned} \frac{\partial \lambda_{24}}{\partial \eta} &= U_{11,2} \overline{\sigma}_{114}(\xi,\eta) + U_{21,2} \overline{\sigma}_{214}(\xi,\eta) - \Sigma_{111,2} \overline{u}_{14}(\xi,\eta) - \Sigma_{211,2} \overline{u}_{24}(\xi,\eta) \\ \frac{\partial \lambda_{24}}{\partial \xi} &= -U_{11,2} \overline{\sigma}_{124}(\xi,\eta) - U_{21,2} \overline{\sigma}_{224}(\xi,\eta) + \Sigma_{121,2} \overline{u}_{14}(\xi,\eta) + \Sigma_{221,2} \overline{u}_{24}(\xi,\eta) \end{aligned}\right\} \tag{4.69}$$

where the expressions for the gradients of the Kelvin kernel tensors are given by Eq. (II.29) and,

$$\left\{ \begin{array}{c} \overline{u}_{14}(\xi,\eta) \\ \overline{u}_{24}(\xi,\eta) \end{array} \right\} = \left\{ \begin{array}{c} 0 \\ 1 \end{array} \right\} \tag{4.70}$$

$$\left\{ \begin{array}{c} \overline{\sigma}_{114}(\xi,\eta) \\ \overline{\sigma}_{224}(\xi,\eta) \\ \overline{\sigma}_{124}(\xi,\eta) \end{array} \right\} = \left\{ \begin{array}{c} 0 \\ 0 \\ 0 \end{array} \right\} \tag{4.71}$$

Finally, the solution of system (4.69) is

$$\lambda_{24}(\xi,\eta) = \frac{\eta}{4\pi(1-\nu)r^2} \left(\frac{2\xi^2}{r^2} + 1 - 2\nu \right) \tag{4.72}$$

4.11 DSCs and the concept of material derivative

Let us begin with the quantitative definition of DSCs. The initial design configuration having b as the design variable under consideration is analysed to obtain a physical response $F(b)$. Then the configuration is perturbed with a step size δb and the analysis of this new problem yields $F(b+\delta b)$. The DSC is thus defined as

$$DSC = \lim_{\delta b \to 0} \frac{F(b+\delta b) - F(b)}{\delta b} \tag{4.73}$$

The FDA approximatively evaluates the DSCs by calculating the ratio in the right hand side of (4.73) with a small value of δb instead of taking the limit, i.e.

$$DSC \approx \frac{F(b+\delta b) - F(b)}{\delta b} \tag{4.74}$$

The DDA uses the definition of derivative to evaluate the limit in (4.73), so conceptually, this is an exact approach

$$DSC = \frac{dF}{db} \tag{4.75}$$

However, it should be noted that the concept of material derivative has to be employed here because of the following reasoning.

It can be seen that the physical response F (von Mises stress, for example) is a function of not only the design variable b, but also the coordinates of the point where F is evaluated, i.e. $F = F(b,x,y)$ in 2-D problems. In considering the partial derivative $\partial F/\partial b$, this (Eulerian) derivative measures the change in F at a fixed spatial point (x,y) in the body, and is often referred to as local derivative

$$\frac{\partial F}{\partial b} = \left.\frac{dF}{db}\right|_{(x,y)=constant}$$

The (Lagrangian) derivative that measures the change in F at a *fixed material point* needs to take account also the change in (x,y) of this material point as b changes. This derivative is called the material derivative or the total derivative of F and is denoted as $\dot{F} = dF/db$.

Typically, the material derivative is more physically interesting than the partial derivative. For example, if we change the shape of a hole boundary to relieve stress concentration at that boundary, we would like the DSC of the stress at the boundary rather than at a point with fixed coordinates because sometimes this fixed point is out of the material domain due to the shape design modification!

The total derivative of $F(b, x, y)$ with respect to b is given by the total derivative rule as

$$\begin{aligned} \dot{F} = \frac{dF}{db} &= \frac{\partial F}{\partial b} + \frac{\partial F}{\partial x}\frac{dx}{db} + \frac{\partial F}{\partial y}\frac{dy}{db} \\ &= F_{,b} + F_{,x}\,\dot{x} + F_{,y}\,\dot{y} \end{aligned} \tag{4.76}$$

Or, in tensor notation

$$\dot{F} = F_{,b} + v_i F_{,i} \tag{4.77}$$

where the quantities $v_1 = \dot{x}$ and $v_2 = \dot{y}$ are components of the design velocity field.

CHAPTER V
SUMMARY

Two novel methods of the same *boundary contour* family, namely the BCM and HBCM for 2-D linear elasticity, along with their successful application in stress analysis and shape optimization, are presented in this dissertation.

- **Original contributions**

The original contributions of this study can be summarized as follows:

- A further development of the BCM has been carried out in which the numerical implementation with quadratic boundary elements and post-processing analysis are introduced to 2-D problems.
- A new and full development of the HBCM in 2-D linear elasticity.
- A new and full development of design sensitivity analysis using the 2-D BCM.
- A successful development of a C program that couples a 2-D BCM code, its design sensitivity code and a SQP function of the commercial IMSL library in order to solve shape optimization problems in 2-D linear elasticity. The fourth paper dealing with this development is in fact the first contribution to the literature for the topic of shape optimization using the BCM.

While this research was being conducted, there have been investigations of the HBCM and design sensitivity analysis by the BCM in 3-D cases. However, for the time being, only some preliminary (non general) results for special cases have been obtained from the above investigations as opposed to complete validation with general results presented through this study. Therefore, this study can serve as an excellent reference for a successful implementation of the HBCM and BCM design sensitivity analysis for 3-D linear elasticity in a near future.

- **Discussions**

As shown from this study, the 2-D BCM and HBCM exhibit the following remarkable advantages:

- Simplicity in meshing (only boundary meshing as opposed to domain meshing required by the FEM).

- The methods do not require any numerical integration. In other words, the line integrals in these methods are evaluated analytically by using the potential functions. This advantage, as well as the fact that the BCM and HBCM use shape functions satisfying the Navier-Cauchy equations and Hooke's law, may explain why numerical results obtained from these methods are generally better than those from the BEM.

- Unlike the conventional BEM, special treatments for singularity are completely avoided in stress analysis as well as in design sensitivity analysis by the BCM. Hence, the computation of DSCs using the BCM is much more effective than that using the BEM.

These advantages confirm that the BCM is very attractive and suitable for optimal shape design. Besides the aforementioned major advantages offered by the BCM and HBCM in 2-D linear elasticity, these methods still have some shortcomings as follows:

- Stresses are numerically discontinuous across boundary elements due to the configuration of BCM boundary elements. However, the stress discontinuities are very slight where stresses are physically continuous. On the other hand, this configuration makes the corner modeling straightforward.

- Due to the nature of the HBIE used, stress discontinuities across boundary elements can be much improved by the HBCM. However, this method requires finer meshes than the BCM and it is expected that higher order elements such as cubic would overcome this meshing drawback.

- As the conventional BEM, the BCM and HBCM system matrices are not symmetric. Furthermore, the primary system of equations is, in general, overdetermined. Although this does not raise any problem in solving the system because there are effective rectangular solvers (such as those based on the least-squares or singular value decompositions and generalized inverses algorithms), the programming for a BCM or HBCM code requires more effort by the fact that the column dimension of the system matrices depends upon the type of problems to be analyzed.

It should be recalled that the BEM can solve a wide range of engineering problems such as steady state potential flows, elastodynamics and wave propagation, thermoelasticity and consolidation, plate-bending, anisotropic and viscoelastic materials, elastoplasticity and viscoplasticity, etc. The BEM has also been applied to bimaterial and nonhomogeneous problems, but these applications are not as efficient as in the context of the FEM.

As a variant of the BEM, in principle, the BCM is applicable to the above problems providing that the BIE integrands in such cases are divergent-free. However, the method is not recommended for nonlinear problems such as elastoplasticity or viscoplasticity, because the advantage of a further reduction in dimensionality with respect to the BEM could be lost in these cases. Also, body forces, that can be modeled as a particular integral in the BEM, can also be treated in the same manner in the BCM.

Finally, this study shows that the BCM has great potential advantages over other numerical methods in shape optimization. Therefore, the present work certainly motivates future research on this kind of application in 3-D cases.

REFERENCES

AITHAL, R. and SAIGAL, S. (1990). Adjoint structure approach for shape-sensitivity analysis using BEM. *Journal of Engineering Mechanics*, *116*, 2663-2680.

AITHAL, R., SAIGAL, S. and MUKHERJEE, S. (1991). Three dimensional boundary element implicit differentiation formulation for design sensitivity analysis. *Math. Comput. Modelling*, *15*, 1-10.

BONNET, M. (1995-a). Regularized direct and indirect symmetric variational BIE formulations for three-dimensional elasticity. *Engineering Analysis with Boundary Elements*, *15*, 93-102.

BONNET, M. (1995-b). Regularized BIE formulations for first- and second-order shape sensitivity of elastic fields. *Computers & Structures*, *56*, 799-811.

BANERJEE, P.K. and BUTTERFIELD, R. (1981). *Boundary Element Method In Engineering Science*, McGraw-Hill.

BARONE, M.R. and CAULK, D.A. (1982). Optimal arrangement of holes in a two-dimensional heat conductor by a special boundary integral method. *International Journal for Numerical Methods in Engineering*, *18*, 675-685.

BARONE, M.R. and YANG, R.J. (1988). Boundary integral equations for recovery of design sensitivities in shape optimization. *AIAA Journal*, *26*, 589-594.

BREBBIA, C.A., TELLES, J.C.F. and WROBEL, L.C. (1984). *Boundary Element Techniques, Theory and Applications in Engineering*, Springer-Verlag.

CHANDRA, A. and MUKHERJEE, S. (1997). *Boundary element methods in manufacturing*, Oxford University Press.

CHOI, J.H. and KWAK, B.M. (1988). Boundary integral equation method for shape optimization of elastic structures. *International Journal for Numerical Methods in Engineering*, *26*, 1579-1595.

GRAY, L.J., BALAKRISHNA, C. and KANE, J.H. (1995). Symmetric Galerkin fracture analysis. *Engineering Analysis with Boundary Elements*, *15*, 103-109.

GRAY, L.J., MARTHA, L.F. and INGRAFFEA, A.R. (1990). Hypersingular integrals in boundary element fracture analysis. *International Journal for Numerical Methods in Engineering*, *29*, 1135-1158.

GRAY, L.J. and PAULINO, G.H. (1997-a). Crack tip interpolation, revisited. *SIAM Journal on Numerical Analysis*. (In press).

GRAY, L.J. and PAULINO, G.H. (1997-b). Symmetric Galerkin boundary integral formulation for interface and multy-zone problems. *International Journal for Numerical Methods in Engineering*. (In press).

GUIGGIANI, M., KRISHNASAMY, G., RUDOLPHI, T.J. and RIZZO, F.J. (1992). A general algorithm for the numerical solution of the hypersingular boundary integral equations. *ASME Journal of Applied Mechanics*, *59*, 604-614.

HAFTKA, R.T., GÜRDAL, Z. and KAMAT, M.P. (1990). *Elements of Structural Optimization*, Kluwer Academic Publishers, Dordrecht, The Netherlands.

HALL, W.S. (1994). *The Boundary Element Method*, Kluwer Academic Publishers, Dordrecht, The Netherlands.

KANE, J.H. and PRASAD, K.G. (1993). Boundary formulations for sensitivity analysis without matrix derivatives. *AIAA Journal*, *31*, 1731-1734.

KANE, J.H. and SAIGAL, S. (1988). Design sensitivity analysis of solids using BEM. *Journal of Engineering Mechanics*, *114*, 1703-1722.

KANE, J.H., ZHAO, G., WANG, H. and PRASAD, K.G. (1992). Boundary formulations for three-dimensional continuum structural shape sensitivity analysis. *ASME Journal of Applied Mechanics*, *59*, 827-834.

KRISHNASAMY, G., RIZZO, F.J. and RUDOLPHI, T.J. (1992). Hypersingular boundary integral equations: their occurrence, interpretation, regularization and

computation. In: *Developments in boundary element methods, vol. 7* (Banerjee, P.K., Kobayashi, S. ed.), 207-252, Elsevier Applied Science, London.

LEE, B.Y. (1996). Consideration of body forces in axisymmetric design sensitivity analysis using the BEM. *Computers & Structures, 61*, 587-596.

LUTZ, E.D., INGRAFFEA, A.R. and GRAY, L.J. (1992). Use of 'simple solutions' for boundary integral methods in elasticity and fracture analysis. *International Journal for Numerical Methods in Engineering, 35*, 1737-1751.

MELLINGS, S.C. and ALIABADI, M.H. (1995). Flaw identification using the boundary element method. *International Journal for Numerical Methods in Engineering*, **38**, 399-419.

MENON, G. (1996). *Hypersingular error estimates in boundary element methods.* M.S. thesis, Cornell University, Ithaca, New York, U.S.A.

MENON, G., PAULINO, G.H. and MUKHERJEE, S. (1997). Analysis of hypersingular residual error estimates for potential problems using boundary element methods. (Submitted for publication).

MUKHERJEE, S. (1982). *Boundary Element Methods in Creep and Fracture*, Elsevier Applied Science, London.

MUKHERJEE, S. and CHANDRA, A. (1989). A boundary element formulation for design sensitivities in materially nonlinear problems. *Acta Mechanica, 78*, 243-253.

MUKHERJEE, S. and CHANDRA, A. (1991). A boundary element formulation for design sensitivities in problems involving both geometric and material nonlinearities. *Math. Computer Modelling, 15*, 245-255.

MUKHERJEE, S. and MUKHERJEE, Y.X. (1977-a). The hypersingular boundary contour method for three-dimensional linear elasticity - Part I: General theory. (Submitted for publication).

MUKHERJEE, S. and MUKHERJEE, Y.X. (1977-b). The hypersingular boundary

contour method for three-dimensional linear elasticity - Part II: Special cases and numerical examples. (Submitted for publication).

MUKHERJEE Y.X., MUKHERJEE, S., SHI, X. and NAGARAJAN, A. (1997). The boundary contour method for three-dimensional linear elasticity with a new quadratic boundary element. *Engineering Analysis with Boundary Elements.* (In press).

NAGARAJAN, A., LUTZ, E.D. and MUKHERJEE, S. (1994). A novel boundary element method for linear elasticity with no numerical integration for two-dimensional and line integrals for three-dimensional problems. *ASME Journal of Applied Mechanics, 61,* 264-269.

NAGARAJAN, A., LUTZ, E.D. and MUKHERJEE, S. (1996). The boundary contour method for three-dimensional linear elasticity. *ASME Journal of Applied Mechanics, 63,* 278-286.

PAULINO, G.H. (1995). *Novel formulations of the boundary element method for fracture mechanics and error estimation.* Ph.D. dissertation, Cornell University, Ithaca, New York, U.S.A.

PAULINO, G.H., GRAY, L.J. and ZARKIAN, V. (1996). Hypersingular residuals - A new approach for error estimation in the boundary element method. *International Journal for Numerical Methods in Engineering, 39,* 2005-2029.

PHAN, Anh-Vũ, MUKHERJEE, S. and MAYER, J.R.R. (1997-a). The boundary contour method for two-dimensional linear elasticity with quadratic boundary elements. *Computational Mechanics.* (In press).

PHAN, Anh-Vũ, MUKHERJEE, S. and MAYER, J.R.R. (1997-b). The hypersingular boundary contour method for two-dimensional linear elasticity. *Acta Mechanica.* (In press).

PHAN, Anh-Vũ, MUKHERJEE, S. and MAYER, J.R.R. (1997-c). A boundary contour formulation for design sensitivity analysis in two-dimensional linear elasticity.

International Journal of Solids and Structures. (In press).

PHAN, Anh-Vũ, MUKHERJEE, S. and MAYER, J.R.R. (1997-d). Stresses, stress sensitivities and shape optimization by the usual and hypersingualr boundary contour method. (Submitted for publication).

RICE, J.R. and MUKHERJEE, S. (1990) Design sensitivity coefficients for axisymmetric elasticity problems by boundary element methods. *Engineering Analysis with Boundary Elements*, *7*, 13-20.

SAIGAL, S., BORGGAARD, J.T. and KANE, J.H. (1989). Boundary element implicit differentiation equations for design sensitivities of axisymmetric structures. *International Journal of Solids and Structures*, *25*, 527-538.

SAIGAL, S. and KANE, J.H. (1990). Boundary-element shape optimization system for aircraft structural components. *AIAA Journal*, *28*, 1203-1204.

SANDGREN, E. and WU, S.J. (1988). Shape optimization using the boundary element method with substructuring. *International Journal for Numerical Methods in Engineering*, *26*, 1913-1924.

SCHMITH, L.A. (1960). Structural design by systematic synthesis. *Proceedings of 2nd Conference on Electronic Computations*, ASCE, New York, 105-122.

TAFRESHI, A. and FENNER, R.T. (1995). General-purpose computer program for shape optimization of engineering structures using the boundary element method. *Computers & Structures*, *56*, 713-720.

WEI, X., CHANDRA, A., LEU, L.J. and MUKHERJEE, S. (1994). Shape optimization in elasticity and elasto-viscoplasticity by the boundary element method. *International Journal of Solids and Structures*, *31*, 533-550.

WU, S.J. (1986). *Applications of the boundary element method for structural shape optimization.* Ph.D. thesis, University of Missouri at Columbia, U.S.A.

YAMAZAKI, K., SAKAMOTO, J. and KITANO, M. (1994). Three-dimensional

shape optimization using the boundary element method. *AIAA Journal*, *32*, 1295-1301.

YANG, R.J. (1990). Component shape optimization using BEM. *Computers & Structures*, *37*, 561-568.

ZHANG, Q. and MUKHERJEE, S. (1991). Design sensitivity coefficients for linear elastic bodies with zones and corners by the derivative boundary element method. *International Journal of Solids and Structures*, *27*, 983-998.

ZHAO, Z. (1991). *Shape Design Sensitivity Analysis and Optimization Using the Boundary Element Method*, Springer-Verlag, Berlin and New York.

ZHAO, Z. (1993). Direct continuum approach to three-dimensional sensitivity analysis. *Journal of Engineering Mechanics*, *119*, 2143-2156.

ZIENKIEWICZ, O.C. and CAMPBELL, J.S. (1973). Shape optimization and sequential linear programming. *Optimum Structural Design*, Gallagher, R.H., Zienkiewicz, O.C., Wiley, 109-126.

APPENDIX I

The boundary contour method for two-dimensional linear elasticity with quadratic boundary elements.

THE BOUNDARY CONTOUR METHOD FOR TWO-DIMENSIONAL LINEAR ELASTICITY WITH QUADRATIC BOUNDARY ELEMENTS

(Final revised version, January 1997.
Accepted for publication in *Computational Mechanics*)

Anh-Vũ Phan
Graduate Student
Department of Mechanical Engineering
Ecole Polytechnique
Montréal, Québec
Canada H3C 3A7

Subrata Mukherjee
Professor
Department of Theoretical and Applied Mechanics
Cornell University
Ithaca, NY 14853
USA

J.R. René Mayer
Assistant Professor
Department of Mechanical Engineering
Ecole Polytechnique
Montréal, Québec
Canada H3C 3A7

Abstract

This paper presents a further development of the Boundary Contour Method (BCM) for two-dimensional linear elasticity. The new developments are : (a) explicit use of the rigid body motion solution to regularize the BCM and avoid computation of the corner tensor, (b) quadratic boundary elements compared to linear elements in previous work and (c) evaluation of stresses both inside and on the boundary of a body. This method allows boundary stress computations at regular points (i.e. at points where the boundary is locally smooth) inside boundary elements without the need of any special algorithms for the numerical evaluation of hypersingular integrals. Numerical solutions for illustrative examples are compared with analytical ones. The numerical results are uniformly accurate.

1 Introduction

1.1 Previous work

The conventional Boundary Element Method (BEM) for linear elasticity requires the numerical evaluation of line integrals for two-dimensional (2-D) problems and surface integrals for three-dimensional (3-D) ones (see, for example, Hall, 1994; Mukherjee, 1982). By observing that the integrand vector of the usual linear elasticity BEM equation without body forces is divergence free, Nagarajan et al. (1994) have proposed a novel approach, called the BCM, that achieves a further reduction in dimension. The divergence free property allows, for 3-D problems, the use of Stokes' theorem to transform surface integrals on the usual boundary elements into line integrals on the bounding contours of these elements. For 2-D problems, a similar transformation, using the simple idea of path-independent integrals, eliminates numerical integration altogether. The above transformations are quite general and apply to boundary elements of arbitrary shapes. Thus, the BCM requires only numerical evaluation of line integrals for 3-D problems and simply the evaluation of functions (called potential functions) at points on the boundary of a body for 2-D

cases. The above idea also works for other linear problems such as potential theory.

The BCM has been presented in the literature for 2-D (see Nagarajan et al., 1994) and for 3-D (see Nagarajan et al., 1996) linear elasticity problems. In both these papers, however, only the "first" BCM problem, i.e. the determination of boundary tractions and displacements, has been addressed. Also, the idea of rigid body modes, to regularize Cauchy singular intergrals, was not employed in the above papers in an explicit manner.

1.2 Paper Outline

This paper presents a BCM formulation and numerical implementation for 2-D problems in linear elasticity. Quadratic boundary elements are used. The idea of rigid body modes is employed at the outset to regularize the Cauchy singular integrand. Also, the "second" BCM problem, namely the calculation of stresses both inside and on the body boundary, as well as the "first" BCM problem, are addressed in this paper.

Numerical results are presented for several illustrative examples including the Lamé and Kirsch problems. The numerical results are uniformly accurate. An interesting observation is that the BCM approach allows one to calculate boundary stresses, at regular points that are not at the ends of boundary elements, directly, without the need of any special algorithm for the numerical evaluation of hypersingular integrals.

1.3 2-D BCM basic formulations

The idea of dimensional reduction starts from the standard Boundary Integral Equation (BIE) without body forces (see Rizzo, 1967)

$$c_{ik}(P)u_i(P) = \int_{\partial B}[U_{ik}(P,Q)\sigma_{ij}(Q) - \Sigma_{ijk}(P,Q)u_i(Q)]\mathbf{e}_j \cdot d\mathbf{S} \qquad (1)$$

where c_{ik} is the corner tensor, P, Q, u_i and σ_{ij} are source point, field point, displacement vector and stress tensor respectively, U_{ik} and Σ_{ijk} are the Kelvin kernel tensors,

and $\mathbf{e}_j$ are global Cartesian unit vectors. In 2-D problems, ∂B is the boundary of a body B, and $d\mathbf{S}$ is an infinitesimal boundary length vector.

Here are the expressions for the Kelvin kernel tensors for plane strain problems

$$\left.\begin{aligned} U_{ik} &= \frac{-1}{8\pi(1-\nu)\mu}[(3-4\nu)\delta_{ik}\ln(r) - r_{,i}r_{,k}] \\ \Sigma_{ijk} &= \frac{-1}{4\pi(1-\nu)r}[2r_{,i}r_{,j}r_{,k} + (1-2\nu)(\delta_{ik}r_{,j} + \delta_{jk}r_{,i} - \delta_{ij}r_{,k})] \end{aligned}\right\} \tag{2}$$

where $\mu = G$ is the shear modulus, ν is the Poisson's ratio, δ_{ij} is the Kronecker delta ($\equiv 1$ for $i = j$ and $\equiv 0$ for $i \neq j$), and $r = \sqrt{(x_Q - x_P)^2 + (y_Q - y_P)^2}$.

Let $\mathbf{F}_k = [U_{ik}(P,Q)\sigma_{ij}(Q) - \Sigma_{ijk}(P,Q)u_i(Q)]\mathbf{e}_j$, so Eq. (1) has the form

$$c_{ik}(P)u_i(P) = \int_{\partial B} \mathbf{F}_k \cdot d\mathbf{S} \tag{3}$$

If we take the divergence of $\mathbf{F}_k$ at a field point Q, as shown in related work by Nagarajan et al. (1994), this vector is divergence free, i.e.

$$\nabla_Q \cdot \mathbf{F}_k = 0 \tag{4}$$

everywhere except at the source point P.

Equation (4) shows the existence of a function Φ_k such that

$$\mathbf{F}_k = \frac{\partial \Phi_k}{\partial y}\mathbf{e}_1 - \frac{\partial \Phi_k}{\partial x}\mathbf{e}_2 \tag{5}$$

The boundary is now discretized into n elements, thus

$$\int_{\partial B} \mathbf{F}_k \cdot d\mathbf{S} = \sum_{\ell=1}^{n} \int_{E_{\ell 1}}^{E_{\ell 2}} \mathbf{F}_k \cdot d\mathbf{S} \tag{6}$$

Equation (5) may now be substituted into Eq. (6) to obtain

$$\int_{E_{\ell 1}}^{E_{\ell 2}} \mathbf{F}_k \cdot d\mathbf{S} = \int_{E_{\ell 1}}^{E_{\ell 2}} \left(\frac{\partial \Phi_k}{\partial y}\mathbf{e}_1 - \frac{\partial \Phi_k}{\partial x}\mathbf{e}_2\right) \cdot \mathbf{n} dS \tag{7}$$

where $d\mathbf{S} = \mathbf{n}dS$ with $\mathbf{n}$ the unit outward normal vector to ∂B.

Since (see a similar proof on page 179 of Timoshenko et al., 1970)

$$\mathbf{n} = \frac{dy}{dS}\mathbf{e}_1 - \frac{dx}{dS}\mathbf{e}_2 \tag{8}$$

equation (7) becomes

$$\int_{E_{\ell 1}}^{E_{\ell 2}} \mathbf{F}_k \cdot d\mathbf{S} = \int_{E_{\ell 1}}^{E_{\ell 2}} (\frac{\partial \Phi_k}{\partial y}\frac{dy}{dS} + \frac{\partial \Phi_k}{\partial x}\frac{dx}{dS})dS = \int_{E_{\ell 1}}^{E_{\ell 2}} d\Phi_k = \Phi_k(E_{\ell 2}) - \Phi_k(E_{\ell 1}) \quad (9)$$

which means that there is no need for any numerical integration for 2-D linear elasticity.

Finally, the 2-D BCM discretized equation corresponding to Eq. (1) is written as follows

$$c_{ik}(P)u_i(P) = \sum_{\ell=1}^{n}[\Phi_k^{(\ell)}(E_{\ell 2}) - \Phi_k^{(\ell)}(E_{\ell 1})] \quad (10)$$

2 Formulations using the rigid body motion technique

2.1 General formulation

Consider an arbitrary rigid body translation where $u_i(Q) = u_i(P) =$ constant. Thus, $\sigma_{ij}(Q) = 0$. Use of this rigid body motion solution in Eq. (1) gives

$$c_{ik}(P)u_i(P) = -\int_{\partial B} \Sigma_{ijk}(P,Q)u_i(P)\mathbf{e}_j \cdot d\mathbf{S} \quad (11)$$

Subtracting Eq. (11) from Eq. (1) yields a new BEM equation

$$\int_{\partial B}\{U_{ik}(P,Q)\sigma_{ij}(Q) - \Sigma_{ijk}(P,Q)[u_i(Q) - u_i(P)]\}\mathbf{e}_j \cdot d\mathbf{S} = 0 \quad (12)$$

Thus, the corner tensor c_{ik} is now eliminated from the BEM equation. Its evaluation is avoided and this is the first advantage of using the rigid body motion technique.

As mentioned above, $\mathbf{F}_k = [U_{ik}(P,Q)\sigma_{ij}(Q) - \Sigma_{ijk}(P,Q)u_i(Q)]\mathbf{e}_j$ is divergence free. The extra term $\Sigma_{ijk}(P,Q)u_i(P)\mathbf{e}_j$ is also divergence free (except at the source point P) since the divergence is taken with respect to the field point Q. Thus, for this purpose, $u_i(P)$ can be treated as a constant.

Therefore, the new integrand vector of Eq. (12)

$$\mathbf{G}_k = \{U_{ik}(P,Q)\sigma_{ij}(Q) - \Sigma_{ijk}(P,Q)[u_i(Q) - u_i(P)]\}\mathbf{e}_j \quad (13)$$

also has the property

$$\nabla_Q \cdot \mathbf{G}_k = 0 \tag{14}$$

everywhere except at the source point P.

2.2 2-D BCM formulation

The 2-D BCM discretized equation corresponding to Eq. (12) is obtained in a manner analogous to the process that led to Eq. (9) from Eq. (6). The result is

$$\sum_{\ell=1}^{n} [\Psi_k^{(\ell)}(E_{\ell 2}) - \Psi_k^{(\ell)}(E_{\ell 1})] = 0 \tag{15}$$

3 2-D boundary contour analysis with quadratic boundary elements

3.1 Shape functions

$\mathbf{G}_k$ contains the unknown fields u_i and σ_{ij}. In order for the property (14) to be valid in general, the displacement shape functions u_i must satisfy, a priori, the Navier-Cauchy equations, i.e. the equilibrium equations in terms of displacements

$$\nabla^2 \mathbf{u} + \frac{1}{1-2\nu} \nabla(\nabla \cdot \mathbf{u}) = \mathbf{0} \tag{16}$$

and the stress shape functions σ_{ij} must be derived from those of u_i using Hooke's law,

$$\sigma_{ij} = \lambda \delta_{ij} u_{k,k} + \mu(u_{i,j} + u_{j,i}) \tag{17}$$

where λ and μ are Lamé constants of the material.

The determination of quadratic shape functions that satisfy Eq. (16) was addressed in Nagarajan's Ph.D. dissertation (1994). There are a total of 12 linearly independent quadratic (vector) shape functions. The equilibrium constraint eliminates two of them, leaving 10. The displacement components are written as arbitrary

linear combinations of these 10 functions as follows,

$$\left\{ \begin{array}{c} u_1 \\ u_2 \end{array} \right\} = \beta_1 \left\{ \begin{array}{c} 1 \\ 0 \end{array} \right\} + \beta_2 \left\{ \begin{array}{c} x \\ 0 \end{array} \right\} + \beta_3 \left\{ \begin{array}{c} y \\ 0 \end{array} \right\} + \beta_4 \left\{ \begin{array}{c} 0 \\ 1 \end{array} \right\} + \beta_5 \left\{ \begin{array}{c} 0 \\ x \end{array} \right\} + \beta_6 \left\{ \begin{array}{c} 0 \\ y \end{array} \right\}$$
$$+ \beta_7 \left\{ \begin{array}{c} x^2 \\ k_2 xy \end{array} \right\} + \beta_8 \left\{ \begin{array}{c} y^2 \\ k_1 xy \end{array} \right\} + \beta_9 \left\{ \begin{array}{c} k_1 xy \\ x^2 \end{array} \right\} + \beta_{10} \left\{ \begin{array}{c} k_2 xy \\ y^2 \end{array} \right\} \quad (18)$$

where $k_1 = -2(1-2\nu)$ and $k_2 = -4(1-\nu)$.

In matrix form,

$$\left\{ \begin{array}{c} u_1 \\ u_2 \end{array} \right\} = [T_u(x,y)]\{\beta\} \quad (19)$$

where

$$\{\beta\} = \langle \beta_1 \ \beta_2 \ \ldots \ \beta_{10} \rangle^T \quad (20)$$

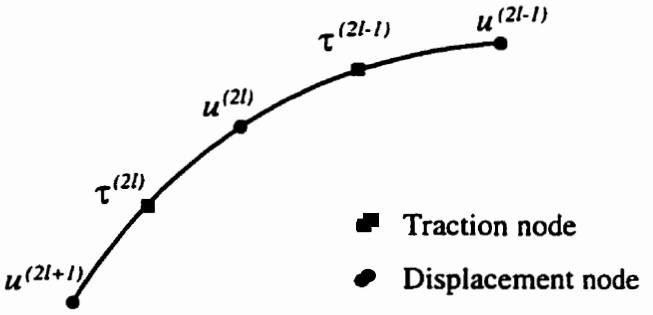

Figure 1: Quadratic boundary element.

These 10 artificial variables require quadratic elements with 10 physical variables. The configuration of a chosen quadratic boundary element is shown in Fig. 1. Each element is divided into 4 equal segments by 2 traction and 3 displacement nodes. Thus, it has 10 physical variables and the way they are numbered globally on the element (ℓ) is also shown in the figure. It should be noted that the BCM equations are enforced at the displacement nodes only.

The tractions on the boundary are given by the following relation

$$\tau_i = \sigma_{ij} n_j = [\lambda \delta_{ij} u_{k,k} + \mu(u_{i,j} + u_{j,i})] n_j \quad (21)$$

By using the Eqs. (18) and (21), the physical variables $\{p\}$ on the element (ℓ) can be described as

$$\begin{aligned}\{p^{(\ell)}\} &= \left\langle u_1^{(2\ell-1)}\ u_2^{(2\ell-1)}\ \tau_1^{(2\ell-1)}\ \tau_2^{(2\ell-1)}\ u_1^{(2\ell)}\ u_2^{(2\ell)}\ \tau_1^{(2\ell)}\ \tau_2^{(2\ell)}\ u_1^{(2\ell+1)}\ u_2^{(2\ell+1)}\right\rangle^T \\ &= [T^{(\ell)}(x,y)]\{\beta^{(\ell)}\} \end{aligned} \tag{22}$$

Therefore,

$$\{\beta^{(\ell)}\} = [T^{(\ell)}(x,y)]^{-1}\{p^{(\ell)}\} \tag{23}$$

An important issue here is the invertibility of $[T^{(\ell)}(x,y)]$. As mentioned by Nagarajan (1994), the chosen quadratic element whose configuration is shown in Fig. 1 ensures this invertibility.

A new coordinate system (ξ,η) centered at each source point is introduced at this stage. This is done in order to make the shape function variables conform to those of the kernels U_{ik} and Σ_{ijk} (which are functions of ξ and η only). The ξ and η axes are parallel to the global x and y axes, thus

$$\begin{aligned}\xi &= x(Q) - x(P) \\ \eta &= y(Q) - y(P)\end{aligned} \tag{24}$$

So, if this new coordinate system is centered at the source point j, by substituting (24) into Eq. (19) the displacement shape functions can be rewritten as

$$\left\{ \begin{array}{c} u_1 \\ u_2 \end{array} \right\} = [T_u(\xi,\eta)]\{\hat{\beta}\} \tag{25}$$

where,

$$\{\hat{\beta}\} = \left\langle \hat{\beta}_1\ \hat{\beta}_2\ \ldots\ \hat{\beta}_{10}\right\rangle^T = [B_j]\{\beta\} \tag{26}$$

in which $[B_j]$ is a transformation matrix that depends only on the coordinates of the source point j.

If (h) is the element containing the source point at its first or middle displacement node, with this new coordinate system $u_1(P) = \hat{\beta}_1^{(h)}$ and $u_2(P) = \hat{\beta}_4^{(h)}$. So, for the element (ℓ), we have

$$\left\{ \begin{array}{c} u_1(Q) - u_1(P) \\ u_2(Q) - u_2(P) \end{array} \right\} = [T_u(\xi,\eta)]\{\tilde{\beta}^{(\ell)}\} \tag{27}$$

where the columns of $[T_u(\xi,\eta)]$ are the ten shape functions

$$\left\{\begin{array}{c}1\\0\end{array}\right\},\left\{\begin{array}{c}\xi\\0\end{array}\right\},\left\{\begin{array}{c}\eta\\0\end{array}\right\},\left\{\begin{array}{c}0\\1\end{array}\right\},\left\{\begin{array}{c}0\\\xi\end{array}\right\},\left\{\begin{array}{c}0\\\eta\end{array}\right\},$$
$$\left\{\begin{array}{c}\xi^2\\k_2\xi\eta\end{array}\right\},\left\{\begin{array}{c}\eta^2\\k_1\xi\eta\end{array}\right\},\left\{\begin{array}{c}k_1\xi\eta\\\xi^2\end{array}\right\},\left\{\begin{array}{c}k_2\xi\eta\\\eta^2\end{array}\right\} \tag{28}$$

and

$$\{\tilde{\beta}^{(\ell)}\} = \left\langle [\hat{\beta}_1^{(\ell)} - \hat{\beta}_1^{(h)}]\ \hat{\beta}_2^{(\ell)}\ \hat{\beta}_3^{(\ell)}\ [\hat{\beta}_4^{(\ell)} - \hat{\beta}_4^{(h)}]\ \hat{\beta}_5^{(\ell)}\ \hat{\beta}_6^{(\ell)}\ \hat{\beta}_7^{(\ell)}\ \hat{\beta}_8^{(\ell)}\ \hat{\beta}_9^{(\ell)}\ \hat{\beta}_{10}^{(\ell)}\right\rangle^T \tag{29}$$

Expression (27) for $[u_i(Q) - u_i(P)]$ is used in Eq. (13).

3.2 Potential functions

By substituting the 10 displacement shape functions from (28) and their corresponding stress shape functions (using Eq. (17)) into Eq. (13), we obtain 20 sub-vectors $\mathbf{g}_{ki}$ (10 corresponding to $k = 1$ and 10 corresponding to $k = 2$). For example, $\mathbf{g}_{1,1}$ is obtained from $\mathbf{G}_1$ with $\mathbf{u}(Q) - \mathbf{u}(P) = \left\{\begin{array}{c}1\\0\end{array}\right\}$ and $\sigma_{ij} = 0$. Equation (5) in this case takes the form

$$\mathbf{g}_{ki} = \frac{\partial \phi_{i+10(k-1)}(\xi,\eta)}{\partial \eta}\mathbf{e}_1 - \frac{\partial \phi_{i+10(k-1)}(\xi,\eta)}{\partial \xi}\mathbf{e}_2 \tag{30}$$

where $k = 1, 2$ and $i = 1, 2, \ldots, 10$.

Equation (30) is solved to give 10 potential functions $(\phi_1, \ldots, \phi_{10})$ corresponding to $k = 1$ and 10 more $(\phi_{11}, \ldots, \phi_{20})$ corresponding to $k = 2$.

These potential functions are listed in the Appendix. They are numbered according to the order of shape functions in Eq. (28) with, as mentioned above, the first ten for $k = 1$ and the next ten for $k = 2$. Thus, for example, ϕ_1 corresponds to $\left\{\begin{array}{c}1\\0\end{array}\right\}$ with $k = 1$ and ϕ_{14} corresponds to $\left\{\begin{array}{c}0\\1\end{array}\right\}$ with $k = 2$.

3.3 Discretized equations

Now, with the potential functions already derived, the BCM discretized equations are developed as follows.

For the source point j (source points are only placed at the ends and mid-point, i.e. displacement nodes, of each boundary element, see Fig. 1)

$$\sum_{\ell=1}^{n}[\Psi_k^{(\ell)}(E_{\ell 2}) - \Psi_k^{(\ell)}(E_{\ell 1})] = \sum_{\ell=1}^{n}\sum_{i=1}^{10} \phi_{ki}^{j\ell}\ \tilde{\beta}_i^{(\ell)} = 0 \tag{31}$$

where,

$$\left.\begin{aligned} \phi_{1i}^{j\ell} &= \phi_i(\xi_{\ell 2}, \eta_{\ell 2}) - \phi_i(\xi_{\ell 1}, \eta_{\ell 1}) \\ \phi_{2i}^{j\ell} &= \phi_{i+10}(\xi_{\ell 2}, \eta_{\ell 2}) - \phi_{i+10}(\xi_{\ell 1}, \eta_{\ell 1}) \end{aligned}\right\} \tag{32}$$

It should be noted that the potential functions $\phi_1(\xi,\eta)$, $\phi_4(\xi,\eta)$, $\phi_{11}(\xi,\eta)$, and $\phi_{14}(\xi,\eta)$ corresponding to constant shape functions are singular when a field point $Q \rightarrow$ the source point P, i.e. when $(\xi,\eta) \rightarrow (0,0)$. But in this case $u_k(Q) - u_k(P) = O(r)$, and Eqs. (27) lead to

$$\left.\begin{aligned} \tilde{\beta}_1^{(\ell)} &= [\hat{\beta}_1^{(\ell)} - \hat{\beta}_1^{(h)}] = 0 \\ \tilde{\beta}_4^{(\ell)} &= [\hat{\beta}_4^{(\ell)} - \hat{\beta}_4^{(h)}] = 0 \end{aligned}\right\} \tag{33}$$

so the evaluation of these potential functions can be avoided, i.e. expression (31) is now completely regular. This is the second advantage of the approach using the rigid body motion technique.

A further development of expression (31) leads to

$$\begin{aligned} \left\{ \begin{array}{c} \sum_{\ell=1}^{n}\sum_{i=1}^{10} \phi_{1i}^{j\ell}\ \tilde{\beta}_i^{(\ell)} \\ \sum_{\ell=1}^{n}\sum_{i=1}^{10} \phi_{2i}^{j\ell}\ \tilde{\beta}_i^{(\ell)} \end{array} \right\} &= \sum_{\ell=1}^{n}[\Psi^{(j\ell)}]\{\hat{\beta}^{(\ell)}\} = \sum_{\ell=1}^{n}[\Psi^{(j\ell)}][B_j]\{\beta^{(\ell)}\} \\ &= \sum_{\ell=1}^{n}[\Psi^{(j\ell)}][B_j][T^{(\ell)}]^{-1}\{p^{(\ell)}\} \\ &= \sum_{\ell=1}^{n}[M^{(j\ell)}]\{p^{(\ell)}\} = \{0\} \end{aligned} \tag{34}$$

The last system of equations (34) is now condensed to reflect the continuity of displacements across elements. This results in the following relation

$$[M^{(j)}]\{p\} = \{0\} \tag{35}$$

where $\{p\}$ are degrees of freedom (DOF) on the whole boundary ∂B.

With $2n$ source points corresponding to $2n$ displacement nodes on the boundary ∂B, one gets $2n$ relations of the form (35) which are now combined into the final BCM linear system of equations

$$[M]\{p\} = \{0\} \tag{36}$$

Finally, the system of equations (36) needs to be reordered in accordance with the boundary conditions to form

$$[A]\{X\} = [B]\{Y\} \tag{37}$$

where $\{X\}$ and $\{Y\}$ contain, respectively, the unknown and known (from the boundary conditions) quantities. Let $[B]\{Y\} = \{Z\}$, so $\{Z\}$ is a known vector and (37) can be rewritten as

$$[A]\{X\} = \{Z\} \tag{38}$$

The global system (38) is generally overdetermined ($[A]$ is a rectangular matrix) but always consistent as discussed in earlier papers (see, for example, Nagarajan et al., 1994).

After the solution of the global equation system (38) is obtained, one can easily derive the artificial variables $\{\beta^{(\ell)}\}$ from Eq. (23). At this stage, the remaining physical variables (displacements, tractions, stresses) at any point on the boundary can be easily calculated from (18) and the corresponding relations for stresses and tractions in terms of their shape functions.

4 Stresses

4.1 Internal stresses

The internal stresses are also evaluated using Eq. (17). To this end, the first step is to determine the displacement gradient tensor $u_{i,j}$ inside the body B.

4.1.1 Displacement gradient tensor

There are two approaches to evaluate $u_{i,j}$. The first one starts from the standard BIE (1) written for the displacement at an internal point p. This expression is first differentiated with respect to a source point. The new integrand is still divergence free and allows one to derive appropriate potential functions. In other words, here one first differentiates the BEM equations and then converts the resulting surface integrals to line integrals for 3-D problems, or line integrals to function evaluations for 2-D problems. This idea has been mentioned in earlier work (see Nagarajan et al., 1994 and 1996) but no numerical examples are given in these papers.

The second approach follows the opposite process, i.e. we first convert the BIE to the corresponding BCM version and then differentiate it. This technique has been proposed by Mukherjee (1995) for 3-D problems and is also used in this work, because of its simplicity in 2-D problems as we will see later. Since the BCM version is available at this stage, the starting point is the BCM Eq. (10) at an internal point. For 2-D problems this equation can be written as (see Eqs. (10), (15) and (34))

$$\{u_k(p)\} = \sum_{\ell=1}^{n} [\Phi^{(p\ell)}][B_p]\{\beta^{(\ell)}\} \tag{39}$$

where $[B_p]$ is the transformation matrix corresponding to the internal source point p where stresses are computed.

Now the displacement gradient tensor is (M is a source point index for the coordinate system (x, y), i.e. $_{,1} \equiv \partial/\partial x(p)$ and $_{,2} \equiv \partial/\partial y(p)$)

$$\{u_{k,M}(p)\} = \sum_{\ell=1}^{n} ([\Phi^{(p\ell)}][B_p]_{,M} + [\Phi^{(p\ell)}]_{,M}[B_p])\{\beta^{(\ell)}\} \tag{40}$$

Using expresion (24) we derive the relationship $[\Phi^{(p\ell)}]_{,M} = -[\Phi^{(p\ell)}]_{,\mu}$ (where μ is a field point index for the coordinate system (ξ, η)). In other words, $\dfrac{\partial}{\partial x(p)}[\Phi^{(p\ell)}] = -\dfrac{\partial}{\partial \xi}[\Phi^{(p\ell)}]$, and similarly for y and η. Finally,

$$\{u_{k,M}(p)\} = \sum_{\ell=1}^{n}([\Phi^{(p\ell)}][B_p]_{,M} - [\Phi^{(p\ell)}]_{,\mu}[B_p])\{\beta^{(\ell)}\} \tag{41}$$

4.1.2 Gradients of potential functions

At this stage, we know $\{\beta^{(\ell)}\}$ from the solution of Eqs. (38) and (23). Thus, in order to calculate displacement gradient tensor (41), one needs the evaluation of $[B_p]_{,M}$ and $[\Phi^{(p\ell)}]_{,\mu}$. There is no problem with $[B_p]_{,M}$. The evaluation of $[\Phi^{(p\ell)}]_{,\mu}$ is also straightforward because it contains the gradients of potential functions $\dfrac{\partial \phi_i}{\partial \xi}$; $\dfrac{\partial \phi_i}{\partial \eta}$ which do not need to be calculated from the known potential functions because it can be seen from (30) that

$$\left.\begin{aligned} \frac{\partial \phi_{i+10(k-1)}}{\partial \xi} &= -g_{ki2} \\ \frac{\partial \phi_{i+10(k-1)}}{\partial \eta} &= g_{ki1} \end{aligned}\right\} \tag{42}$$

where g_{ki1} and g_{ki2} are the first and second components of $\mathbf{g}_{ki}$, respectively.

Hence, this method for evaluating the stresses inside a body is simple and easy for numerical implementation.

4.2 Stresses at regular points on the boundary

One simple way to compute boundary stresses is to use the quantities $\{\beta^{(\ell)}\}$ on each boundary element (ℓ), together with the appropriate stress shape functions. However, another approach is to take the limit of Eq. (41) as an internal point $p \rightarrow$ a boundary point P. This approach is developed below for the case where P is a regular point on ∂B (i.e. ∂B is locally smooth at P) and does not lie at an end of a boundary element.

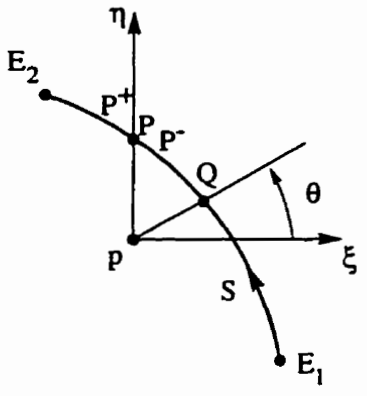

Figure 2: Internal source point approaching the boundary.

It can be shown that the potential functions that must be treated carefully during this limit process are ϕ_1 and ϕ_{14} (see the Appendix). These functions are related to the first vector shape function with $k = 1$ and the fourth with $k = 2$, according to the ordering in Eqs. (28).

Fig. 2 shows an internal source point p approaching a boundary point P on E_1E_2. P is a regular point on ∂B and does not coincide with either of the end points E_1 or E_2 of the boundary element. The potential functions ϕ_1 and ϕ_{14} are associated with the integral (see Eq. (2))

$$\int_{E_1}^{E_2} \frac{r_{,j}\, n_j}{r} dS = \int_{E_1}^{E_2} \frac{d\theta}{dS} dS = \int_{E_1}^{E_2} d\theta \tag{43}$$

As $p \to P$, the angle θ suffers a jump discontinuity from 0 to π as Q crosses P, i.e.

$$\int_{P-}^{P+} d\theta = [\theta]_{P-}^{P+} = \pi \tag{44}$$

so that (see the formula for ϕ_1 in the Appendix and note that $\tan\theta = \eta/\xi$)

$$[\phi_1]_{P-}^{P+} = \frac{2(1-\nu)}{4\pi(1-\nu)} [\theta]_{P-}^{P+} = 0.5 \tag{45}$$

Similarly,

$$[\phi_{14}]_{P-}^{P+} = 0.5 \tag{46}$$

Thus, for the singular case $P \in \partial B$,

$$\int_{E_1}^{E_2} \mathbf{f}_{1,1} \cdot d\mathbf{S} = [\phi_1(E_2) - \phi_1(P^+)] + [\phi_1(P^-) - \phi_1(E_1)] + 0.5 \tag{47}$$

$$\int_{E_1}^{E_2} \mathbf{f}_{2,4} \cdot d\mathbf{S} = [\phi_{14}(E_2) - \phi_{14}(P^+)] + [\phi_{14}(P^-) - \phi_{14}(E_1)] + 0.5 \qquad (48)$$

The effect of Eqs. (47) and (48) on (41) as $p \to P$ can be assessed by observing Eqs. (26) and (27) and noting that $u_1(P) = \hat{\beta}_1^{(h)}$; $u_2(P) = \hat{\beta}_4^{(h)}$. (Note that $\hat{\beta}_1$ is associated with ϕ_1 and $\hat{\beta}_4$ is associated with ϕ_{14} and that these are the only potential functions with jump discontinuities.) These jump terms change the constant multiplying $u_{k,M}$ on the left hand side of Eq. (41) from 1 to 0.5. The displacement gradient equation now becomes

$$0.5\{u_{k,M}(P)\} = \sum_{\ell=1}^{n} ([\Phi^{(P\ell)}][B_P]_{,M} - [\Phi^{(P\ell)}]_{,\mu}[B_P])\{\beta^{(\ell)}\} \qquad (49)$$

where one must now use expressions for the integrals in Eqs. (47) and (48) *without* the constant 0.5 terms, i.e. their Cauchy Principal Values (CPV)

$$\int_{E_1}^{E_2} \mathbf{f}_{1,1} \cdot d\mathbf{S} = \phi_1(E_2) - \phi_1(E_1) - 0.5 \qquad (50)$$

$$\int_{E_1}^{E_2} \mathbf{f}_{2,4} \cdot d\mathbf{S} = \phi_{14}(E_2) - \phi_{14}(E_1) - 0.5 \qquad (51)$$

Note that Eqs. (47) and (48) have been used to get the above expressions.

The fact that Eq. (49) holds for a regular boundary point P (provided that P does not lie on one of the end nodes), is quite remarkable. In the conventional BEM, the equations corresponding to (39) and (49) are strongly singular and hypersingular, respectively, and need to be regularized before the appropriate surface integrals can be evaluated. The above formulae are used to calculate stresses at regular boundary points in all of the following numerical examples.

5 Numerical examples

Four examples are illustrated in this section. All of them use the same material data as follows : Young's modulus $E = 2.5$ (in consistent units) and Poisson's ratio $\nu = 0.3$. In all these examples, boundary stresses are calculated from Eqs. (49) and (17).

5.1 Displacement field problems

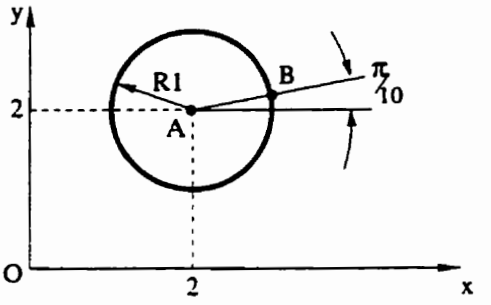

Figure 3: Circular body with imposed displacement fields.

Consider a circular body of unit radius centered at the point $(2,2)$ in the global (x,y) coordinate system as shown in Fig. 3. Two displacement fields which are the exact solutions of the elasticity Navier-Cauchy equations (16) have been imposed at the displacement nodes on the boundary.

5.1.1 Planar field

$$\left.\begin{aligned} u_1 &= \frac{x}{x^2+y^2} \\ u_2 &= \frac{y}{x^2+y^2} \end{aligned}\right\} \tag{52}$$

This is the field used in the linear 2-D BCM paper (see Nagarajan et al., 1994). The same problem is chosen here in order to compare the performance of quadratic elements against the linear ones.

5.1.2 Cubic field

$$\left.\begin{aligned} u_1 &= y^3 - 3yx^2 \\ u_2 &= -x^3 + 3xy^2 \end{aligned}\right\} \tag{53}$$

The idea here is to test the accuracy of 2-D BCM code with quadratic displacement shape functions for a problem with a cubic global displacement field.

The circular boundary is discretized by 10 quadratic elements spaced at equal increments. Tractions on traction nodes have been derived by solving the "first"

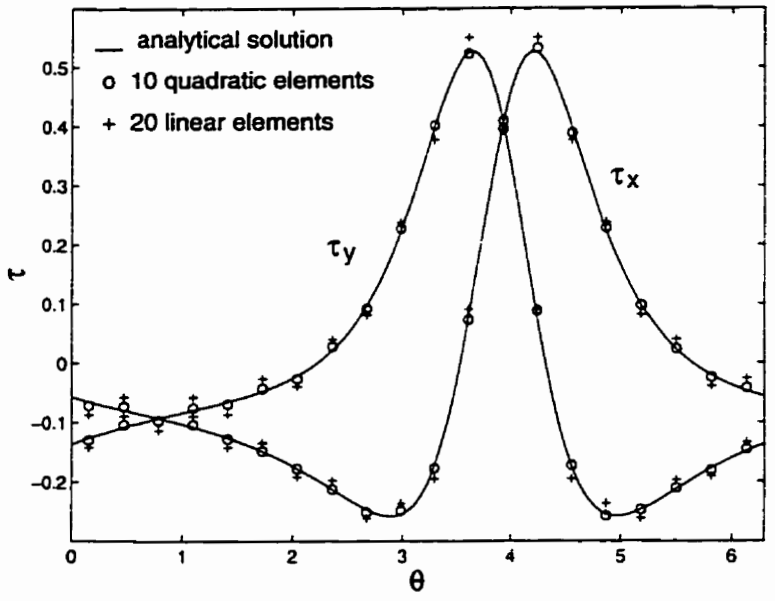

Figure 4: Traction components τ_x and τ_y for the planar displacement field.

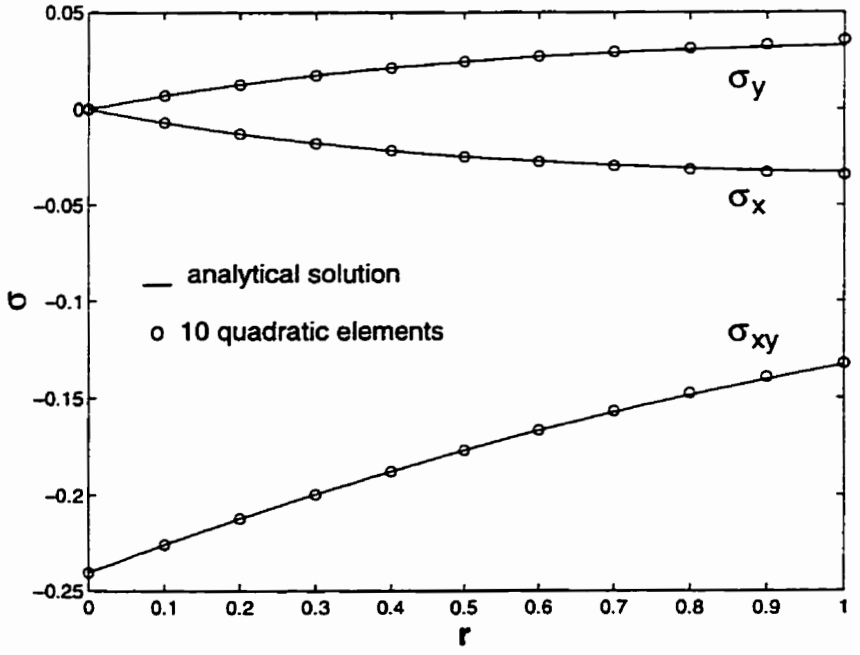

Figure 5: Stress components along the line AB (see Fig. 3) for the planar displacement field.

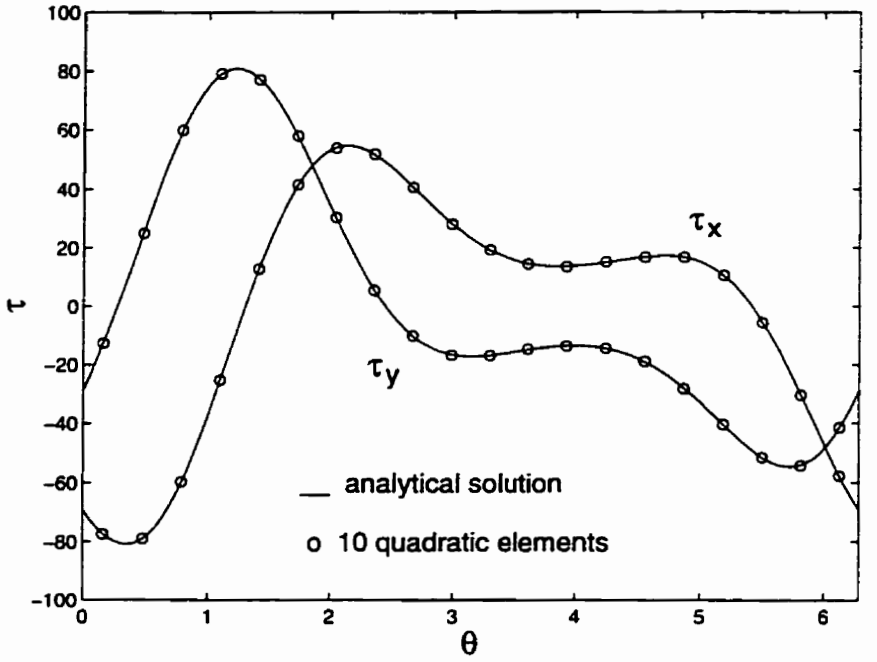

Figure 6: Traction components τ_x and τ_y for the cubic displacement field.

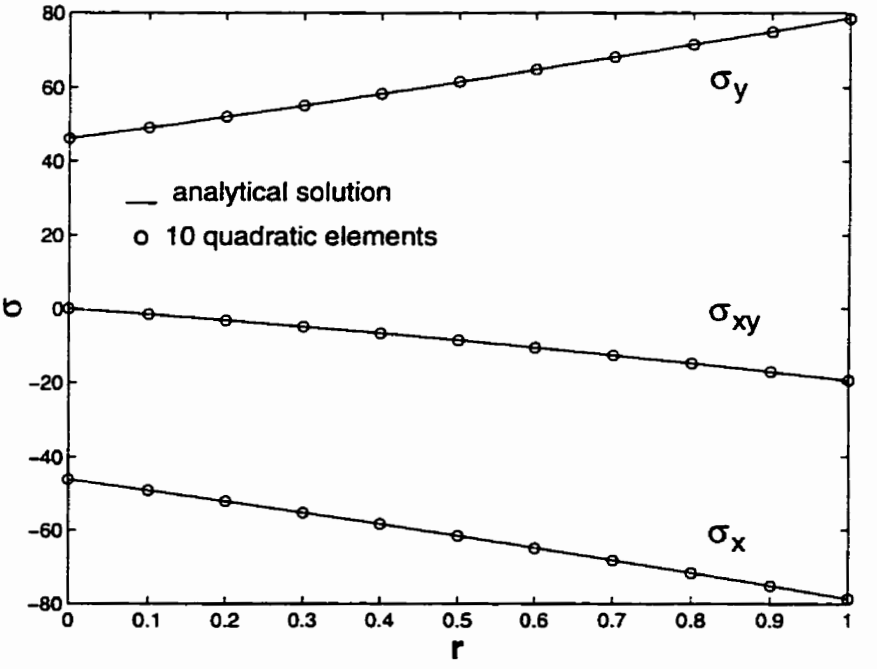

Figure 7: Stress components along the line AB (see Fig. 3) for the cubic displacement field.

BCM problem. Stresses on the segment AB, where B is a regular boundary point, have been calculated next. These numerical results show very good agreement with the exact analytical solution as illustrated in Figs. 4, 5, 6 and 7.

Also, it can be seen on Fig. 4 that with the same boundary discretization, i.e. 10 quadratic elements versus 20 linear elements, quadratic elements show better results as expected.

5.2 Lamé's problem

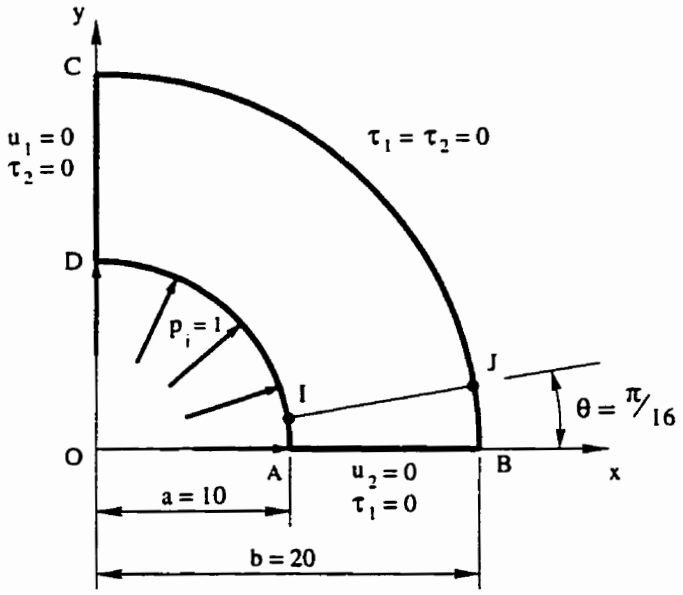

Figure 8: Modeling of Lamé's problem.

The third example involves the well-known Lamé's problem in which a hollow cylinder is subjected to uniform pressure on the inner surface. Let a and b denote the inner and outer radii of the cylinder, and p_i the uniform internal pressure. The stress components σ_r in the radial direction and σ_θ in the circumferential direction at a point (r, θ) are given by Timoshenko and Goodier (1970)

$$\left.\begin{aligned} \sigma_r &= \frac{a^2 p_i}{b^2 - a^2}\left(1 - \frac{b^2}{r^2}\right) \\ \sigma_\theta &= \frac{a^2 p_i}{b^2 - a^2}\left(1 + \frac{b^2}{r^2}\right) \end{aligned}\right\} \tag{54}$$

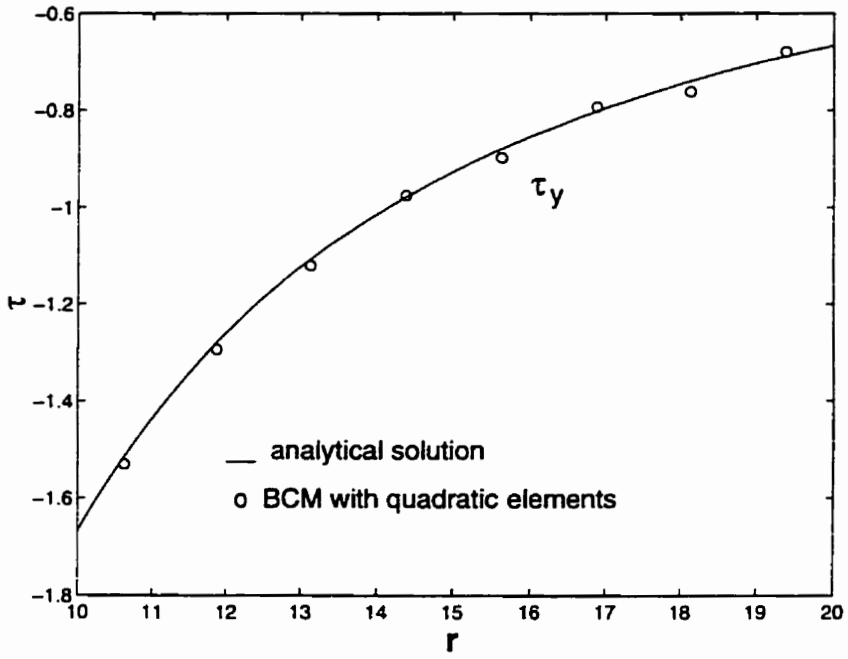

Figure 9: The traction component τ_y on the edge AB (see Fig. 8) for Lamé's problem.

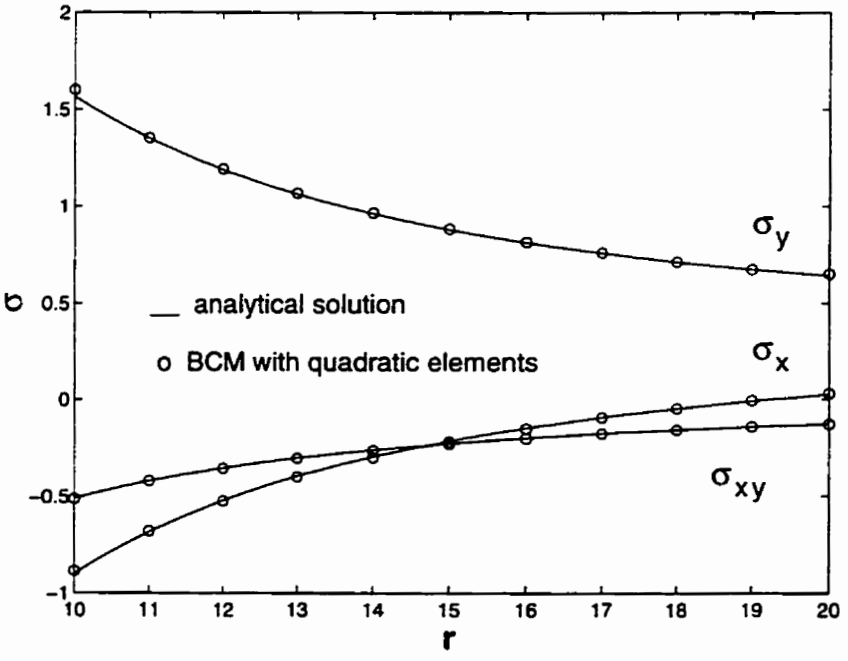

Figure 10: Stress components along the line IJ (see Fig. 8) for Lamé's problem.

The xy stress components can be expressed in terms of σ_r and σ_θ by the following relations (see Timoshenko and Goodier, 1970)

$$\left.\begin{aligned} \sigma_x &= \sigma_r \cos^2\theta + \sigma_\theta \sin^2\theta \\ \sigma_y &= \sigma_r \sin^2\theta + \sigma_\theta \cos^2\theta \\ \sigma_{xy} &= (\sigma_r - \sigma_\theta)\sin\theta\cos\theta \end{aligned}\right\} \tag{55}$$

Due to the symmetry of the problem, only a quarter of the structure is modeled as shown in Fig. 8. A total of 16 quadratic elements are used for the numerical results (4 elements are spaced at equal increments on each edge AB, BC, CD and DA). The traction τ_y on the edge AB is shown in Fig. 9 and the stresses calculated along the line segment IJ, where I and J are regular boundary points, are shown in Fig. 10. Observe that agreement between the analytical solutions and the corresponding BCM results are excellent, especially those in Fig. 10.

5.3 Kirsch's problem

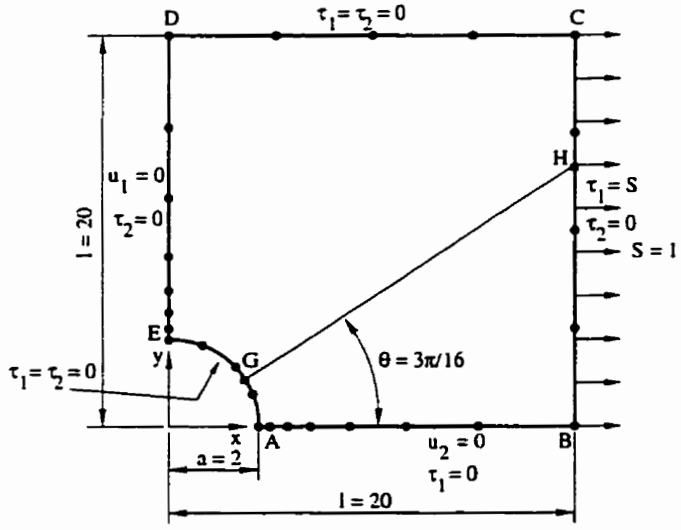

Figure 11: Modeling of Kirsch's problem.

The last example deals with Kirsch's problem. Fig. 11 displays a quarter symmetry model of a square plate with a central circular hole subjected to a unit uniaxial tensile load. The boundary contour analysis model was made up of 26 quadratic

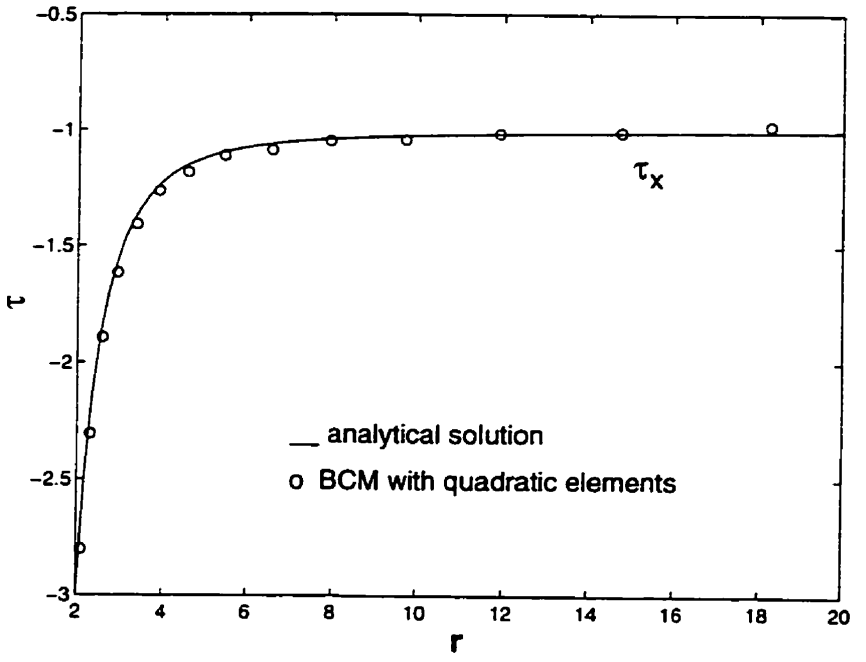

Figure 12: The traction component τ_x on the edge DE (see Fig. 11) for Kirsch's problem.

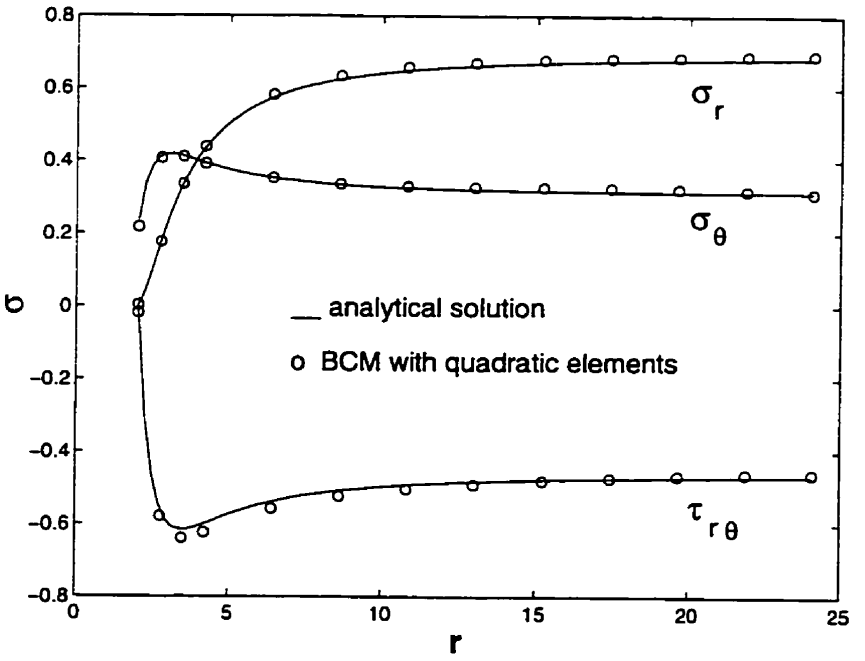

Figure 13: Stress components along the line GH (see Fig. 11) for Kirsch's problem.

elements. Due to stress concentration at the corners A and E, the mesh in this zone needs to be densified : the density of elements on AB and DE is nonuniform, with short elements being placed near the point A and E.

In polar coordinates, the stress component σ_r in the radial direction, the stress component σ_θ in the circumferential direction and the shearing stress component $\tau_{r\theta}$, at a point (r, θ) in an infinite plate with a circular hole are given by Timoshenko and Goodier (1970)

$$\left.\begin{aligned} \sigma_r &= \frac{S}{2}(1 - \frac{a^2}{r^2}) + \frac{S}{2}(1 + \frac{3a^4}{r^4} - \frac{4a^2}{r^2})\cos 2\theta \\ \sigma_\theta &= \frac{S}{2}(1 + \frac{a^2}{r^2}) - \frac{S}{2}(1 + \frac{3a^4}{r^4})\cos 2\theta \\ \tau_{r\theta} &= -\frac{S}{2}(1 - \frac{3a^4}{r^4} + \frac{2a^2}{r^2})\sin 2\theta \end{aligned}\right\} \tag{56}$$

For the cross section of the plate along the y axis ($\theta = \pi/2$), tractions in the x-direction along the edge DE can be found from Eqs. (56)

$$\tau_x = -\sigma_\theta = -\frac{S}{2}(2 + \frac{a^2}{r^2} + \frac{3a^4}{r^4}) \tag{57}$$

As seen in Fig. 12, results from the "first" BCM problem are in good agreement with the analytical solution. For the "second" BCM problem, polar coordinates are used to compute stresses on the line GH (see Fig. 11), and again, Fig. 13 reveals that the accuracy of internal and boundary stresses at regular points (G and H), calculated by the BCM, is excellent.

6 Conclusions

A further development for the BCM for 2-D linear elasticity is presented in this paper. An implementation is carried out with quadratic boundary elements and the idea of rigid body modes is used in explicit fashion. This approach does not require any numerical integration at all for 2-D problems, even with curved boundary elements. Also, corner modeling is trivial since only (continuous) displacement degrees of freedom are used at corners.

A remarkable feature of the BCM approach is that stresses at regular boundary points, inside boundary elements, are directly obtained from Eqs. (49) and (17), without the need for regularization of hypersingular integrals as must be done for the conventional BEM (see, for example, Guiggiani et al., 1992; Toh and Mukherjee, 1994 or Chien et al., 1991). In other words, Eq. (49) is already regularized by the use of Stokes' theorem!

Numerical results for illustrative problems are shown to be uniformly accurate. In particular, stress components at internal and boundary points, for the "second" BCM problem, match almost perfectly (within plotting accuracy) with the analytical solutions.

While the central issue in the present paper is not regularization of hypersingular boundary integral equations (HBIEs), it is useful to briefly discuss an ongoing controversy regarding numerical implementation of HBIEs. To be specific, consider a regular point P (where the boundary is locally smooth) on the bounding surface of a (2-D or 3-D) body, that lies on an interelement boundary. Also, let the displacement gradient field $\nabla \mathbf{u}$ (and therefore the stress) be continuous at P. Of course, in this case it is obvious that the boundary data (tangential derivatives of the displacement as well as the traction) are also continuous at P. (Please note that if the traction vector is prescribed at P and is discontinuous, so will, in general, be the displacement gradient and stress there). Other issues such as points on edges or corners are of obvious technological importance, but these are not discussed here in the interest of brevity.

There is general agreement that an HBIE has a unique limiting value at P. At issue are the smoothness requirements of *shape functions* of the boundary displacement for collocating an HBIE at a point such as P. Martin and Rizzo (1996), in a recent paper, claim that while the previously proved *sufficiency* requirement of $C^{1,\alpha}$ shape functions can be somewhat relaxed, $C^{0,\alpha}$ shape functions are certainly not permissible. Cruse and Richardson (1996), on the other hand, claim that $C^{0,\alpha}$ shape functions for $\mathbf{u}$ are *sufficient* in this case, provided that one specifically develops a scheme that allows the numerical solution for the stress to be multi-valued

at P. Further, these authors claim that logarithmically singular terms (see for example, Martin and Rizzo, 1996), at a point such as P, arise as a consequence of not incorporating the continuity constraint on the $\nabla \mathbf{u}$ field at P prior to developing the BEM representation.

Acknowledgements Anh-Vũ Phan acknowledges the financial support from the Quebec Ministry of Education through the "Programme québécois de bourses d'excellence". Part of the present work was carried out while this author was visiting Cornell University.

References

Chien, C.C.; Rajiyah, H.; Atluri, S.N. (1991): On the evaluation of hypersingular integrals integrals arising in the boundary element method for linear elasticity. Comp. Mech. 8: 57-70

Cruse, T.A.; Richardson, J.D. (1996): Non-singular Somigliana stress identities in elasticity. Int. J. Num. Meth. Eng. 39: 3273-3304

Guiggiani, M.; Krishnasamy, G.; Rudolphi, T.J.; Rizzo, F.J. (1992): A general algorithm for the numerical solution of the hypersingular boundary integral equations. J. Appl. Mech. 59: 604-614

Hall, W.S. (1994): The Boundary Element Method. Kluwer Academic Publishers, Dordrecht, The Netherlands

Kaplan, W. (1984): Advanced Calculus. Addison-Wesley

Martin, P.A.; Rizzo, F.J. (1996): Hypersingular integrals: how smooth must the density be? Int. J. Num. Meth. Eng. 39: 687-704

Mukherjee, S. (1982): Boundary Element Methods in Creep and Fracture. Elsevier Applied Science, London, UK

Mukherjee, Y.X. (1995): Optimal shape design by the boundary contour method. National Science Foundation Phase I Final Report, Dehan Engineering Numerics, Ithaca, New York, USA

Nagarajan, A.; Lutz, E.D.; Mukherjee, S. (1994): A novel boundary element method for linear elasticity with no numerical integration for two-dimensional and line integrals for three-dimensional problems. J. Appl. Mech. 61: 264-269

Nagarajan, A.; Lutz, E.D.; Mukherjee, S. (1996): The boundary contour method for three-dimensional linear elasticity. J. Appl. Mech. 63:278-286

Nagarajan, A. (1994): A novel boundary element method for linear elasticity. Ph.D. dissertation, Department of Theoretical and Applied Mechanics, Cornell University, Ithaca. New York, USA

Rizzo, F.J. (1967): An integral equation approach to boundary value problems of classical elastostatics. Quart. Appl. Math. 25: 83-95

Timoshenko, S.P.; Goodier, J.N. (1970): Theory of Elasticity. McGraw-Hill. New York, USA

Toh, K.C.; Mukherjee, S. (1994): Hypersingular and finite part integrals in the boundary element method. Int. J. Solids Struct. 31: 2299-2312

APPENDIX

POTENTIAL FUNCTIONS

$$\phi_1(\xi,\eta) = k\left[2(1-\nu)\arctan\left(\frac{\eta}{\xi}\right)+\frac{\xi\eta}{r^2}\right]$$

$$\phi_2(\xi,\eta) = k\eta\left[\frac{4\nu^2-9\nu+4-(1-\nu)(3-4\nu)\ln(r)}{(1-2\nu)}-\frac{\eta^2}{r^2}\right]$$

$$\phi_3(\xi,\eta) = k\xi\left[\frac{(3-4\nu)}{2}\ln(r)-\frac{\xi^2}{r^2}-1+2\nu\right]$$

$$\phi_4(\xi,\eta) = k\left[(1-2\nu)\ln(r)+\frac{\eta^2}{r^2}\right]$$

$$\phi_5(\xi,\eta) = k\xi\left[\frac{(3-4\nu)}{2}\ln(r)-\frac{\xi^2}{r^2}\right]$$

$$\phi_6(\xi,\eta) = k\eta\left\{\frac{\eta^2}{r^2}-\frac{\nu[(3-4\nu)\ln(r)-1]}{(1-2\nu)}\right\}$$

$$\phi_7(\xi,\eta) = k\xi\eta\left[(5-4\nu)\frac{\xi^2}{r^2}-(8\nu^2-14\nu+6)\ln(r)\right]$$

$$\phi_8(\xi,\eta) = k\xi\eta\left[2\nu(3-4\nu)\ln(r)+(1-4\nu)\frac{\xi^2}{r^2}+2\nu-1\right]$$

$$\phi_9(\xi,\eta) = k\left\{(3-4\nu)\left[\nu\xi^2+(1-\nu)\eta^2\right]\ln(r)+(1-4\nu)\frac{\xi^4}{r^2}+(4\nu^2-3\nu+1)\xi^2 - (3-4\nu)(1-\nu)\frac{r^2}{2}\right\}$$

$$\phi_{10}(\xi,\eta) = k\left\{(3-4\nu)\left[(2-\nu)\eta^2-(1-\nu)\xi^2\right]\ln(r)+(5-4\nu)\left[\frac{\xi^4}{r^2}-\nu\xi^2-(1-\nu)\frac{r^2}{2}\right]\right\}$$

$$\phi_{11}(\xi,\eta) = -\phi_4(\eta,\xi) \qquad \phi_{12}(\xi,\eta) = -\phi_6(\eta,\xi)$$

$$\phi_{13}(\xi,\eta) = -\phi_5(\eta,\xi) \qquad \phi_{14}(\xi,\eta) = -\phi_1(\eta,\xi)$$

$$\phi_{15}(\xi,\eta) = -\phi_3(\eta,\xi) \qquad \phi_{16}(\xi,\eta) = -\phi_2(\eta,\xi)$$

$$\phi_{17}(\xi,\eta) = -\phi_{10}(\eta,\xi) \qquad \phi_{18}(\xi,\eta) = -\phi_9(\eta,\xi)$$

$$\phi_{19}(\xi,\eta) = -\phi_8(\eta,\xi) \qquad \phi_{20}(\xi,\eta) = -\phi_7(\eta,\xi)$$

where,

$$k = \frac{1}{4\pi(1-\nu)} \quad \& \quad r^2 = \xi^2+\eta^2$$

APPENDIX II

The hypersingular boundary contour method for two-dimensional linear elasticity.

THE HYPERSINGULAR BOUNDARY CONTOUR METHOD FOR TWO-DIMENSIONAL LINEAR ELASTICITY

(Final revised version, September 1997.
Accepted for publication in *Acta Mechanica*)

Anh-Vũ Phan
Graduate Student
Department of Mechanical Engineering
Ecole Polytechnique
Montréal, Québec
Canada H3C 3A7

Subrata Mukherjee
Professor
Department of Theoretical and Applied Mechanics
Cornell University
Ithaca, NY 14853
USA

J.R. René Mayer
Assistant Professor
Department of Mechanical Engineering
Ecole Polytechnique
Montréal, Québec
Canada H3C 3A7

Summary

This paper presents a novel method called the Hypersingular Boundary Contour Method (HBCM) for two-dimensional (2-D) linear elastostatics. This new method can be considered to be a variant of the standard Boundary Element Method (BEM) and the Boundary Contour Method (BCM) because: (a) a regularized form of the hypersingular boundary integral equation (HBIE) is employed as the starting point, and (b) the above regularized form is then converted to a boundary contour version based on the divergence free property of its integrand. Therefore, as in the 2-D BCM, numerical integrations are totally eliminated in the 2-D HBCM. Furthermore, the regularized HBIE can be collocated at any boundary point on a body where stresses are physically continuous. A full theoretical development for this new method is addressed in the present work. Selected examples are also included and the numerical results obtained are uniformly accurate.

1 Introduction

The conventional Boundary Element Method (BEM) for linear elasticity requires the numerical evaluation of line integrals for two-dimensional (2-D) problems and surface integrals for three-dimensional (3-D) ones (see, e.g., Mukherjee [14]). By observing that the integrand vector of the Boundary Integral Equation (BIE) without body forces is divergence free, Nagarajan et al. [16], [17] have pioneered a novel approach, called the BCM, that achieves a further reduction in dimension. The divergence free property allows, for 3-D problems, the use of Stokes' theorem to transform surface integrals on the usual boundary elements into line integrals on the bounding contours of these elements. For 2-D problems, a similar transformation eliminates numerical integration altogether. The above transformations are quite general and apply to boundary elements of arbitrary shape. Thus, the BCM reduces the dimensionality of analysis problems by two: the method only requires numerical evaluation of 1-D line integrals for 3-D problems and simply the evaluation of functions (called potential functions) at points on the boundary of a body for 2-D cases.

The BCM for 2-D linear elastostatics has been presented in the literature by Nagarajan et al. [16] and by Phan et al. [20]. A numerical implementation with linear boundary elements is carried out in the former paper whereas a full development with quadratic boundary elements is performed in the latter one. Also, design sensitivity analysis by the BCM for 2-D linear elasticity has been carried out by Phan et al. [21]. For 3-D elasticity problems, the BCM with quadratic boundary elements is the subject of Nagarajan et al. [17] and Mukherjee et al. [15].

Regularized HBIEs have various important applications such as in computation of boundary stresses (e.g. Guiggiani et al. [7]), in wave scattering (e.g. Krishnasamy et al. [8]), in fracture mechanics (e.g. Gray et al. [3]; Lutz et al. [10]; Paulino [18]; Gray and Paulino [5]), in obtaining symmetric Galerkin boundary element formulations (e.g. Gray et al. [4]; Bonnet [1]; Gray and Paulino [6]), and in adaptative analysis (e.g. Paulino et al. [19]; Menon [12] and Menon et al. [13]).

Again, since the integrand vector of the regularized HBIE under consideration is divergence free, this equation can be converted into a boundary contour version in order to achieve a reduction in dimensionality as in the standard BCM. This work presents the general theory regarding the conversion of the regularized HBIE into a hypersingular boundary contour equation for 2-D linear elasticity. A numerical implementation with quadratic domain shape functions is also performed for both the primary analysis and post-processing.

The rest of this paper is outlined as follows. First, the BCM for 2-D linear elasticity is briefly recalled. This is followed by an introduction to a regularized HBIE, its conversion into a 2-D hypersingular boundary contour version and numerical implementation. Three numerical examples are then solved. Finally, some concluding remarks complete the paper.

2 2-D BCM formulations

The information presented in this section is summarized from Phan et al. [20] where more details can be found.

2.1 Basic formulation

The idea of dimensional reduction starts from the standard Boundary Integral Equation (BIE) without body forces (see Rizzo [23]),

$$c_{ik}(P)u_i(P) = \int_{\partial B} [U_{ik}(P,Q)\sigma_{ij}(Q) - \Sigma_{ijk}(P,Q)u_i(Q)]\,\mathbf{e}_j \cdot d\mathbf{S} \tag{1}$$

where c_{ik} is the corner tensor, P, Q, u_i and σ_{ij} are the source point, field point, displacement vector and stress tensor respectively, U_{ik} and Σ_{ijk} are the Kelvin kernel tensors (Rizzo [23]), and $\mathbf{e}_j$ are global Cartesian unit vectors. In 2-D problems, ∂B is the boundary of a body B, and $d\mathbf{S}$ is an infinitesimal boundary length vector.

Let

$$\mathbf{F}_k = [U_{ik}(P,Q)\sigma_{ij}(Q) - \Sigma_{ijk}(P,Q)u_i(Q)]\,\mathbf{e}_j \tag{2}$$

By discretizing the boundary ∂B into n elements, the BIE (1) becomes

$$c_{ik}(P)u_i(P) = \int_{\partial B} \mathbf{F}_k \cdot d\mathbf{S} = \sum_{\ell=1}^{n} \int_{E_{\ell 1}}^{E_{\ell 2}} \mathbf{F}_k \cdot d\mathbf{S} \tag{3}$$

where $E_{\ell 1}$ and $E_{\ell 2}$ are the endpoint nodes of element (ℓ).

Since the divergence of $\mathbf{F}_k$ at a field point Q is zero (see Nagarajan et al. [16]), i.e.

$$\nabla_Q \cdot \mathbf{F}_k = 0 \tag{4}$$

everywhere except at the source point P, so for non-singular elements (elements that do not contain the source point P), functions Φ_k can be found by solving the following identity that satisfies Eq. (4)

$$\mathbf{F}_k = \frac{\partial \Phi_k}{\partial y}\mathbf{e}_1 - \frac{\partial \Phi_k}{\partial x}\mathbf{e}_2 \tag{5}$$

Hence, for a non-singular element (ℓ), substitution of (5) into (3) yields:

$$\int_{E_{\ell 1}}^{E_{\ell 2}} \mathbf{F}_k \cdot d\mathbf{S} = \Phi_k^{(\ell)}(E_{\ell 2}) - \Phi_k^{(\ell)}(E_{\ell 1}) \tag{6}$$

In view of the above identity, Φ_k are called global potential functions. A numerical implementation of Eq. (6) does not require any numerical integration!

It is noted that the evaluation of boundary integrals on singular elements (elements containing the source point P) can be avoided by using the rigid body motion technique as it is often performed in the standard BEM. A formulation using this technique explicitly is addressed in the next section.

2.2 Formulation using the rigid body motion technique

In order to regularize the Cauchy singular integrals in the BIE (1), a rigid body motion solution is applied to this equation to produce a new equation

$$\int_{\partial B} \{U_{ik}(P,Q)\sigma_{ij}(Q) - \Sigma_{ijk}(P,Q)\,[u_i(Q) - u_i(P)]\}\,\mathbf{e}_j \cdot d\mathbf{S} = 0 \tag{7}$$

As a result, it can be seen that potentially singular integrals in (7) only need to be evaluated on non-singular boundary elements.

Let the new (regularized) integrand vector

$$\mathbf{G}_k = \{U_{ik}(P,Q)\sigma_{ij}(Q) - \Sigma_{ijk}(P,Q)[u_i(Q) - u_i(P)]\}\mathbf{e}_j \tag{8}$$

The vector $\mathbf{G}_k$ is still divergence free (everywhere except at P). With a procedure anologous to that described in the previous section, one gets:

$$\int_{E_{\ell 1}}^{E_{\ell 2}} \mathbf{G}_k \cdot d\mathbf{S} = \Psi_k^{(\ell)}(E_{\ell 2}) - \Psi_k^{(\ell)}(E_{\ell 1}) \tag{9}$$

where Ψ_k is determined by solving the following identity

$$\mathbf{G}_k = \frac{\partial \Psi_k}{\partial y}\mathbf{e}_1 - \frac{\partial \Psi_k}{\partial x}\mathbf{e}_2 \tag{10}$$

2.3 Implementation with quadratic boundary elements

$\mathbf{G}_k$ contains the unknown fields u_i and σ_{ij}. In order for the divergence free property of $\mathbf{F}_k$ and $\mathbf{G}_k$ to hold, the displacement shape functions u_i must satisfy, a priori, the Navier-Cauchy equations:

$$\nabla^2 \mathbf{u} + \frac{1}{1-2\nu}\nabla(\nabla \cdot \mathbf{u}) = \mathbf{0} \tag{11}$$

and the stress shape functions σ_{ij} must be derived from those of u_i using Hooke's law,

$$\sigma_{ij} = \lambda \delta_{ij} u_{k,k} + \mu(u_{i,j} + u_{j,i}) \tag{12}$$

where λ and μ are Lamé constants of the material, δ_{ij} is the Kronecker delta ($\equiv 1$ for $i = j$ and $\equiv 0$ for $i \neq j$).

Quadratic domain shape functions that ensure the divergence free property of $\mathbf{F}_k$ and $\mathbf{G}_k$ are given by

$$\begin{Bmatrix} u_1 \\ u_2 \end{Bmatrix} = \beta_1 \begin{Bmatrix} 1 \\ 0 \end{Bmatrix} + \beta_2 \begin{Bmatrix} x \\ 0 \end{Bmatrix} + \beta_3 \begin{Bmatrix} y \\ 0 \end{Bmatrix} + \beta_4 \begin{Bmatrix} 0 \\ 1 \end{Bmatrix} + \beta_5 \begin{Bmatrix} 0 \\ x \end{Bmatrix} + \beta_6 \begin{Bmatrix} 0 \\ y \end{Bmatrix}$$
$$+ \beta_7 \begin{Bmatrix} x^2 \\ k_2 xy \end{Bmatrix} + \beta_8 \begin{Bmatrix} y^2 \\ k_1 xy \end{Bmatrix} + \beta_9 \begin{Bmatrix} k_1 xy \\ x^2 \end{Bmatrix} + \beta_{10} \begin{Bmatrix} k_2 xy \\ y^2 \end{Bmatrix} \tag{13}$$

where $k_1 = -2(1 - 2\nu)$, $k_2 = -4(1 - \nu)$ and ν is the Poisson's ratio.

Equation (13) can also be written for element (ℓ) as

$$\begin{Bmatrix} u_1 \\ u_2 \end{Bmatrix}^{(\ell)} = \sum_{h=1}^{10} \beta_h^{(\ell)} \begin{Bmatrix} \overline{u}_{1h}(x,y) \\ \overline{u}_{2h}(x,y) \end{Bmatrix}^{(\ell)} \tag{14}$$

or in matrix form,

$$\left\{u^{(\ell)}\right\} = [T_u^{(\ell)}(x,y)]\{\beta^{(\ell)}\} \tag{15}$$

where $\{\beta^{(\ell)}\} = \langle \beta_1^{(\ell)} \ \beta_2^{(\ell)} \ \ldots \ \beta_{10}^{(\ell)} \rangle^T$.

The configuration of a chosen quadratic boundary element is shown in Fig. 1. The relationship between the physical variable vector $\left\{p^{(\ell)}\right\}$ and the artificial variable vector $\left\{\beta^{(\ell)}\right\}$ of boundary element (ℓ) is

$$\{p^{(\ell)}\} = \left\langle u_1^{(2\ell-1)} \ u_2^{(2\ell-1)} \ \tau_1^{(2\ell-1)} \ \tau_2^{(2\ell-1)} \ u_1^{(2\ell)} \ u_2^{(2\ell)} \ \tau_1^{(2\ell)} \ \tau_2^{(2\ell)} \ u_1^{(2\ell+1)} \ u_2^{(2\ell+1)} \right\rangle^T$$
$$= [T^{(\ell)}(x,y)]\{\beta^{(\ell)}\} \tag{16}$$

where $\{\beta^{(\ell)}\} = \langle \beta_1^{(\ell)} \ \ldots \ \beta_{10}^{(\ell)} \rangle^T$.

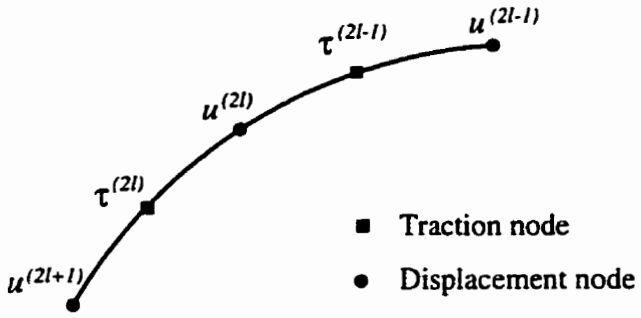

Figure 1: Quadratic boundary element (ℓ).

A new coordinate system (ξ, η) centered at each source point is introduced. Equations (14) and (15) become respectively,

$$\left\{ \begin{array}{c} u_1 \\ u_2 \end{array} \right\}^{(\ell)} = \sum_{h=1}^{10} \hat{\beta}_h^{(\ell)} \left\{ \begin{array}{c} \overline{u}_{1h}(\xi, \eta) \\ \overline{u}_{2h}(\xi, \eta) \end{array} \right\}^{(\ell)} \tag{17}$$

$$\left\{ u^{(\ell)} \right\} = [T_u^{(\ell)}(\xi, \eta)] \{ \hat{\beta}^{(\ell)} \} \tag{18}$$

In Eq. (18),

$$\{ \hat{\beta}^{(\ell)} \} = \langle \hat{\beta}_1^{(\ell)} \ \ldots \ \hat{\beta}_{10}^{(\ell)} \rangle^T = [B_j] \{ \beta^{(\ell)} \} \tag{19}$$

where $\hat{\beta}_h^{(\ell)} = \beta_h^{(\ell)}$ for $h = 7, \ldots, 10$, and $[B_j]$ is a matrix depending only on the coordinates of the source point j (since it arises from a coordinate transformation from the global system (x, y) to a system (ξ, η) centered at j).

Since the coordinates of a source point P are always $(0, 0)$, the displacement field used in Eq. (7) can easily be found from Eq. (17) as

$$\left\{ \begin{array}{c} u_1(Q) - u_1(P) \\ u_2(Q) - u_2(P) \end{array} \right\}^{(\ell)} = \sum_{h=1}^{10} \tilde{\beta}_h^{(\ell)} \left\{ \begin{array}{c} \overline{u}_{1h}(\xi, \eta) \\ \overline{u}_{2h}(\xi, \eta) \end{array} \right\}^{(\ell)} \tag{20}$$

in which, with (q) the element containing the source point, i.e., the singular element,

$$\left. \begin{array}{ll} \tilde{\beta}_h^{(\ell)} = \hat{\beta}_h^{(\ell)} - \hat{\beta}_h^{(q)} & \text{if} \quad h = 1, 4 \\ \tilde{\beta}_h^{(\ell)} = \beta_h^{(\ell)} & \text{if} \quad h = 7, \ldots, 10 \\ \tilde{\beta}_h^{(\ell)} = \hat{\beta}_h^{(\ell)} & \text{otherwise} \end{array} \right\} \tag{21}$$

It can be seen that the displacement shape vectors in Eqs. (14) and (20) are the same. Thus, by substituting each of these ten displacement shape vectors and its corresponding stress shape vector (using (12)) into Eqs. (2) and (8), one obtains

$$\mathbf{F}_{kh} = \mathbf{G}_{kh} = [U_{ik}\overline{\sigma}_{ijh}(\xi,\eta) - \Sigma_{ijk}\overline{u}_{ih}(\xi,\eta)]\,\mathbf{e}_j \tag{22}$$

Equations (5) and (10) in this case take the following form

$$\mathbf{F}_{kh} = \mathbf{G}_{kh} = \frac{\partial \phi_z}{\partial \eta}\mathbf{e}_1 - \frac{\partial \phi_z}{\partial \xi}\mathbf{e}_2 \tag{23}$$

where $z = h + 10(k-1)$; $h = 1, 2, \ldots, 10$ and $k = 1, 2$.

Equation (23) implies that the BIE (1) and its regularized form (7) have the same potential functions ϕ_z.

For a given value of h, the solution of (23) using (22) yields two potential functions ϕ_z associated with $k = 1, 2$. The 20 resulting potential functions (for $h = 1, \ldots, 10; k = 1, 2$) are listed in the Appendix of Phan et al. [20]. It can be observed from this Appendix that only half of these 20 potential functions need to be determined.

By using these potential functions, Eqs. (6) and (9) become respectively

$$\int_{E_{\ell 1}}^{E_{\ell 2}} \mathbf{F}_k \cdot d\mathbf{S} = \sum_{h=1}^{10} \hat{\beta}_h^{(\ell)} [\phi_z(E_{\ell 2}) - \phi_z(E_{\ell 1})] \tag{24}$$

$$\int_{E_{\ell 1}}^{E_{\ell 2}} \mathbf{G}_k \cdot d\mathbf{S} = \sum_{h=1}^{10} \tilde{\beta}_h^{(\ell)} [\phi_z(E_{\ell 2}) - \phi_z(E_{\ell 1})] \tag{25}$$

As shown in Phan et al. [20], a development of (25) for all boundary elements leads to the following final BCM system of equations

$$[A]\{X\} = [B]\{Y\} \tag{26}$$

Or,

$$[A]\{X\} = \{Z\} \tag{27}$$

In eqns (26) and (27), $[A]$ and $[B]$ are the BCM matrices which are associated with the potential functions ϕ_z; $\{X\}$ and $\{Y\}$ contain, respectively, the unknown

and known (from boundary conditions) physical quantities. Thus, $\{Z\}$ is a known vector. Finally, system (27) can easily be solved to find the unknowns $\{X\}$.

3 A regularized hypersingular boundary integral equation

The starting point of the HBCM is the following regularized form of the HBIE (see, e.g., Krishnasamy et al. [9], Lutz et al. [10] and Cruse and Richardson [2]):

$$\int_{\partial B} \left\{ U_{ik,m}(P,Q)\left[\sigma_{ij}(Q)-\sigma_{ij}(P)\right] - \Sigma_{ijk,m}(P,Q)\left[u_i(Q)-u_i^{(L)}\right]\right\} \mathbf{e}_j \cdot d\mathbf{S} = 0 \quad (28)$$

where, for plane strain problems, the gradients with respect to a field point $(\ )_{,m}$ of the Kelvin kernel tensors are given by

$$\left.\begin{aligned} U_{ik,m} &= \frac{-1}{8\pi\mu(1-\nu)r}\left[(3-4\nu)\delta_{ik}r_{,m} - \delta_{im}r_{,k} - \delta_{mk}r_{,i} + 2r_{,i}r_{,m}r_{,k}\right] \\ \Sigma_{ijk,m} &= \frac{1}{4\pi(1-\nu)r^2}\left[8r_{,i}r_{,j}r_{,k}r_{,m} - 2(\delta_{im}r_{,j}r_{,k} + \delta_{jm}r_{,i}r_{,k} + \delta_{km}r_{,i}r_{,j}) + (1-2\nu)\right. \\ &\left.(-\delta_{ik}\delta_{jm} - \delta_{jk}\delta_{im} + \delta_{ij}\delta_{km}) + 2(1-2\nu)(\delta_{ik}r_{,j}r_{,m} + \delta_{jk}r_{,i}r_{,m} - \delta_{ij}r_{,k}r_{,m})\right] \end{aligned}\right\} \quad (29)$$

where $i,j,k,m = 1,2$ for 2-D problems, δ_{ij} is the Kronecker delta, and r is the Euclidean distance between a field point Q and a source point P.

In Eq. (28),

$$u_i^{(L)} = u_i(P) + u_{i,s}(P)\left[x_s(Q) - x_s(P)\right] \quad (30)$$

which yields

$$u_{i,m}^{(L)} = u_{i,m}(P) \quad (31)$$

In others words, the linear displacement field $u_i^{(L)}$ gives the stress field $\sigma_{ij}(P)$. Therefore, the stress field $\sigma_{ij}(Q) - \sigma_{ij}(P)$ is obtained from the displacement field $u_i(Q) - u_i^{(L)}$. Based on this remark, a similarity in structure can be observed between the regularized HBIE (28) and the regularized BIE (7).

According to Cruse and Richardson [2], Eq. (28) is valid at any boundary point, including corners, provided that the stress tensor is continuous there. The singular gradients of the kernels are regularized in this case because the quantities inside the square brackets in Eq. (28) are ($O(r)$ and $O(r^2)$, respectively, as $Q \to P$.

Therefore, the regularized HBIE (28) can be collocated at any boundary point P, including corners, provided that the stress is continuous at that point. Collocation of the boundary contour version of Eq. (28) at corners is successfully carried out in some of the numerical examples presented later in this paper.

4 2-D HBCM formulations

Let the integrand vector of Eq. (28) be $\mathbf{J}_{km}$, i.e.

$$\mathbf{J}_{km} = \left[U_{ik,m}(P,Q)\left[\sigma_{ij}(Q) - \sigma_{ij}(P)\right] - \Sigma_{ijk,m}(P,Q)\left[u_i(Q) - u_i^{(L)}\right]\right]\mathbf{e}_j \qquad (32)$$

The divergence free property of (2) is valid for any pair (u_i, σ_{ij}) which satisfies the Navier-Cauchy equations (11) and Hooke's law (12). Let such a pair be called admissible. Then, since the pair $\left(u_i(Q) - u_i^{(L)}, \sigma_{ij}(Q) - \sigma_{ij}(P)\right)$ is also admissible, by analogy with $\mathbf{F}_k$, the following vectors:

$$\mathbf{K}_k = \left[U_{ik}(P,Q)\left[\sigma_{ij}(Q) - \sigma_{ij}(P)\right] - \Sigma_{ijk}(P,Q)\left[u_i(Q) - u_i^{(L)}\right]\right]\mathbf{e}_j \qquad (33)$$

$$\mathbf{I}_{kM} = \left[U_{ik,M}(P,Q)\left[\sigma_{ij}(Q) - \sigma_{ij}(P)\right] - \Sigma_{ijk,M}(P,Q)\left[u_i(Q) - u_i^{(L)}\right]\right]\mathbf{e}_j \qquad (34)$$

are divergence free, i.e. $\nabla_Q \cdot \mathbf{K}_k = \nabla_Q \cdot \mathbf{I}_{kM} = 0$, (everywhere except at the source point P).

Therefore,

$$\nabla_Q \cdot \mathbf{J}_{km} = -\nabla_Q \cdot \mathbf{J}_{kM} = -\nabla_Q \cdot \mathbf{I}_{kM} = 0 \qquad (35)$$

everywhere except at P. Here, as usual, the gradients of the kernel tensors with respect to a field point are converted to those with respect to a source point by a sign change.

By discretizing the boundary ∂B into n elements, the regularized HBIE (28) becomes

$$\int_{\partial B} \mathbf{J}_{km} \cdot d\mathbf{S} = \sum_{\ell=1}^{n} \int_{E_{\ell 1}}^{E_{\ell 2}} \mathbf{J}_{km} \cdot d\mathbf{S} = 0 \qquad (36)$$

Due to (35), for a boundary element (ℓ), the boundary contour version of the 2-D HBCM can be written as

$$\int_{E_{\ell 1}}^{E_{\ell 2}} \mathbf{J}_{km} \cdot d\mathbf{S} = \Lambda_{km}^{(\ell)}(E_{\ell 2}) - \Lambda_{km}^{(\ell)}(E_{\ell 1}) \qquad (37)$$

where Λ_{km} is defined by the equation

$$\mathbf{J}_{km} = \frac{\partial \Lambda_{km}}{\partial y}\mathbf{e}_1 - \frac{\partial \Lambda_{km}}{\partial x}\mathbf{e}_2 \tag{38}$$

5 Numerical implementation for the 2-D HBCM

As in the BCM, a new coordinate system (ξ, η) centered at each source point is employed at this stage. Here, source points are only placed at the endpoint nodes.

Quadratic shape functions used in Eq. (28) can be obtained easily from Eq. (17) as

$$\left\{ \begin{array}{l} u_1(Q) - u_1^{(L)} \\ u_2(Q) - u_2^{(L)} \end{array} \right\} = \sum_{h=1}^{10} \check{\beta}_h^{(\ell)} \left\{ \begin{array}{l} \overline{u}_{1h}(\xi, \eta) \\ \overline{u}_{2h}(\xi, \eta) \end{array} \right\}^{(\ell)} \tag{39}$$

where,

$$\left. \begin{array}{ll} \check{\beta}_h^{(\ell)} = \hat{\beta}_h^{(\ell)} - \hat{\beta}_h^{(q)} & \text{if} \quad h = 1, \ldots, 6 \\ \check{\beta}_h^{(\ell)} = \beta_h^{(\ell)} & \text{if} \quad h = 7, \ldots, 10 \end{array} \right\} \tag{40}$$

5.1 Potential functions

The 2-D HBCM potential functions can be determined by using the same procedure for obtaining the potential functions ϕ_z described in section 2.3. In other words, each of the ten displacement shape vectors in (39) (see also Eq. (13)), together with its corresponding stress shape vector (obtained from (12)) are employed in Eq. (32) to result in

$$\mathbf{J}_{kmh} = \left[U_{ik,m} \overline{\sigma}_{ijh}(\xi, \eta) - \Sigma_{ijk,m} \overline{u}_{ih}(\xi, \eta) \right] \mathbf{e}_j \tag{41}$$

Equation (38) in this case has the following form

$$\mathbf{J}_{kmh} = \frac{\partial \lambda_w}{\partial \eta}\mathbf{e}_1 - \frac{\partial \lambda_w}{\partial \xi}\mathbf{e}_2 \tag{42}$$

where $w = h + 10(k-1) + 20(m-1)$; $h = 1, 2, \ldots, 10$; $k = 1, 2$ and $m = 1, 2$.

For a given value of h, the solution of (42) using (41) yields four potential functions λ_w (corresponding to $k = 1, 2$ and $m = 1, 2$). The 40 resulting potential functions (for $h = 1, \ldots, 10$) are listed in the Appendix. Once again, it can be seen that only half of them need to be determined.

By using these potential functions, Eq. (37) becomes

$$\int_{E_{\ell 1}}^{E_{\ell 2}} \mathbf{J}_{km} \cdot d\mathbf{S} = \sum_{h=1}^{10} \tilde{\beta}_h^{(\ell)} \left[\lambda_w(E_{\ell 2}) - \lambda_w(E_{\ell 1})\right] \tag{43}$$

For singular elements $(\ell) = (q)$ (see (40)), one has

$$\int_{E_{q1}}^{E_{q2}} \mathbf{J}_{km} \cdot d\mathbf{S} = \sum_{h=7}^{10} \beta_h^{(q)} \left[\lambda_w(E_{q2}) - \lambda_w(E_{q1})\right] \tag{44}$$

i.e., the singular potential functions λ_w only need to be evaluated on non-singular elements.

5.2 Primary system of equations

For the source point j, the right hand sides of Eqs. (43) and (44) can be developed into the following matrix forms:

$$\begin{aligned} \int_{E_{\ell 1}}^{E_{\ell 2}} \mathbf{J}_{km} \cdot d\mathbf{S} &= \left[\Lambda^{(j\ell)}\right] \left\{\tilde{\beta}^{(\ell)}\right\} = \left[\Lambda^{(j\ell)}\right] [B_j] \left\{\beta^{(\ell)}\right\} \\ &= \left[\Lambda^{(j\ell)}\right] [B_j] \left[T^{(\ell)}\right]^{-1} \left\{p^{(\ell)}\right\} = \left[M^{(j\ell)}\right] \left\{p^{(\ell)}\right\} \end{aligned} \tag{45}$$

where $(\ell) = (q)$ for singular elements.

Hence,

$$\int_{\partial B} \mathbf{J}_{km} \cdot d\mathbf{S} = \sum_{\ell=1}^{n} \int_{E_{\ell 1}}^{E_{\ell 2}} \mathbf{J}_{km} \cdot d\mathbf{S} = \sum_{\ell=1}^{n} \left[M^{(j\ell)}\right] \left\{p^{(\ell)}\right\} = 0 \tag{46}$$

The last system of equations (46) is now condensed to reflect displacement continuity across elements. The result is:

$$\left[M^{(j)}\right] \{p\} = \{0\} \tag{47}$$

where $\{p\}$ is the vector with physical variables on the whole boundary ∂B.

With n source points corresponding to n endpoint nodes on the boundary ∂B, one gets n relations (47) which are now combined into the following linear system of equations

$$[M]\{p\} = \{0\} \tag{48}$$

Finally, system (48) needs to be reordered in accordance with the boundary conditions to build the primary HBCM system of equations. The resulting system of equations has the same form as Eq. (27). As in the BCM, the HBCM primary system is generally overdetermined but always consistent.

5.3 Post-processing for displacements and stresses

After the solution of the HBCM primary system is obtained, one can easily derive $\{\hat{\beta}^{(\ell)}\}$ from (16) and (19). The post-processing stage involves using the known $\{\hat{\beta}^{(\ell)}\}$ to compute displacements and stresses at any point P in the domain B.

The set of points B^* contains the interior as well as the boundary ∂B of a body, except the nodes at the ends of boundary elements. At a regular boundary point, ∂B is locally smooth. A corner is always an end point.

Displacements on the entire domain B can be calculated from the boundary contour version of the standard BIE (see (1) and (24)) as follows

$$c_{ik}u_i(P) = \sum_{\ell=1}^{n}\sum_{h=1}^{10}\hat{\beta}_h^{(\ell)}\left[\phi_z(E_{\ell 2}) - \phi_z(E_{\ell 1}) - k_\phi\right] \tag{49}$$

However, since the endpoint displacements are already known from the primary HBCM analysis described in the previous section, only the displacements on B^* need to be calculated from (49). For this calculation, $c_{ik} = 0.5\delta_{ik}$ for regular points on the boundary ∂B and $c_{ik} = \delta_{ik}$ for points inside the body B. Also, $k_\phi = 0.5$ if P is a regular point on ∂B and $z = 1$ or 14 (see [20]). At regular boundary points on ∂B with other values of z, as well as at points inside the body, $k_\phi = 0$.

Stresses on B can be evaluated from the boundary contour version of the regualrized HBIE (see (28) and (43)) as

$$\sum_{\ell=1}^{n}\sum_{h=1}^{10}\hat{\beta}_h^{(\ell)}\left[\lambda_w(E_{\ell 2}) - \lambda_w(E_{\ell 1}) + k_\lambda\right] = 0 \tag{50}$$

where $k_\lambda = 0.5$ if P is a regular point on ∂B and $w = 2, 16, 23$ or 35 (see [20] and the Appendix of this paper). Again, at regular boundary points on ∂B with other values of w, as well as at points inside the body, $k_\lambda = 0$.

In Eq. (50), it can be shown that

$$\left.\begin{array}{lll} \check{\beta}_1^{(\ell)} = \hat{\beta}_1^{(\ell)} - u_1(P)\ ; & \check{\beta}_2^{(\ell)} = \hat{\beta}_2^{(\ell)} - u_{1,1}(P)\ ; & \check{\beta}_3^{(\ell)} = \hat{\beta}_3^{(\ell)} - u_{1,2}(P) \\ \check{\beta}_4^{(\ell)} = \hat{\beta}_4^{(\ell)} - u_2(P)\ ; & \check{\beta}_5^{(\ell)} = \hat{\beta}_5^{(\ell)} - u_{2,1}(P)\ ; & \check{\beta}_6^{(\ell)} = \hat{\beta}_6^{(\ell)} - u_{2,2}(P) \end{array}\right\} \tag{51}$$

where $u_1(P)$, $u_2(P)$ and $\hat{\beta}_h^{(\ell)}, h = 1, 2, \ldots, 6$ are known from the primary solution or from (49). Now $u_{1,1}(P)$, $u_{1,2}(P)$,$u_{2,1}(P)$ and $u_{2,2}(P)$ are four unknowns which can be found by solving the system (50) of four equations (corresponding to $k = 1, 2$ and $m = 1, 2$).

It should be pointed out that values of k_λ are not required at endpoint nodes on ∂B because it is particularly easy to find the stresses at these nodes. By comparing $\check{\beta}_h^{(\ell)}$ $(h = 2, 3, 5, 6)$ between (51) and (40), it can be seen that the displacement gradients at endpoint nodes are exactly the values of $\hat{\beta}_2^{(q)}$, $\hat{\beta}_3^{(q)}$, $\hat{\beta}_5^{(q)}$ and $\hat{\beta}_6^{(q)}$, where q is either of the elements containing the endpoint node P under consideration.

Once the displacement gradients are found, Hooke's law (12) is employed to compute the stresses.

6 Numerical examples

Three examples are presented in this section. All of them use the following material data: Young's modulus $E = 2.5$ (in consistent units) and Poisson's ratio $\nu = 0.3$.

6.1 Displacement field problem

Consider an elliptical body as shown in Fig. 2. The following displacement field, which is an exact solution of the elasticity Navier-Cauchy equations (11), is imposed at the displacement nodes on the boundary.

$$\left.\begin{array}{l} u_1 = y^3 - 3yx^2 \\ u_2 = -x^3 + 3xy^2 \end{array}\right\} \tag{52}$$

The circular boundary is discretized by 16 quadratic elements spaced at equal increments. Tractions on the boundary and stresses along the line AB are obtained

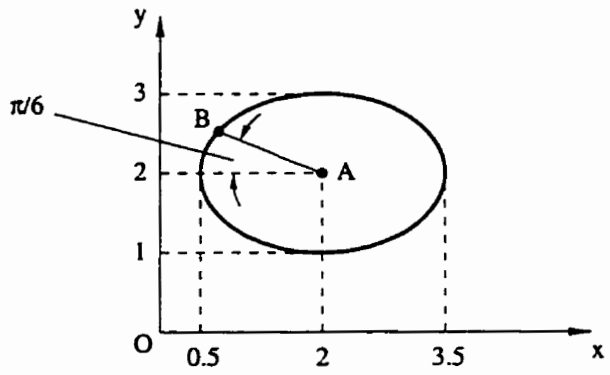

Figure 2: Elliptical body with imposed displacement fields.

from the primary analysis and from post-processing respectively. The numerical results are compared against analytical solutions as shown in Figs. 3 and 4. Excellent agreement between the solutions is achieved in both figures.

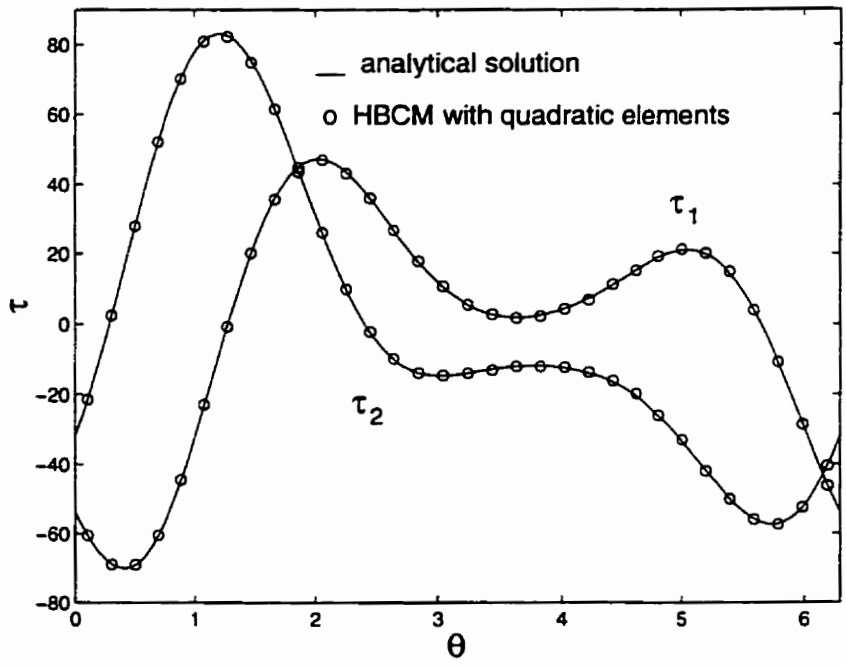

Figure 3: Traction components for the cubic displacement field.

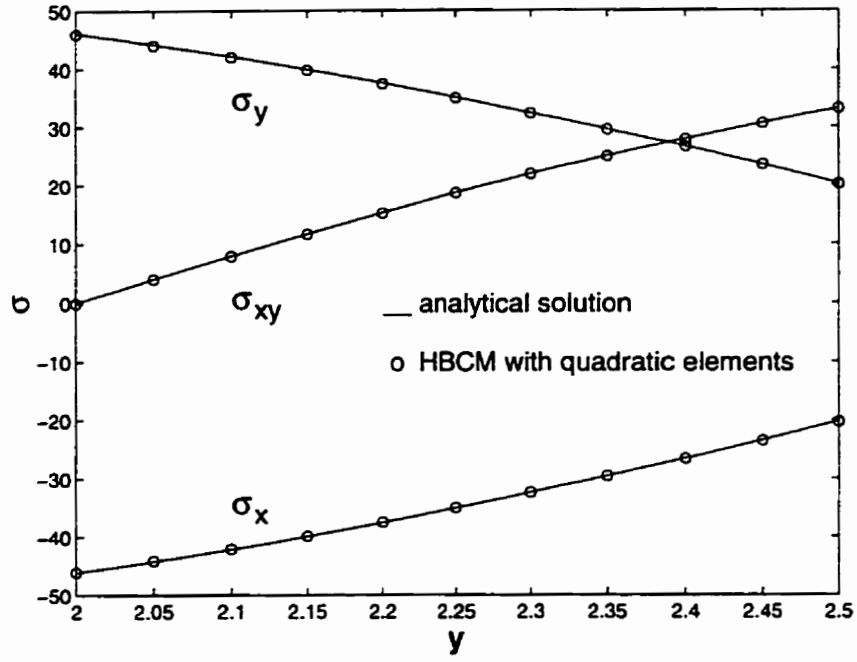

Figure 4: Stress components along AB (see Fig. 2) for the cubic displacement field.

6.2 Lamé's problem

Consider a thick hollow cylinder subjected to uniform pressures p_i and p_o on the inner and outer surfaces, respectively. Let a and b be the inner and outer radii of the cylinder.

Due to symmetry of the problem, only a quarter of the structure is modeled as shown in Fig. 5. A total of 80 quadratic elements is required to discretize the boundary: 18 and 8 elements of equal size are placed on arcs BC and DA, respectively; 27 elements of unequal size are placed on each of the edges AB and CD, with shorter elements being used near B and C.

The analytical expressions in polar coordinates (r, θ), for the stress fields of Lamé's problem, are given by Timoshenko and Goodier [24],

$$\sigma_{r/\theta} = \pm \frac{a^2 b^2 (p_o - p_i)}{(b^2 - a^2) r^2} + \frac{p_i a^2 - p_o b^2}{b^2 - a^2} \tag{53}$$

in which the expressions for σ_r and σ_θ correspond to the upper and lower signs, respectively.

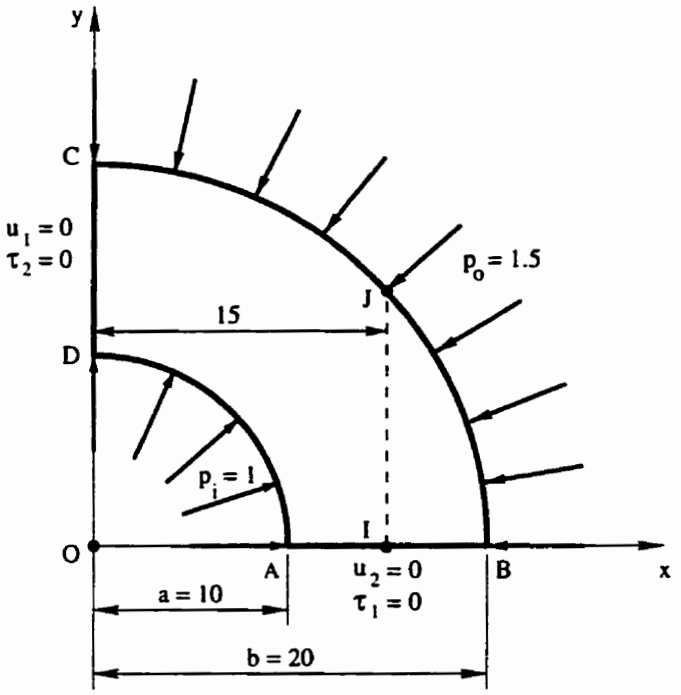

Figure 5: Modeling of Lamé's problem.

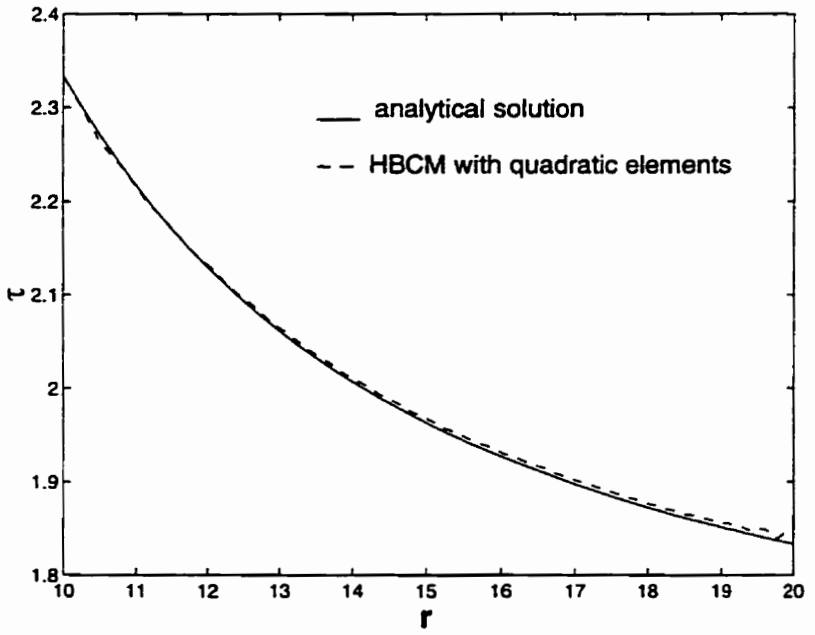

Figure 6: The traction component τ_2 on the edge AB (see Fig. 5) for Lamé's problem.

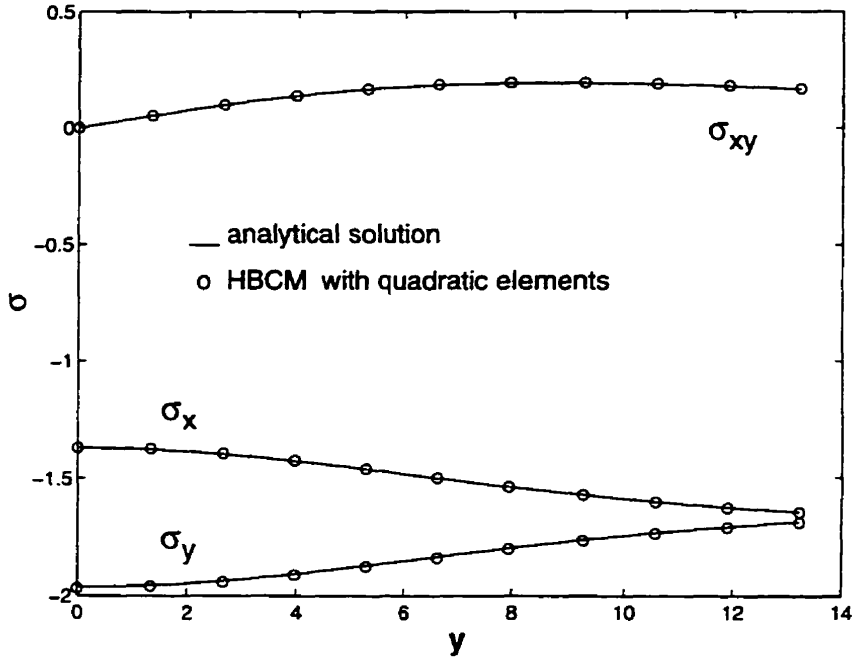

Figure 7: Stresses along IJ (see Fig. 5) for Lamé's problem.

Numerical results for $\tau_2 = -\sigma_\theta$ along AB are obtained from the HBCM primary analysis. These results are compared with the analytical solution in Fig. 6 where a very good correlation is observed. Numerical results for the stress components along the segment IJ are computed from the post-processing stage and these results are in excelent agreement with the analytical solution as seen in Fig. 7.

6.2 Kirsch's problem

The third example deals with Kirsch's problem. Fig. 8 displays a quarter symmetry model of a square plate with a central circular hole subjected to a unit uniaxial tensile load. The boundary contour analysis model is made up of 78 quadratic elements. Due to stress concentration at the corners A and E, the mesh around this zone needs to be densified : the density of elements on AB and DE is nonuniform, with short elements being placed near the points A and E.

In polar coordinates, the stress component σ_r in the radial direction, the stress component σ_θ in the circumferential direction and the shearing stress component

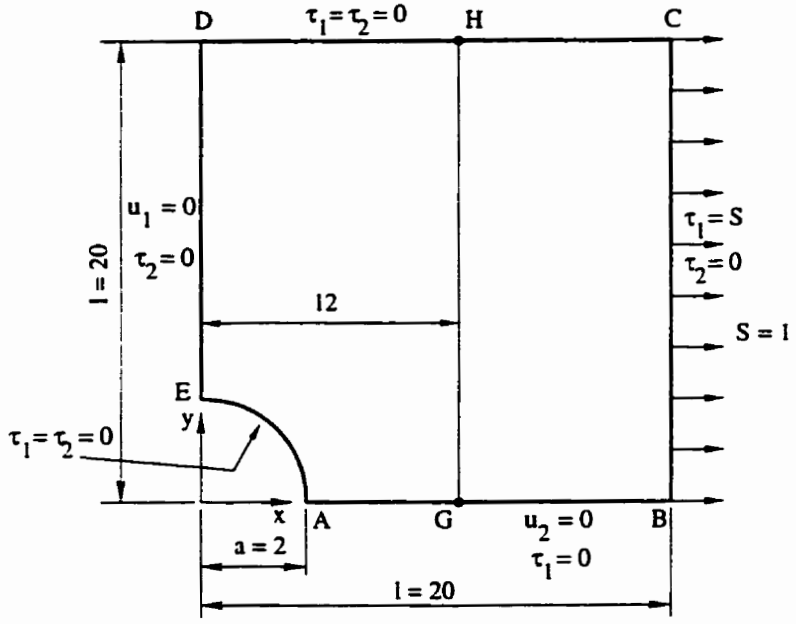

Figure 8: Modeling of Kirsch's problem.

$\tau_{r\theta}$, at a point (r, θ) in an infinite plate with a circular hole are given by Timoshenko and Goodier [24],

$$\left.\begin{aligned} \sigma_r &= \frac{S}{2}(1-\frac{a^2}{r^2}) + \frac{S}{2}(1+\frac{3a^4}{r^4}-\frac{4a^2}{r^2})\cos 2\theta \\ \sigma_\theta &= \frac{S}{2}(1+\frac{a^2}{r^2}) - \frac{S}{2}(1+\frac{3a^4}{r^4})\cos 2\theta \\ \tau_{r\theta} &= -\frac{S}{2}(1-\frac{3a^4}{r^4}+\frac{2a^2}{r^2})\sin 2\theta \end{aligned}\right\} \tag{54}$$

For the cross section of the plate along the y axis ($\theta = \pi/2$), tractions in the x-direction along the edge DE can be found from Eqs. (54) as

$$\tau_1 = -\sigma_\theta = -\frac{S}{2}(2+\frac{a^2}{r^2}+\frac{3a^4}{r^4}) \tag{55}$$

Numerical results from the primary and post-processing stages are compared with the analytical solutions in Figs. 9 and 10. Here, polar coordinates are used to evaluate the stresses along the line GH. Once again, very good agreement is achieved.

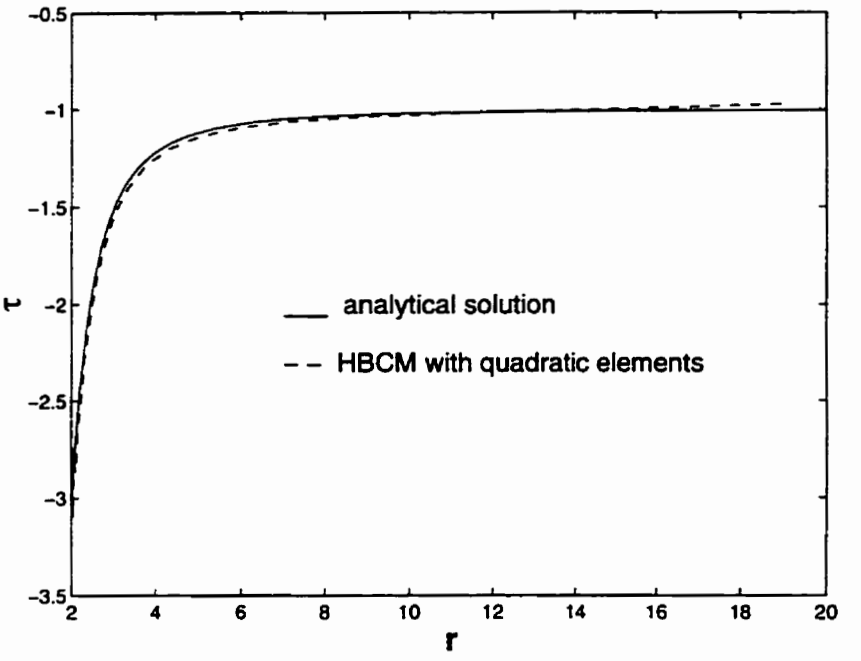

Figure 9: The traction component τ_1 on the edge DE (see Fig. 8) for Kirsch's problem.

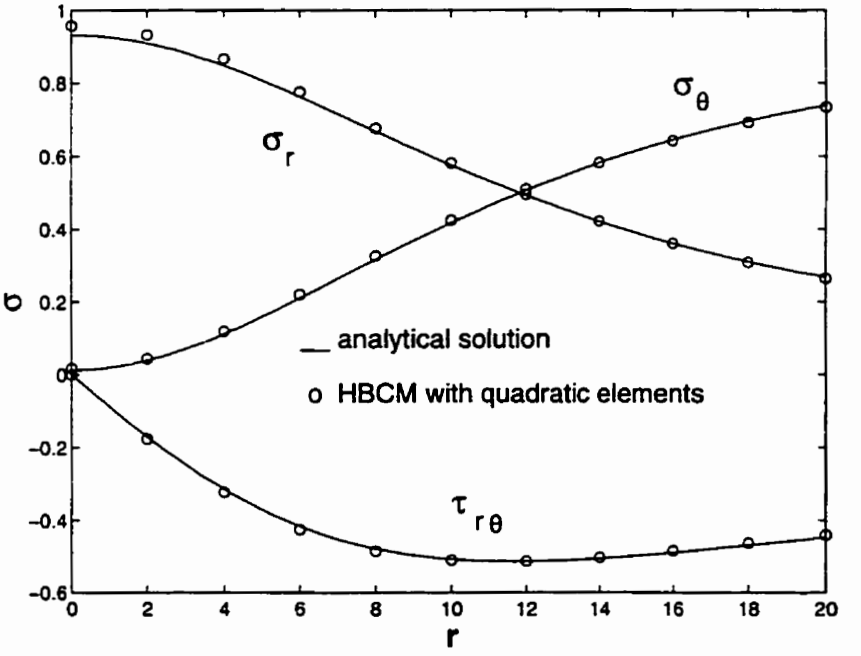

Figure 10: Stresses along GH (see Fig. 8) for Kirsch's problem.

7 Conclusions

A formulation and numerical implementation of the HBCM for 2-D linear elasticity is presented by this work. The method is based on a regularized HBIE which can be collocated at any boundary point where the stress is continuous. A numerical implementation with quadratic domain shape functions is carried out. Potential functions are required for obtaining integrals (without numerical integration) in the regularized HBIE. These functions, used in both the primary and post-processing stages, are determined and included in this paper. From three examples in the present work, it is noted that the HBCM can provide accurate numerical results, especially those for post-processing stress analysis. It should be pointed out that numerical enforcement of stress continuity at endpoint nodes, with sufficient accuracy, is crucial for the regularization of Eq. (28). In order to achieve this, and consequently obtain accurate numerical results, the meshes used for the HBCM need, in general, to be finer than those used for the BCM. It is expected that higher order elements such as cubic would offer the required accuracy without the need of these fine meshes.

There is an ongoing debate in the literature regarding smoothness requirements of *shape functions* of the boundary displacement for collocating a regularized HBIE (such as Eq. (28)) at a boundary point where the stress is continuous. Martin and Rizzo [11], in a recent paper, claim that while the previously proved *sufficiency* requirement of $C^{1,\alpha}$ shape functions can be somewhat relaxed, $C^{0,\alpha}$ shape functions are certainly not permissible. Cruse and Richardson [2], on the other hand, claim that $C^{0,\alpha}$ shape functions for $\mathbf{u}$ are *sufficient* in this case, provided that one specifically develops a scheme that allows the numerical solution for the stress to be multi-valued at the boundary collocation point. It is very interesting to note that the HBCM formulation presented in this paper uses domain shape functions that are C^{∞} (see Eq. (13)). Thus, numerical collocation of the regularized HBCM (46), at boundary points where the stress is continuous, is mathematically sound. This fact is supported by the excellent numerical results, including at end points and corners, for the Lamé and Kirsch problems presented in Figs. 6, 7, 9 and 10 in this paper.

Acknowledgement

Anh-Vũ Phan is grateful for the support provided by the Quebec Ministry of Education through the "Programme québécois de bourses d'excellence".

References

[1] Bonnet, M.: Regularized direct and indirect symmetric variational BIE formulations for three-dimensional elasticity. Engng. Anal. with Boundary Elem. **15,** 93-102 (1995).

[2] Cruse, T.A., Richardson, J.D.: Non-singular somigliana stress identities in elasticity. Int. J. Num. Meth. Eng. **39,** 3273-3304 (1996).

[3] Gray, L.J., Martha, L.F., Ingraffea, A.R.: Hypersingular integrals in boundary element fracture analysis. Int. J. Num. Meth. Eng. **29,** 1135-1158 (1990).

[4] Gray, L.J., Balakrishna, C., Kane, J.H.: Symmetric Galerkin fracture analysis. Engineering Analysis with Boundary Elements. **15,** 103-109 (1995).

[5] Gray, L.J., Paulino, G.H.: Crack tip interpolation, revisited. SIAM Journal on Numerical Analysis. (In press).

[6] Gray, L J., Paulino, G.H.: Symmetric Galerkin boundary integral formulation for interface and multy-zone problems. Int. J. Num. Meth. Eng. (In press).

[7] Guiggiani, M., Krishnasamy, G., Rudolphi, T.J., Rizzo, F.J.: A general algorithm for the numerical solution of hypersingular boundary integral equations. ASME J. Appl. Mech. **59,** 604-614 (1992).

[8] Krishnasamy, G., Schmerr, L.W., Rudolphi, T.J., Rizzo, F.J.: Hypersingular boundary integral equations: some applications in acoustics and elastic wave scattering. ASME J. Appl. Mech. **57,** 404-414 (1990).

[9] Krishnasamy, G., Rizzo, F.J., Rudolphi, T.J.: Hypersingular boundary integral equations: their occurrence, interpretation, regularization and computation. In: Developments in boundary element methods, vol. 7 (Banerjee, P.K., Kobayashi, S. ed.), pp. 207-252. London: Elsevier Applied Science 1992.

[10] Lutz, E.D., Ingraffea, A.R., Gray, L.J.: Use of 'simple solutions' for boundary integral methods in elasticity and fracture analysis. Int. J. Num. Meth. Eng. **35,** 1737-1751 (1992).

[11] Martin, P.A., Rizzo, F.J.: Hypersingular integrals: how smooth must the density be? Int. J. Num. Meth. Eng. **39,** 687-704 (1996).

[12] Menon, G.: Hypersingular error estimates in boundary element methods. M.S. thesis. Cornell University, Ithaca, New York, U.S.A., 1996.

[13] Menon, G., Paulino, G.H., Mukherjee S.: Analysis of hypersingular residual error estimates for potential problems using boundary element methods. (Submitted for publication).

[14] Mukherjee, S.: Boundary element methods in creep and fracture. New York: Elsevier 1982.

[15] Mukherjee, Y.X., Mukherjee, S., Shi, X., Nagarajan, A.: The boundary contour method for three-dimensional linear elasticity with a new quadratic boundary element. Engng. Anal. with Boundary Elem. (In press).

[16] Nagarajan, A., Lutz, E.D., Mukherjee, S.: A novel boundary element method for linear elasticity with no numerical integration for two-dimensional and line integrals for three-dimensional problems. ASME J. Appl. Mech. **61,** 264-269 (1994).

[17] Nagarajan, A., Lutz, E.D., Mukherjee, S.: The boundary contour method for three-dimensional linear elasticity. ASME J. Appl. Mech. **63,** 278-286 (1996).

[18] Paulino, G.H.: Novel formulations of the boundary element method for fracture mechanics and error estimation. Ph.D. dissertation. Cornell University, Ithaca, New York, U.S.A., 1995.

[19] Paulino, G.H., Gray, L.J., Zarkian V.: Hypersingular residuals - A new approach for error estimation in the boundary element method. Int. J. Num. Meth. Eng. **39,** 2005-2029 (1996).

[20] Phan, A.V., Mukherjee, S., Mayer, J.R.R.: The boundary contour method for two-dimensional linear elasticity with quadratic boundary elements. Comput. Mech. (In press).

[21] Phan, A.V., Mukherjee, S., Mayer, J.R.R.: A boundary contour formulation for design sensitivity analysis in two-dimensional linear elasticity. Int. J. Solids Struct. (In press).

[22] Phan, A.V., Mukherjee, S., Mayer, J.R.R.: Stresses, stress sensitivities and shape optimization in two-dimensional linear elasticity by the boundary contour method. (Submitted for publication).

[23] Rizzo, F.J.: An integral equation approach to boundary value problems of classical elastostatics. Qly. Appl. Math. **25,** 83-95 (1967).

[24] Timoshenko, S.P., Goodier, J.N.: Theory of Elasticity. New York: McGraw-Hill 1970.

APPENDIX

POTENTIAL FUNCTIONS

$$\lambda_1(\xi,\eta) = -\frac{k\eta}{r^2}\left(\frac{2\xi^2}{r^2}+1-2\nu\right)$$

$$\lambda_2(\xi,\eta) = k\left[\frac{\xi\eta}{r^2}\left(\frac{4\nu^2-5\nu+2}{2\nu-1}-\frac{2\xi^2}{r^2}\right)-2(1-\nu)\arctan\left(\frac{\eta}{\xi}\right)\right]$$

$$\lambda_3(\xi,\eta) = k\left[\frac{\xi^2}{r^2}\left(\frac{2\xi^2}{r^2}-2\nu-\frac{3}{2}\right)+\left(\frac{3}{2}-2\nu\right)\ln r\right]$$

$$\lambda_4(\xi,\eta) = \frac{k\xi}{r^2}\left(\frac{2\xi^2}{r^2}-1-2\nu\right)$$

$$\lambda_5(\xi,\eta) = k\left[\frac{\xi^2}{r^2}\left(\frac{2\xi^2}{r^2}-2\nu-\frac{1}{2}\right)+\frac{1}{2}\ln r\right]$$

$$\lambda_6(\xi,\eta) = \frac{k\xi\eta}{r^2}\left(\frac{4\nu^2+\nu-2}{1-2\nu}+\frac{2\xi^2}{r^2}\right)$$

$$\lambda_7(\xi,\eta) = k\eta\left\{2(\nu-1)+\frac{\xi^2}{r^2}\left[3+6\nu-8\nu^2+\frac{2\xi^2}{r^2}(4\nu-5)\right]\right\}$$

$$\lambda_8(\xi,\eta) = k\eta\left\{1+\frac{\xi^2}{r^2}\left[1-2\nu-8\nu^2+\frac{2\xi^2}{r^2}(4\nu-1)\right]\right\}$$

$$\lambda_9(\xi,\eta) = k\xi\left\{-8\nu^2+8\nu-1+\frac{\eta^2}{r^2}\left[8\nu^2-14\nu+3+\frac{2\eta^2}{r^2}(4\nu-1)\right]\right\}$$

$$\lambda_{10}(\xi,\eta) = k\xi\left\{-8\nu^2+14\nu-6+\frac{\eta^2}{r^2}\left[8\nu^2-22\nu+13+\frac{2\eta^2}{r^2}(4\nu-5)\right]\right\}$$

$$\lambda_{11}(\xi,\eta) = -\lambda_4(\eta,\xi)$$

$$\lambda_{12}(\xi,\eta) = -\lambda_6(\eta,\xi)$$

$$\lambda_{13}(\xi,\eta) = -\lambda_5(\eta,\xi)$$

$$\lambda_{14}(\xi,\eta) = -\lambda_1(\eta,\xi)$$

$$\lambda_{15}(\xi,\eta) = -\lambda_3(\eta,\xi)$$

$$\lambda_{16}(\xi,\eta) = -\lambda_2(\eta,\xi)$$

$$\lambda_{17}(\xi,\eta) = -\lambda_{10}(\eta,\xi)$$

$$\lambda_{18}(\xi,\eta) = -\lambda_9(\eta,\xi)$$

$$\lambda_{19}(\xi,\eta) = -\lambda_8(\eta,\xi)$$

$$\lambda_{20}(\xi,\eta) = -\lambda_7(\eta,\xi)$$

$$
\begin{aligned}
\lambda_{21}(\xi,\eta) &= \frac{k\xi}{r^2}\left(\frac{2\xi^2}{r^2}+1-2\nu\right)\\
\lambda_{22}(\xi,\eta) &= k\left[\frac{\xi^2}{r^2}\left(\frac{4\nu^2-5\nu+2}{1-2\nu}+\frac{2\xi^2}{r^2}\right)-\left(\frac{4\nu^2-7\nu+3}{1-2\nu}\right)\ln r\right]\\
\lambda_{23}(\xi,\eta) &= k\left[\frac{\xi\eta}{r^2}\left(\frac{1}{2}-2\nu-\frac{2\xi^2}{r^2}\right)-2(1-\nu)\arctan\left(\frac{\eta}{\xi}\right)\right]\\
\lambda_{24}(\xi,\eta) &= \frac{k\eta}{r^2}\left(\frac{2\xi^2}{r^2}+1-2\nu\right)\\
\lambda_{25}(\xi,\eta) &= \frac{k\xi\eta}{r^2}\left(\frac{2\xi^2}{r^2}+\frac{3}{2}-2\nu\right)\\
\lambda_{26}(\xi,\eta) &= k\left[\frac{\xi^2}{r^2}\left(\frac{4\nu^2+\nu-2}{2\nu-1}-\frac{2\xi^2}{r^2}\right)-\left(\frac{\nu-1}{2\nu-1}\right)\ln r\right]\\
\lambda_{27}(\xi,\eta) &= k\xi\left\{1+\frac{\eta^2}{r^2}\left[-8\nu^2+22\nu-17+\frac{2\eta^2}{r^2}(5-4\nu)\right]\right\}\\
\lambda_{28}(\xi,\eta) &= k\xi\left\{2(1-\nu)+\frac{\eta^2}{r^2}\left[-8\nu^2+14\nu-3+\frac{2\eta^2}{r^2}(1-4\nu)\right]\right\}\\
\lambda_{29}(\xi,\eta) &= k\eta\left\{8\nu^2-14\nu+6+\frac{\xi^2}{r^2}\left[-8\nu^2+6\nu-1+\frac{2\xi^2}{r^2}(4\nu-1)\right]\right\}\\
\lambda_{30}(\xi,\eta) &= k\eta\left\{8\nu^2-20\nu+11+\frac{\xi^2}{r^2}\left[-8\nu^2+14\nu-3+\frac{2\xi^2}{r^2}(4\nu-5)\right]\right\}\\
\lambda_{31}(\xi,\eta) &= -\lambda_{24}(\eta,\xi)\\
\lambda_{32}(\xi,\eta) &= -\lambda_{26}(\eta,\xi)\\
\lambda_{33}(\xi,\eta) &= -\lambda_{25}(\eta,\xi)\\
\lambda_{34}(\xi,\eta) &= -\lambda_{21}(\eta,\xi)\\
\lambda_{35}(\xi,\eta) &= -\lambda_{23}(\eta,\xi)\\
\lambda_{36}(\xi,\eta) &= -\lambda_{22}(\eta,\xi)\\
\lambda_{37}(\xi,\eta) &= -\lambda_{30}(\eta,\xi)\\
\lambda_{38}(\xi,\eta) &= -\lambda_{29}(\eta,\xi)\\
\lambda_{39}(\xi,\eta) &= -\lambda_{28}(\eta,\xi)\\
\lambda_{40}(\xi,\eta) &= -\lambda_{27}(\eta,\xi)
\end{aligned}
$$

where,

$$k=\frac{1}{4\pi(1-\nu)} \quad \& \quad r^2=\xi^2+\eta^2$$

APPENDIX III

A boundary contour formulation for design sensitivity analysis in two-dimensional linear elasticity.

A BOUNDARY CONTOUR FORMULATION FOR DESIGN SENSITIVITY ANALYSIS IN TWO-DIMENSIONAL LINEAR ELASTICITY

(Final revised version, May 1997.
Accepted for publication in *International Journal of Solids and Structures*)

Anh-Vũ Phan
Graduate Student
Department of Mechanical Engineering
Ecole Polytechnique
Montréal, Québec
Canada H3C 3A7

Subrata Mukherjee
Professor
Department of Theoretical and Applied Mechanics
Cornell University
Ithaca, NY 14853
USA

J.R. René Mayer
Assistant Professor
Department of Mechanical Engineering
Ecole Polytechnique
Montréal, Québec
Canada H3C 3A7

Abstract

A formulation for computing first-order shape design sensitivities in two-dimensional (2-D) linear elastostatics by the boundary contour method (BCM), along with a numerical implementation using quadratic boundary elements, is presented in this paper. Here, the direct differentiation approach is analytically applied to the appropriate boundary contour equations in order to derive the sensitivities of all the physical quantities (displacements, tractions and stresses) on the boundary as well as those for displacements and stresses inside the body under consideration. The nonsingular formulation of the BCM is used for computing the boundary displacements, and boundary stresses at "off contour" regular points. A regular boundary point is a point on the boundary where it is locally smooth; an off contour point lies inside a boundary element. Their corresponding sensitivities are obtained in a straightforward manner from the resulting regular sensitivity formulation. Also, the stress sensitivities at the boundary nodes can be recovered easily from the global displacement shape functions described in a Cartesian coordinate system. Finally, through three numerical examples for which analytical solutions exist, it is shown that the BCM can provide remarkably accurate numerical results for shape sensitivities.

1. INTRODUCTION

The conventional Boundary Element Method (BEM) for linear elasticity requires the numerical evaluation of line integrals for two-dimensional (2-D) problems and surface integrals for three-dimensional (3-D) ones (see, for example, Mukherjee, 1982 or Banerjee, 1994). By observing that the integrand vector of this Boundary Integral Equation (BIE) without body forces is divergence free, Nagarajan *et al.* (1994, 1996) have proposed a novel approach, called the BCM, that achieves a further reduction in dimension. The divergence free property allows, for 3-D problems, the use of Stokes' theorem to transform surface integrals on the usual boundary elements into line integrals on the bounding contours of these elements. For 2-D problems, a similar transformation eliminates numerical integration altogether. The

above transformations are quite general and apply to boundary elements of arbitrary shape. Thus, the BCM requires only numerical evaluation of line integrals for 3-D problems and simply the evaluation of functions (called potential functions) at points on the boundary of a body for 2-D cases.

The BCM is a young method and further developments of this approach are under way. A hypersingular BCM (HBCM) formulation for linear elasticity has been proposed recently (Mukherjee and Mukherjee, 1997-a,-b; Phan *et al.*, 1997-b). This formulation can possibly be extended to solve fracture mechanics problems. It is pointed out in Nagarajan *et al.* (1994) that the divergence free property of the BEM intergrand holds true for other linear problems besides potential therory and linear elasticity. Thus, in principle, it is possible to derive BCM formulations for other linear problems such as plate bending, transient heat conduction with uniform initial temperature, and thermoelasticity; although such formulations have not been derived yet. Finally, body forces that can be modeled as particular integrals in the usual BEM (see, for exemple, Banerjee, 1994) can also be modeled in the same way by the BCM. Thus, at least in principle, the BCM is a fairly general approach for linear problems. The method, however, is not recommended for nonlinear problems, since the primary advantage of a further reduction in dimension, compared to the usual BEM, would, in general, be lost in these cases.

Most shape optimization problems employ mathematical programming methods where design sensitivity coefficients (DSCs), which are defined as the rates of change of physical response quantities with respect to changes in the design variables, are required for determination of the optimum shape of a body.

Unlike the well-known finite element method (FEM), the BEM requires only discretization on the boundary of a body. This characteristic provides significant advantages in its use in shape optimal design where mesh generation needs to be redone after each iterative step of the optimization process. Therefore, several researchers have used the BEM to develop efficient approaches for computing design sensitivities. The reader is referred to a special issue of *Engineering Analysis with Boundary Elements* (Bui and Bonnet, 1995) for a recent discussion of sensitivity

analysis with the BEM. As in the context of the FEM, there are three methods (e.g. Haug *et al.*, 1986 or Sokolowski and Zolesio, 1992), namely, the finite difference approach (FDA), the adjoint structure approach (ASA) and the direct differentiation approach (DDA).

Besides having the same advantage in mesh generation as for the conventional BEM, the BCM offers a further reduction in dimension, and especially, a nonsingular formulation for computing boundary displacements and boundary stresses at regular points inside a boundary element (see Phan *et al.*, 1997-a). Moreover, the stresses at boundary nodes can be recovered easily and exactly from the global displacement shape functions expressed in Cartesian coordinates. These advantages of the BCM are expected to make it very competitive in optimal shape design.

To that purpose, this paper presents a formulation for computing first-order design sensitivities based on a full development of the BCM for 2-D linear elasticity with quadratic boundary elements which has been introduced by Phan *et al.* (1997-a). In this paper, we develop a formulation for design sensitivities by direct differentiation of the BCM equations, i.e. by using the DDA. In the context of the BEM for elastostatics, the DDA has been used by Barone and Yang (1988), Kane and Saigal (1988), Zhang and Mukherjee (1991), and Mellings and Aliabadi (1995) for 2-D problems, by Saigal *et al.* (1989), and Rice and Mukherjee (1990) for axisymmetric problems, by Aithal *et al.* (1991), Kane *et al.* (1992), and Bonnet (1995) for 3-D bodies, and by Mukherjee and Chandra (1991), and Chandra and Mukherjee (1997) for 2-D nonlinear problems.

The DDA may be applied either before or after discretization of the initial BIE. The two processes are expected to lead to the same equations. Kane and Saigal (1988) generated the desired DSCs by differentiating the resulting BEM system matrix analytically. In these formulations, the authors have placed the source points outside the region to avoid singular integrations. Barone and Yang (1988) carried out the opposite process by differentiating the BIE to obtain the DSCs analytically before numerical integration. Here, the rigid body motion technique has been employed to treat singular integral terms in the calculation of displacement sensitivities,

but the integration of strongly singular kernels is required in a direct formula used in computing stress sensitivities. Zhang and Mukherjee (1991) overcame this difficulty related to the singular feature of the governing BIE by using a 2-D elastic BIE formulated in terms of tangential gradient of displacements where the sensitivity of boundary stresses is recovered from the corresponding tractions and tangential gradients of displacements and their sensitivities. In order to avoid strongly singular integrals involved in design sensitivity analysis, Bonnet (1995) applied the material derivative concept to the regularized displacement boundary integral equation.

It can be seen from the above papers that most authors limit their calculations to design sensitivities on the boundary of a body.

The formulation described in this work includes the DSCs of all diplacements and stresses throughout the domain of interest, i.e., on the boundary as well as inside the body. DSCs are obtained from completely regularized equations. There is no need to evaluate any singular integrals as in the BEM work of Barone and Yang (1988). In fact, for 2-D linear elasticity, the BCM does not require the numerical evaluation of any integral at all!

Three examples, including Lamé , Kirsch and a plate with an elliptical cutout, are solved and compared against analytical solutions. The numerical results are very accurate for these illustrative examples.

2. 2-D BCM FORMULATIONS

The information presented in this section is summarized from Phan *et al.* (1997-a) where more details can be found.

2.1. Basic formulation

The idea of dimensional reduction starts from the standard BIE without body forces (see Rizzo, 1967)

$$c_{ik}(P)u_i(P) = \int_{\partial B} [U_{ik}(P,Q)\sigma_{ij}(Q) - \Sigma_{ijk}(P,Q)u_i(Q)]\,\mathbf{e}_j \cdot d\mathbf{S} \qquad (1)$$

where c_{ik} is the corner tensor, P, Q, u_i and σ_{ij} are the source point, field point, displacement vector and stress tensor respectively, U_{ik} and Σ_{ijk} are the Kelvin kernel tensors (Rizzo, 1967), and $\mathbf{e}_j$ are global Cartesian unit vectors. In 2-D problems, ∂B is the boundary of a body B, and $d\mathbf{S}$ is an infinitesimal boundary length vector.

Let $\mathbf{F}_k = [U_{ik}(P,Q)\sigma_{ij}(Q) - \Sigma_{ijk}(P,Q)u_i(Q)]\,\mathbf{e}_j$. Since the divergence of $\mathbf{F}_k$ at a field point Q is zero (see Nagarajan *et al.*, 1994), i.e.

$$\nabla_Q \cdot \mathbf{F}_k = 0 \tag{2}$$

everywhere except at the source point P, so after discretizing the boundary ∂B into n elements, the BIE (1) can be converted to the following BCM version

$$c_{ik}(P)u_i(P) = \sum_{\ell=1}^{n} \left[\Phi_k^{(\ell)}(E_{\ell 2}) - \Phi_k^{(\ell)}(E_{\ell 1})\right] \tag{3}$$

Here, $E_{\ell 1}$ and $E_{\ell 2}$ are the endpoint nodes of element (ℓ), and Φ_k are called the main potential functions that are determined by solving the following identity that satisfies eqn (2)

$$\mathbf{F}_k = \frac{\partial \Phi_k}{\partial y}\mathbf{e}_1 - \frac{\partial \Phi_k}{\partial x}\mathbf{e}_2 \tag{4}$$

A numerical implementation of eqn (3) does not require any numerical integration.

2.2. Formulation using the rigid body motion technique

In order to regularize Cauchy singular integrals in eqn (1), a rigid body motion solution is applied to this equation to produce a new equation

$$\int_{\partial B} \{U_{ik}(P,Q)\sigma_{ij}(Q) - \Sigma_{ijk}(P,Q)\,[u_i(Q) - u_i(P)]\}\,\mathbf{e}_j \cdot d\mathbf{S} = 0 \tag{5}$$

Since the new integrand vector $\mathbf{G}_k = \{U_{ik}(P,Q)\sigma_{ij}(Q) - \Sigma_{ijk}(P,Q)[u_i(Q) - u_i(P)]\}\mathbf{e}_j$ is still divergence free (everywhere except at P), eqn (5) can be converted to the following corresponding BCM version

$$\sum_{\ell=1}^{n} \left[\Psi_k^{(\ell)}(E_{\ell 2}) - \Psi_k^{(\ell)}(E_{\ell 1})\right] = 0 \tag{6}$$

where Ψ_k is determined by solving the following identity

$$\mathbf{G}_k = \frac{\partial \Psi_k}{\partial y}\mathbf{e}_1 - \frac{\partial \Psi_k}{\partial x}\mathbf{e}_2 \tag{7}$$

2.3. Implementation with quadratic boundary elements

Quadratic shape functions that ensure the divergence free property of $\mathbf{F}_k$ and $\mathbf{G}_k$ are given by

$$\begin{Bmatrix} u_1 \\ u_2 \end{Bmatrix} = \beta_1 \begin{Bmatrix} 1 \\ 0 \end{Bmatrix} + \beta_2 \begin{Bmatrix} x \\ 0 \end{Bmatrix} + \beta_3 \begin{Bmatrix} y \\ 0 \end{Bmatrix} + \beta_4 \begin{Bmatrix} 0 \\ 1 \end{Bmatrix} + \beta_5 \begin{Bmatrix} 0 \\ x \end{Bmatrix} + \beta_6 \begin{Bmatrix} 0 \\ y \end{Bmatrix} + \beta_7 \begin{Bmatrix} x^2 \\ k_2 xy \end{Bmatrix} + \beta_8 \begin{Bmatrix} y^2 \\ k_1 xy \end{Bmatrix} + \beta_9 \begin{Bmatrix} k_1 xy \\ x^2 \end{Bmatrix} + \beta_{10} \begin{Bmatrix} k_2 xy \\ y^2 \end{Bmatrix} \tag{8}$$

where $k_1 = -2(1-2\nu)$, $k_2 = -4(1-\nu)$ and ν is the Poisson's ratio.

In matrix form, for element (ℓ)

$$\left\{u^{(\ell)}\right\} = [T_u^{(\ell)}(x,y)]\{\beta^{(\ell)}\} \tag{9}$$

where $\{\beta^{(\ell)}\} = \langle \beta_1^{(\ell)} \ \beta_2^{(\ell)} \ \dots \ \beta_{10}^{(\ell)} \rangle^T$.

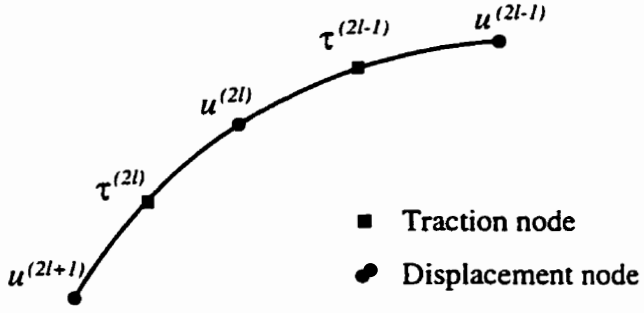

Figure 1: Quadratic boundary element.

The configuration of a chosen quadratic boundary element is shown in Fig. 1. The relationship between the physical variable vector $\left\{p^{(\ell)}(x,y)\right\}$ and the artificial variable vector $\left\{\beta^{(\ell)}\right\}$ of boundary element (ℓ) are

$$\begin{aligned} \{p^{(\ell)}\} &= \left\langle u_1^{(2\ell-1)} \ u_2^{(2\ell-1)} \ \tau_1^{(2\ell-1)} \ \tau_2^{(2\ell-1)} \ u_1^{(2\ell)} \ u_2^{(2\ell)} \ \tau_1^{(2\ell)} \ \tau_2^{(2\ell)} \ u_1^{(2\ell+1)} \ u_2^{(2\ell+1)} \right\rangle^T \\ &= [T^{(\ell)}(x,y)]\{\beta^{(\ell)}\} \end{aligned} \tag{10}$$

A new coordinate system (ξ, η) centered at each source point is introduced. Equation (9) becomes

$$\left\{u^{(\ell)}\right\} = [T_u^{(\ell)}(\xi, \eta)]\{\hat{\beta}^{(\ell)}\} \tag{11}$$

In eqn (11),

$$\{\hat{\beta}^{(\ell)}\} = [B_j]\{\beta^{(\ell)}\} \tag{12}$$

where $[B_j]$ is a matrix depending only on the coordinates of the source point j (since it arises from a coordinate transformation from the global system (x, y) to a system (ξ, η) centerd at j).

3. DESIGN SENSITIVITY ANALYSIS

3.1. Notation

If the boundary ∂B of a 2-D body B is discretized into n boundary elements, then there are n endpoint nodes. Corners are always endpoint nodes. For convenience, let us define

- The boundary ∂B^* as the set of points belonging to the boundary ∂B except the n endpoint nodes. In other words,

  $$\{\text{The whole boundary } \partial B\} \equiv \{\text{The boundary } \partial B^*\} \bigcup \{n \text{ endpoint nodes}\}$$

- The domain B^* as the set of points belonging to the body B except these n endpoint nodes, i.e.

  $$\{\text{The whole domain } B\} \equiv \{\text{The domain } B^*\} \bigcup \{n \text{ endpoint nodes}\}$$

3.2. Boundary displacement sensitivities at displacement nodes and traction sensitivities at traction nodes

As seen in the earlier work by Phan *et al.* (1997-a) the numerical implementation of eqn (6) leads to

$$\left\{\sum_{\ell=1}^{n}\left[\Psi_k^{(\ell)}(E_{\ell 2}) - \Psi_k^{(\ell)}(E_{\ell 1})\right]\right\} = \sum_{\ell=1}^{n}\left[M^{(j\ell)}\right]\left\{p^{(\ell)}\right\} = \{0\} \tag{13}$$

where

$$\left[M^{(j\ell)}\right] = \left[\Psi^{(j\ell)}\right] [B_j] \left[T^{(\ell)}\right]^{-1} \tag{14}$$

in which $\left[\Psi^{(j\ell)}\right]$ is the matrix associated with the main potential functions Ψ_k and is evaluated in the coordinate system (ξ, η).

The DSCs under consideration can be found by differentiating eqn (13) with respect to a design variable b, which is a typical component of a shape design vector $\mathbf{b}$. We have

$$\sum_{\ell=1}^{n} \left(\left[\dot{M}^{(j\ell)}\right] \left\{p^{(\ell)}\right\} + \left[M^{(j\ell)}\right] \left\{\dot{p}^{(\ell)}\right\} \right) = \{0\} \tag{15}$$

where $\dot{(\ )}$ denotes the total derivative with respect to b, i.e. $\dot{(\ )} = d(\ )/db$ and generally,

$$\dot{(\ )} = (\ )_{,b} + v_i (\ )_{,i} \tag{16}$$

It is noted here that in order to avoid any ambiguities that might result from the use of the above notation for the total derivative of a long expresion, the alternative notation $(\ )^{\cdot}$ is used in such cases.

In eqn (16), the quantities $v_i = dx_i/db$ are the components of the design velocity field. For 2-D cases, $x_1 \equiv x$ and $x_2 \equiv y$, thus eqn (16) can be expanded to

$$\dot{(\ )} = (\ )_{,b} + (\ )_{,x} \dot{x} + (\ )_{,y} \dot{y} \tag{17}$$

This total derivative is totally analogous to the concept of the material derivative (often taken with respect to time) in continuum mechanics.

It can be proved that $\left[\dot{\Psi}^{(j\ell)}\right] = \left[\dot{\Phi}^{(j\ell)}\right]$ ($\left[\Phi^{(j\ell)}\right]$ is the matrix associated with the main potential functions Φ_k), therefore eqn (14) leads to

$$\left[\dot{M}^{(j\ell)}\right] = \left[\dot{\Phi}^{(j\ell)}\right] [B_j] \left[T^{(\ell)}\right]^{-1} + \left[\Psi^{(j\ell)}\right] [\dot{B}_j] \left[T^{(\ell)}\right]^{-1} + \left[\Psi^{(j\ell)}\right] [B_j] \left[\left[T^{(\ell)}\right]^{-1}\right]^{\cdot} \tag{18}$$

in which

$$[\dot{B}_j] = [B_j]_{,x} \dot{x}\,(x_j, y_j) + [B_j]_{,y} \dot{y}\,(x_j, y_j) \tag{19}$$

$$\left[\left[T^{(\ell)}\right]^{-1}\right]^{\cdot} = -\left[T^{(\ell)}\right]^{-1} \left[\dot{T}^{(\ell)}\right] \left[T^{(\ell)}\right]^{-1} \tag{20}$$

$$\left[\overset{*}{T}^{(\ell)}\right] = \left[T^{(\ell)}_{gh,n_x}\ \overset{*}{n}_x + T^{(\ell)}_{gh,n_y}\ \overset{*}{n}_y + T^{(\ell)}_{gh,x}\ \overset{*}{x} + T^{(\ell)}_{gh,y}\ \overset{*}{y}\right] \tag{21}$$

($T^{(\ell)}_{gh}$ are the components of matrix $\left[T^{(\ell)}\right]$, n_x and n_y are the components of the outward normal vector to ∂B), and the components of matrix $\left[\overset{*}{\Phi}^{(j\ell)}\right]$ are given by (let $z = h + 10(k-1)$ where $h = 1, \ldots, 10$)

$$\begin{aligned}
\overset{*}{\phi}^{(j\ell)}_{ki} &= \overset{*}{\phi}_z(\xi_{\ell 2}, \eta_{\ell 2}) - \overset{*}{\phi}_z(\xi_{\ell 1}, \eta_{\ell 1}) \\
&= \frac{\partial \phi_z(\xi_{\ell 2}, \eta_{\ell 2})}{\partial \xi}\left[\overset{*}{x}(x_{\ell 2}, y_{\ell 2}) - \overset{*}{x}(x_j, y_j)\right] \\
&+ \frac{\partial \phi_z(\xi_{\ell 2}, \eta_{\ell 2})}{\partial \eta}\left[\overset{*}{y}(x_{\ell 2}, y_{\ell 2}) - \overset{*}{y}(x_j, y_j)\right] \\
&- \frac{\partial \phi_z(\xi_{\ell 1}, \eta_{\ell 1})}{\partial \xi}\left[\overset{*}{x}(x_{\ell 1}, y_{\ell 1}) - \overset{*}{x}(x_j, y_j)\right] \\
&- \frac{\partial \phi_z(\xi_{\ell 1}, \eta_{\ell 1})}{\partial \eta}\left[\overset{*}{y}(x_{\ell 1}, y_{\ell 1}) - \overset{*}{y}(x_j, y_j)\right]
\end{aligned} \tag{22}$$

The potential functions ϕ_z are listed in the Appendix of the paper by Phan *et al.* (1997-a) and the determination of their gradients $\partial\phi_z/\partial\xi$ and $\partial\phi_z/\partial\eta$ are also addressed in that paper. It should be noted that $\partial\phi_z/\partial\xi$ and $\partial\phi_z/\partial\eta$ are singular when $Q(x_\ell, y_\ell) \to P(x_j, y_j)$, i.e. when $(\xi, \eta) \to (0, 0)$. But in this case $\left[\overset{*}{x}(x_\ell, y_\ell) - \overset{*}{x}(x_j, y_j)\right] = \left[\overset{*}{y}(x_\ell, y_\ell) - \overset{*}{y}(x_j, y_j)\right] \sim O(r)$, thus, unlike $\left[\Phi^{(j\ell)}\right]$, the matrix $\left[\overset{*}{\Phi}^{(j\ell)}\right]$ is completely regular.

The advantage of the equality $\left[\overset{*}{\Psi}^{(j\ell)}\right] = \left[\overset{*}{\Phi}^{(j\ell)}\right]$ lies in the fact that the evaluation of $\left[\overset{*}{\Phi}^{(j\ell)}\right]$ is more convenient than that of $\left[\overset{*}{\Psi}^{(j\ell)}\right]$ and the expression (22) can be reused in the computation of DSCs in the domain B^*, as discussed later in this paper.

Displacement continuity across elements is now applied to system (15) which results in the new system of equations

$$\left[\overset{*}{M}^{(j)}\right]\{p\} + \left[M^{(j)}\right]\{\overset{*}{p}\} = \{0\} \tag{23}$$

where $\{p\}$ and $\{\overset{*}{p}\}$ are the degrees of freedom (DOF) and their sensitivities, respectively, on the whole boundary ∂B.

With $2n$ source points corresponding to $2n$ displacement nodes on the boundary ∂B in the numerical implementation using quadratic boundary elements, one gets $2n$ relations of the form (23) which are now combined into the following linear system

$$\dot{[M]}\ \{p\} + [M]\ \dot{\{p\}} = \{0\} \tag{24}$$

System (24) needs to be split in accordance with the boundary conditions to yield

$$\dot{[A]}\ \{X\} + \dot{[B]}\ \{Y\} + [A]\ \dot{\{X\}} + [B]\ \dot{\{Y\}} = \{0\} \tag{25}$$

where $\{X\}$ and $\{Y\}$ contain, respectively, the unknown and known (from boundary conditions) physical quantities. It is noted that, at this stage, $\{X\}$ is known from the solution of the BCM system $[A]\{X\} = \{Z\}$, where $\{Z\} = [B]\{Y\}$. Furthermore, it is assumed that the boundary conditions are kept fixed during the change of the design variables, so that $\dot{\{Y\}} = \{0\}$. By shifting the known terms to the right hand side, eqn (25) becomes

$$[A]\ \dot{\{X\}} = -\dot{[B]}\ \{Y\} - \dot{[A]}\ \{X\} \tag{26}$$

or,

$$[A]\ \dot{\{X\}} = \{W\} \tag{27}$$

This final linear system is very similar to the BCM system $[A]\{X\} = \{Z\}$. The matrix $[A]$ is identical in both equations. Also, it is generally overdetermined but always consistent and therefore, the rectangular system solving algorithm used to solve the usual BCM equations, can be reused here.

3.3. Displacement sensitivities in the domain B^*

The displacement in the domain B^* is evaluated from eqn (3) which can now be written as (see Phan *et al.*, 1997-a)

$$\gamma\ \{u_k(\mathbf{b}, P)\} = \left\{ \sum_{\ell=1}^{n} [\Phi_k^{(\ell)}(E_{\ell 2}) - \Phi_k^{(\ell)}(E_{\ell 1})] \right\} = \sum_{\ell=1}^{n} \left[\Phi^{(P\ell)}\right] [B_P] \left\{\beta^{(\ell)}\right\} \tag{28}$$

where $\gamma = 0.5$ if the source point P (where displacements are to be computed) is on the boundary ∂B^* and $\gamma = 1$ if P is inside the body B.

Thus, displacement sensitivities in the domain B^* can be found by differentiating eqn (28) with respect to a design variable b. That means

$$\gamma \{u_k(\mathbf{b}, P)\}^* =$$

$$\sum_{\ell=1}^{n} \left\{ \left[\overset{*}{\Phi}{}^{(P\ell)}\right] [B_P] \left\{\beta^{(\ell)}\right\} + \left[\Phi^{(P\ell)}\right] [\overset{*}{B}_P] \left\{\beta^{(\ell)}\right\} + \left[\Phi^{(P\ell)}\right] [B_P] \left\{\overset{*}{\beta}{}^{(\ell)}\right\} \right\} \quad (29)$$

in which $[\overset{*}{B}_P]$ and $\left[\overset{*}{\Phi}{}^{(P\ell)}\right]$ are computed by using eqns (19) and (22) respectively, and since $\left\{\beta^{(\ell)}\right\} = \left[T^{(\ell)}\right]^{-1} \left\{p^{(\ell)}\right\}$ (see (10)), one gets

$$\left\{\overset{*}{\beta}{}^{(\ell)}\right\} = \left[\left[T^{(\ell)}\right]^{-1}\right]^* \left\{p^{(\ell)}\right\} + \left[T^{(\ell)}\right]^{-1} \left\{\overset{*}{p}{}^{(\ell)}\right\} \quad (30)$$

where $\left[\left[T^{(\ell)}\right]^{-1}\right]^*$ is determined by eqn (20) and $\left\{\overset{*}{p}{}^{(\ell)}\right\}$ is known at this stage after the solution of (27) because $\left\{\overset{*}{p}{}^{(\ell)}\right\}$ is derived from $\{\overset{*}{p}\}$ which is formed from $\{\overset{*}{X}\}$ with $\{\overset{*}{Y}\} = \{0\}$.

3.4. Stress sensitivity recovery at boundary traction and endpoint nodes

Stresses can be calculated using Hooke's law,

$$\sigma_{ij} = \lambda \delta_{ij} u_{k,k} + \mu(u_{i,j} + u_{j,i}) \quad (31)$$

where λ and μ are Lamé constants of the material, δ_{ij} is the Kronecker delta ($\equiv 1$ for $i = j$ and $\equiv 0$ for $i \neq j$).

The stress sensitivities are determined by taking the total derivative of eqn (31) with respect to a design variable b to yield

$$\overset{*}{\sigma}_{ij} = \lambda \delta_{ij} (u_{k,k})^* + \mu \left[(u_{i,j})^* + (u_{j,i})^*\right] \quad (32)$$

In order to evaluate (recover) the stress sensitivities at traction nodes where the traction sensitivities are available after the solution of eqn (27), their displacement gradient tensor used in (31) needs to be computed first. It starts from the displacement shape functions (9) whose displacement gradient tensor is given by

$$\left\{u^{(\ell)}\right\}_{,m} = \left[T_u^{(\ell)}(x, y)\right]_{,m} \left\{\beta^{(\ell)}\right\} \quad (33)$$

where m is a field point index for the coordinate system (x, y), i.e. $_{,1} \equiv \partial/\partial x$ and $_{,2} \equiv \partial/\partial y$.

Finally, the sensitivity of the displacement gradient tensor required by eqn (32) is derived from eqn (33)

$$\left\{\left\{u^{(\ell)}\right\}_{,m}\right\}^{\cdot} = \left[\left[T_u^{(\ell)}(x,y)\right]_{,m}\right]^{\cdot} \left\{\beta^{(\ell)}\right\} + \left[T_u^{(\ell)}(x,y)\right]_{,m} \left\{\dot{\beta}^{(\ell)}\right\} \tag{34}$$

in which $\left\{\dot{\beta}^{(\ell)}\right\}$ is evaluated using eqn (30).

The above approach is equivalent to the stress recovery procedure in the usual BEM (see, for example, Kane and Saigal, 1988), but more straighforward, since the global displacement shape functions (9) are employed in the BCM.

For computing stress sensitivities at endpoint nodes, the problem is much easier if the starting point is the displacement expression (11). In this case, the displacement gradients at an endpoint node are, simply:

$$\langle u_{1,1}^{(\ell)} \; u_{1,2}^{(\ell)} \; u_{2,1}^{(\ell)} \; u_{2,2}^{(\ell)} \rangle^T = \langle \hat{\beta}_2^{(\ell)} \; \hat{\beta}_3^{(\ell)} \; \hat{\beta}_5^{(\ell)} \; \hat{\beta}_6^{(\ell)} \rangle^T \tag{35}$$

where (ℓ) is the element containing this endpoint node so that its coordinates are $(\xi, \eta) = (0, 0)$. Therefore, the sensitivity of the displacement gradients required by eqn (32) is

$$\langle \left(u_{1,1}^{(\ell)}\right)^{\cdot} \; \left(u_{1,2}^{(\ell)}\right)^{\cdot} \; \left(u_{2,1}^{(\ell)}\right)^{\cdot} \; \left(u_{2,2}^{(\ell)}\right)^{\cdot} \rangle^T = \langle \dot{\hat{\beta}}_2^{(\ell)} \; \dot{\hat{\beta}}_3^{(\ell)} \; \dot{\hat{\beta}}_5^{(\ell)} \; \dot{\hat{\beta}}_6^{(\ell)} \rangle^T \tag{36}$$

in which the components on the right hand side of eqn (36) are derived from the sensitivity of eqn (12), i.e. from

$$\left\{\dot{\hat{\beta}}^{(\ell)}\right\} = [\dot{B}_j] \; \{\beta^{(\ell)}\} + [B_j] \left\{\dot{\beta}^{(\ell)}\right\} \tag{37}$$

The above procedure from eqn (32) to eqn (34) is simple and it can be used to compute the stress sensitivities on the whole boundary ∂B. Stress sensitivities in the domain B^* can be computed by using the direct formulation addressed in the following section.

3.5. Stress sensitivities in the domain B^*

This kind of sensitivity is also computed using eqn (32). To this end, the first step is to determine the displacement gradient tensor $u_{i,j}$ on the body B^* by taking the partial derivative of eqn (28) with respect to a source point P (see Phan *et al.*, 1997-a) to yield

$$\gamma \{u_{k,M}(\mathbf{b}, P)\} = \sum_{\ell=1}^{n} \left(\left[\Phi^{(P\ell)}\right] [B_P]_{,M} - \left[\Phi^{(P\ell)}\right]_{,\mu} [B_P] \right) \left\{\beta^{(\ell)}\right\} \tag{38}$$

where M is a source point index for the coordinate system (x, y), i.e. $_{,1} \equiv \partial/\partial x(P)$ and $_{,2} \equiv \partial/\partial y(P)$, and μ is a field point index for the coordinate system (ξ, η), i.e. in this case $_{,1} \equiv \partial/\partial \xi$ and $_{,2} \equiv \partial/\partial \eta$.

Then, the sensitivity of the displacement gradient tensor is derived from (38) to give

$$\begin{aligned} \gamma \{u_{k,M}(\mathbf{b}, P)\}^* = \sum_{\ell=1}^{n} \Bigg(& \left[\overset{*}{\Phi}{}^{(P\ell)}\right] [B_P]_{,M} + \left[\Phi^{(P\ell)}\right] \left[[B_P]_{,M}\right]^* - \left[\left[\Phi^{(P\ell)}\right]_{,\mu}\right]^* [B_P] \\ & - \left[\Phi^{(P\ell)}\right]_{,\mu} [\overset{*}{B_P}] \Bigg) \left\{\beta^{(\ell)}\right\} + \sum_{\ell=1}^{n} \left(\left[\Phi^{(P\ell)}\right] [B_P]_{,M} - \left[\Phi^{(P\ell)}\right]_{,\mu} [B_P] \right) \left\{\overset{*}{\beta}{}^{(\ell)}\right\} \end{aligned} \tag{39}$$

In eqn (39),

$$\left[[B_P]_{,M}\right]^* = \begin{cases} \dfrac{\partial^2 [B_P]}{\partial x^2} \overset{*}{x}(x_P, y_P) + \dfrac{\partial^2 [B_P]}{\partial x \partial y} \overset{*}{y}(x_P, y_P) & if\ M = 1 \\ \dfrac{\partial^2 [B_P]}{\partial x \partial y} \overset{*}{x}(x_P, y_P) + \dfrac{\partial^2 [B_P]}{\partial y^2} \overset{*}{y}(x_P, y_P) & if\ M = 2 \end{cases} \tag{40}$$

and the components of matrix $\left[\left[\Phi^{(P\ell)}\right]_{,\mu}\right]^*$ are given by

$$(\phi_{ki,\mu})^* = (\phi_{z,\mu}(\xi_{\ell 2}, \eta_{\ell 2}))^* - (\phi_{z,\mu}(\xi_{\ell 1}, \eta_{\ell 1}))^* \tag{41}$$

in which

$$(\phi_{z,\mu}(\xi_\ell,\eta_\ell))^* = \begin{cases} \dfrac{\partial^2\phi_z(\xi_\ell,\eta_\ell)}{\partial\xi^2}[\overset{*}{x}(x_\ell,y_\ell)-\overset{*}{x}(x_P,y_P)]+ \\ \dfrac{\partial^2\phi_z(\xi_\ell,\eta_\ell)}{\partial\xi\partial\eta}[\overset{*}{y}(x_\ell,y_\ell)-\overset{*}{y}(x_P,y_P)] \quad if\ M=1 \\ \dfrac{\partial^2\phi_z(\xi_\ell,\eta_\ell)}{\partial\xi\partial\eta}[\overset{*}{x}(x_\ell,y_\ell)-\overset{*}{x}(x_P,y_P)]+ \\ \dfrac{\partial^2\phi_z(\xi_\ell,\eta_\ell)}{\partial\eta^2}[\overset{*}{y}(x_\ell,y_\ell)-\overset{*}{y}(x_P,y_P)] \quad if\ M=2 \end{cases} \tag{42}$$

It can be seen from eqn (41) that in order to calculate $\left[\left[\Phi^{(P\ell)}\right]_{,\mu}\right]^*$, one needs to evaluate the second-order gradient of the potential functions ϕ_z, i.e. $\dfrac{\partial^2\phi_z}{\partial\xi^2}$, $\dfrac{\partial^2\phi_z}{\partial\eta^2}$ and $\dfrac{\partial^2\phi_z}{\partial\xi\partial\eta}$.

Three points need to be mentioned with regard to the evaluation of displacement and stress sensitivities on the boundary ∂B^*.

- As demonstrated in the work by Phan *et al.* (1997-a), unlike the conventional BEM, eqns (28) and (38) are completely regular when they are used to calculate displacements and stresses on the boundary ∂B^*. This advantage allows one to derive formulae for the corresponding DSCs directly, as presented above. In the usual BEM, a similar procedure for computing the stress sensitivities on the boundary was presented by Barone and Yang (1988), but the formula involves strongly singular integrals. An approximate formula was introduced in the above work in order to overcome the difficulty.

- When the source point P lies on the boundary ∂B^*, the evaluation of matrix $\left[\Phi^{(P\ell)}\right]$ has to be carried out carefully by using the approach addressed in the earlier work by Phan *et al.* (1997-a).

- The matrix $\left[\Phi^{(P\ell)}\right]$ is singular when the source point P (where the DSCs are to be computed) approaches an endpoint node. Thus, eqns (29) and (39) are only used for calculating DSCs in the domain B^* where endpoint nodes are

excluded. However, the displacement and stress sensitivities at endpoint nodes can be obtained from the equations in sections 3.2 and 3.4, respectively.

4. NUMERICAL EXAMPLES

Three examples are illustrated in this section. The same material data for all these examples are as follows: Young's modulus $E = 2.5$ (in consistent units) and Poisson's ratio $\nu = 0.3$.

4.1. Lamé's problem

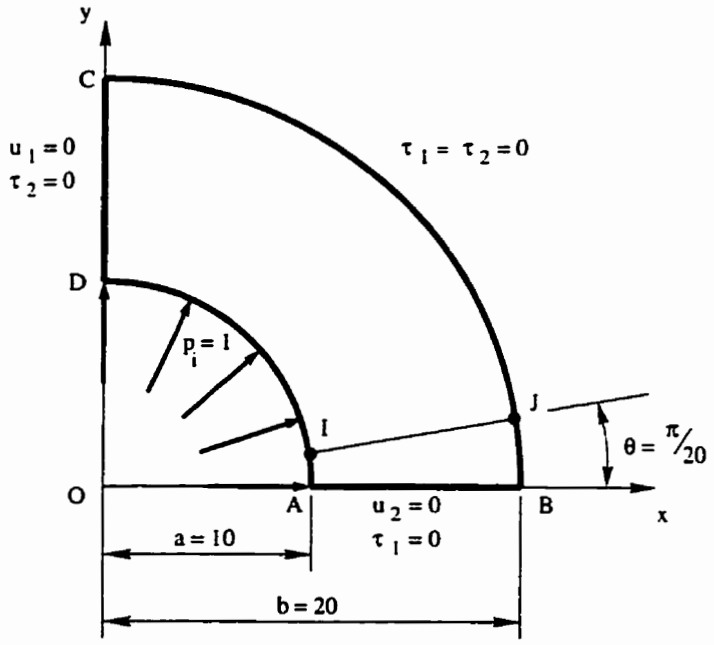

Figure 2: Modeling of Lamé's problem.

Consider a thick cylinder subjected to uniform pressure p_i on the inner surface. Let a and b be the inner and outer radii of the cylinder where a is chosen as the design variable.

The analytical expressions in polar coordinates (r, θ), for the displacement and stress fields of Lamé's problem, are available from Timoshenko and Goodier (1970).

In the case of a plane stress state

$$\left.\begin{aligned} u_r &= \frac{a^2 p_i}{E(b^2-a^2)}\left[(1-\nu)r + (1+\nu)\frac{b^2}{r}\right] \\ \sigma_{r/\theta} &= \frac{a^2 p_i}{b^2-a^2}\left(1 \mp \frac{b^2}{r^2}\right) \end{aligned}\right\} \tag{43}$$

in which, the expressions for σ_r and σ_θ correspond to the upper and lower signs respectively.

By assuming that the geometry changes linearly with the changes of the design variable a, one gets $\dot{r} = (b-r)/(b-a)$ (Chandra and Mukherjee, 1997). So, the analytical sensitivity fields are found by taking the total derivative of eqn (43) with respect to the design variable a (using eqn (16) written in polar coordinates) to give

$$\left.\begin{aligned} \dot{u}_r = & \frac{a^2 p_i}{E(b^2-a^2)}\left[\frac{2b^2}{b^2-a^2}\left\{(1-\nu)r + (1+\nu)\frac{b^2}{r}\right\}\right. \\ & \left. + \frac{a(b-r)}{b-a}\left\{1-\nu-(1+\nu)\frac{b^2}{r^2}\right\}\right] \\ \dot{\sigma}_{r/\theta} = & \frac{2ab^2 p_i}{r^2(b^2-a^2)}\left[\frac{r^2 \mp b^2}{b^2-a^2} \pm \frac{a(b-r)}{r(b-a)}\right] \end{aligned}\right\} \tag{44}$$

Because of the symmetry of the problem, only a quarter of the structure needs to be modeled as shown in Fig. 2. The mesh consists of equal numbers of quadratic boundary elements on each segment of the boundary. Also, all the elements on a given segment are of equal length. In general, a finer mesh ensures better convergence of numerical results, and especially, in the calculation of displacement sensitivities. Figures 3–6 display numerical results obtained by using a total of 60 quadratic elements. Excellent agreement with the analytical solutions is seen. Figures 3 and 4 show numerical results for the DSCs on the boundary AB (see Fig. 2), in which, the approach presented in section 3.4 is employed to recover the stress sensitivities in Fig. 4. Finally, the formulas in section 3.3 and 3.5 are used to compute the displacement sensitivities (Fig. 5) and the stress sensitivities (Fig. 6) on the line segment IJ (see Fig. 2) (domain B^*), respectively.

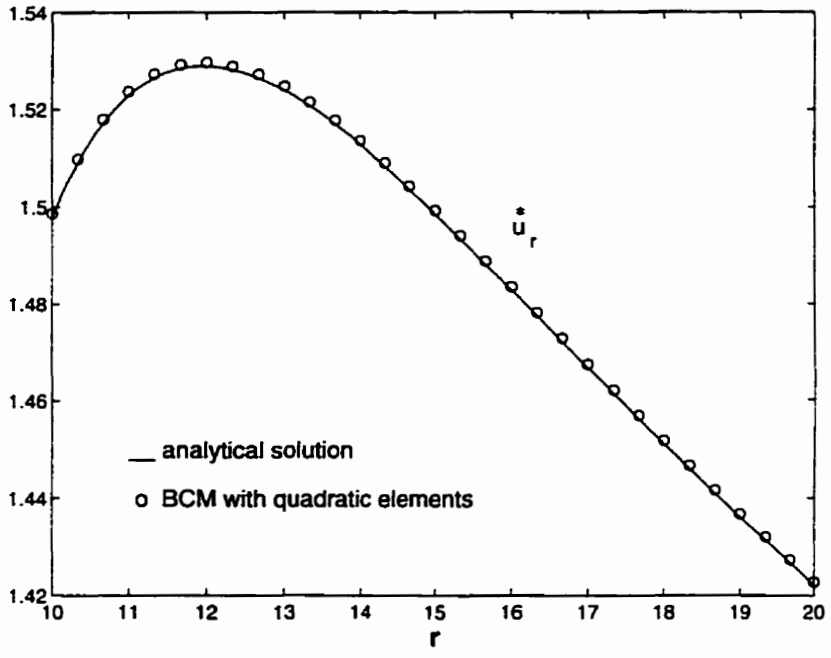

Figure 3: Displacement sensitivity on the edge AB (see Fig. 2).

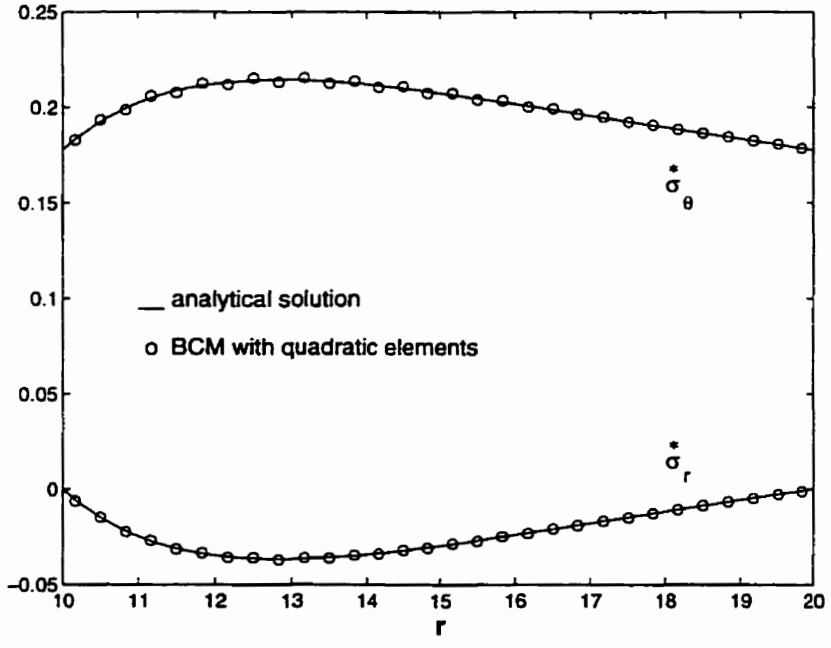

Figure 4: Stress sensitivities on the edge AB (see Fig. 2).

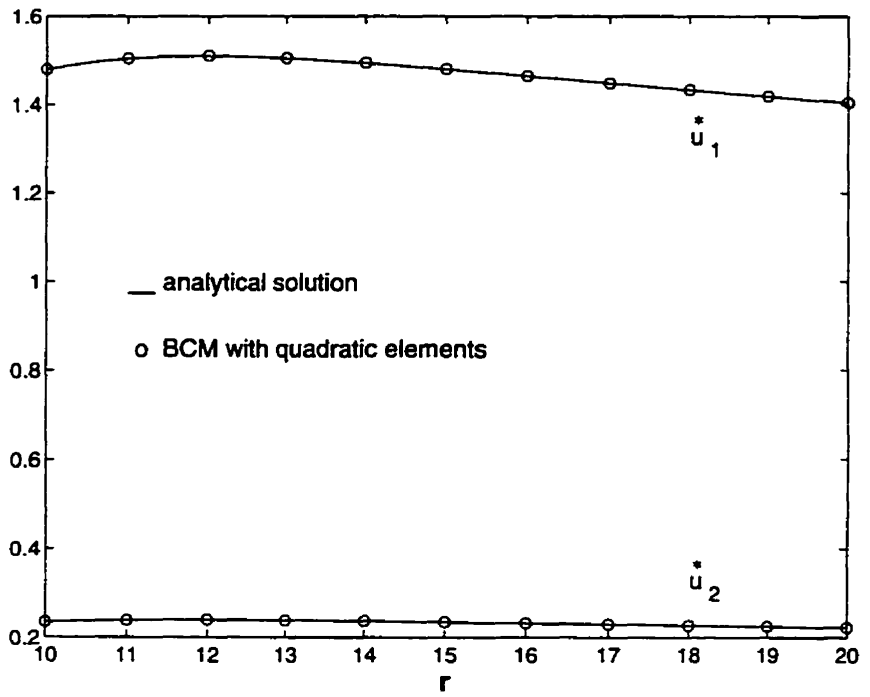

Figure 5: Displacement sensitivities along the line IJ (see Fig. 2).

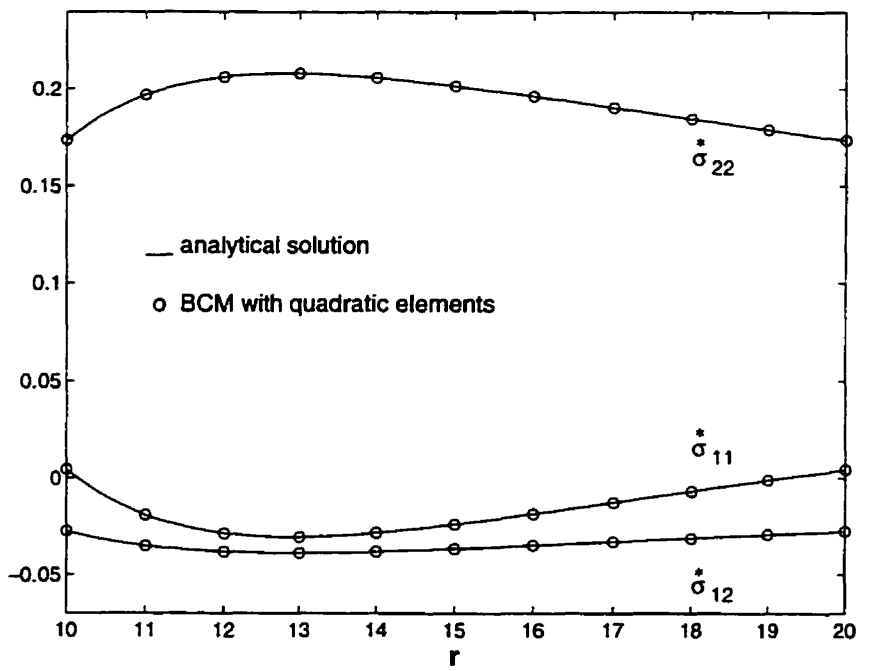

Figure 6: Stress sensitivities along the line IJ (see Fig. 2).

4.2. Kirsch's problem

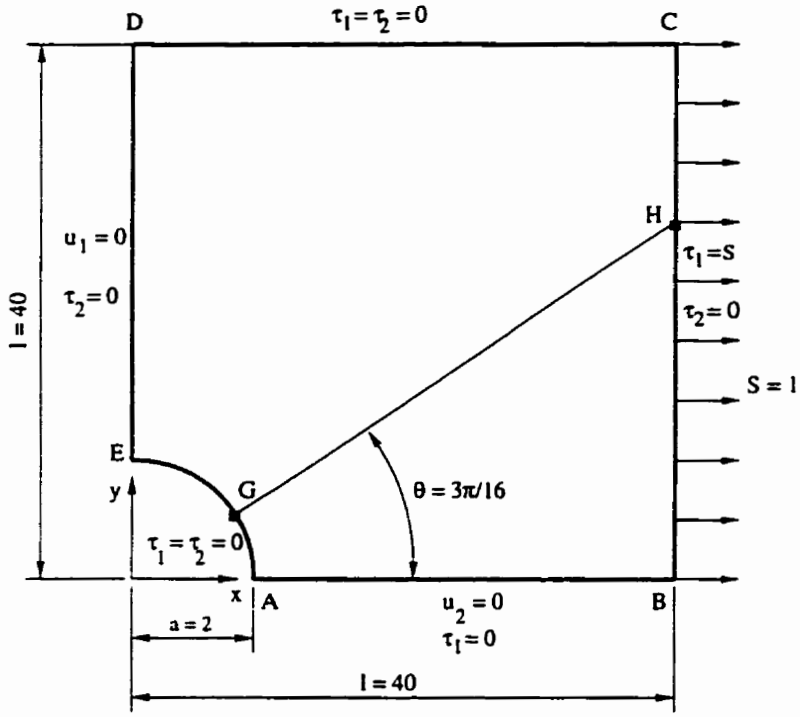

Figure 7: Modeling of Kirsch's problem.

The second example deals with Kirsch's problem. Figure 7 shows a quarter symmetry model of a square plate with a central circular hole of radius a subjected to a unit uniaxial tensile load S. The stress components in polar coordinates (r, θ) are given by Timoshenko and Goodier (1970) as

$$\left.\begin{aligned} \sigma_r &= \frac{S}{2}\left(1-\frac{a^2}{r^2}\right) + \frac{S}{2}\left(1+\frac{3a^4}{r^4}-\frac{4a^2}{r^2}\right)\cos 2\theta \\ \sigma_\theta &= \frac{S}{2}\left(1+\frac{a^2}{r^2}\right) - \frac{S}{2}\left(1+\frac{3a^4}{r^4}\right)\cos 2\theta \\ \tau_{r\theta} &= -\frac{S}{2}\left(1-\frac{3a^4}{r^4}+\frac{2a^2}{r^2}\right)\sin 2\theta \end{aligned}\right\} \tag{45}$$

Here, a is chosen as the design variable. The total derivative of eqn (45) is obtained using the same approach as in the previous example to yield the stress sensitivity fields where, with the same linear assumption as in Lamé's problem, the

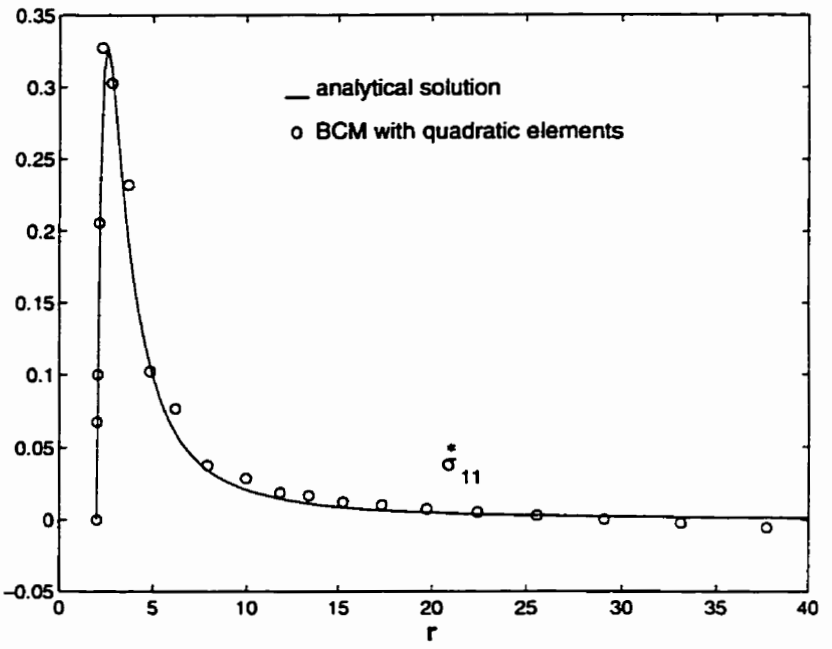

Figure 8: Stress sensitivity $\overset{*}{\sigma}_{11}$ on the edge DE (see Fig. 7).

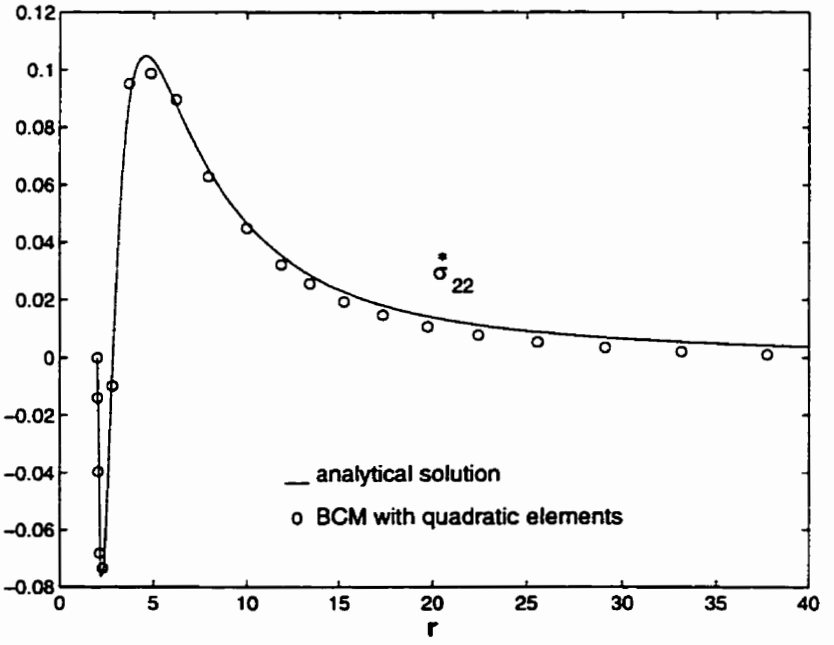

Figure 9: Stress sensitivity $\overset{*}{\sigma}_{22}$ on the edge DE (see Fig. 7).

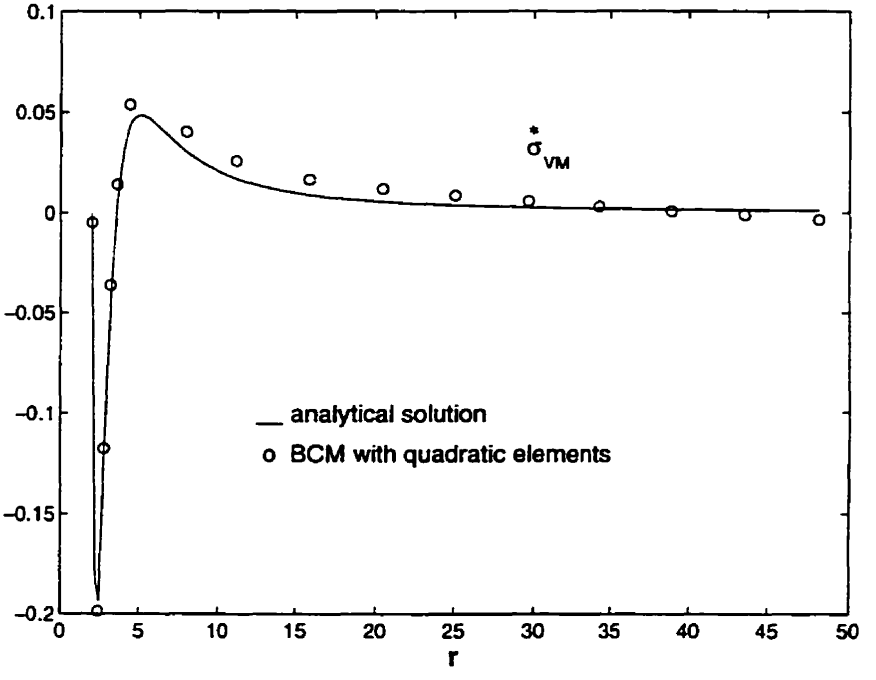

Figure 10: Sensitivity of the von Mises stress along the line GH (see Fig. 7).

geometric sensitivities are given by

$$\left.\begin{aligned} \overset{*}{r} &= \frac{l-r}{l-a} \qquad if \quad r \leq l \\ \overset{*}{r} &= 0 \qquad\quad if \quad r > l \end{aligned}\right\} \tag{46}$$

The boundary contour analysis model is made up of 34 quadratic elements: 10 elements on the edges AB and DE, 4 elements on the edges BC and CD, and 6 elements on the arc EA (see Fig. 7). Due to stress concentrations at the corners A and E, the mesh in this zone needs to be refined: the density of elements on AB and DE is nonuniform, with short elements being placed near the points A and E.

The numerical results for the stress sensitivities on the boundary DE, computed from the approach presented in section 3.4, are shown in Figs 8 and 9. For the stress sensitivities in the domain B^* (along the line segment GH, see Fig. 7), a state of plane stress is employed to analytically compute the sensitivity of the von Mises

stress. The von Mises stress and its sensitivity are:

$$\left.\begin{aligned} \sigma_{VM} &= \sqrt{\sigma_{11}^2 + \sigma_{22}^2 + 3\sigma_{12}^2 - \sigma_{11}\sigma_{22}} \\ \dot{\sigma}_{VM} &= \frac{(2\sigma_{11} - \sigma_{22})\,\dot{\sigma}_{11} + (2\sigma_{22} - \sigma_{11})\,\dot{\sigma}_{22} + 6\sigma_{12}\,\dot{\sigma}_{12}}{2\sigma_{VM}} \end{aligned}\right\} \tag{47}$$

Analytical and numerical results for this quantity are presented in Fig. 10. This time, the formulas in sections 3.3 and 3.5 are used. Reasonably good agreements with the analytical solutions are observed, even though the analytical solutions exhibit some rapid changes along the lines DE and GH in Fig. 7.

4.3. Infinite plate with an elliptical hole

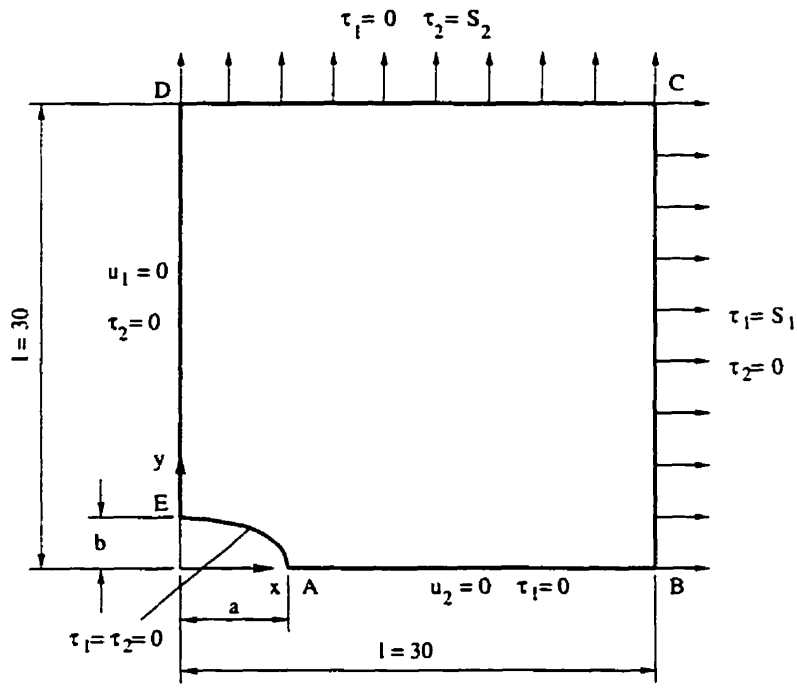

Figure 11: Modeling of a plate with an elliptical hole.

Infinite plates with elliptical holes, subjected to uniform biaxial tensions S_1 and S_2, are studied in this example. Because of symmetry, only a quarter of a plate needs to be modeled as shown in Fig. 11. Let a and b be, respectively, the semi-major and semi-minor axes of the hole. Two cases are considered here:

a) $S_1 = 0$, $S_2 = 1$, $a = 2$ and $b = 1$ in which a is chosen as the design variable. The same data as in the work of Zhang and Mukherjee (1991) (where the derivative BEM was employed) are used here for the purpose of comparison. Graded meshes with 11 elements each are used on each of the sides AB and DE (due to the stress concentration at A), uniform discretizations (with 4 elements each) are used on each of the sides BC and CD, and 10 elements are placed at equal increments of the eccentric angle ϕ on the elliptical arc EA.

The focus here is on the tangential ("skin") stress σ_s on the hole boundary since it is often used as a control parameter in shape design. The analytical solution for σ_s, and its sensitivity for this case, are presented by Barone and Yang (1988).

Numerical and analytical solutions are compared in Figs 12 and 13. It is quite remarkable that the results given from the BCM are seen to have excellent agreement with the exact solution on the entire elliptical hole boundary. Furthermore, Fig. 13 also shows that the present formulation yields better results than those obtained from the BEM by Zhang and Mukherjee (1991). Only very slight numerical oscillations are seen in this figure even though fewer quadratic elements (especially only a half of elements on the elliptical boundary) are employed in this BCM study, as opposed to the previous BEM research. In this work there are 11 elements on each of the segments AB and DE and 10 on EA, compared to 12, 14 and 20 respectively, in the BEM work of Zhang and Mukhejee (1991).

b) $S_1 = 1$, $S_2 = 0.75$ for $\beta = b/a = 0.5, 0.75$ and 1, respectively. The mesh is the same as in the previous case, except that 12 elements each are used on each of the sides AB and DE, and 20 elements are spaced around the arc EA.

The analytical solutions for the stress sentitivities at the points A and E are given by Barone and Yang (1988)

$$\left.\begin{aligned} a\,\dot{\sigma}_{22}\,(A) &= -\frac{1.5}{\beta^2} \\ a\,\dot{\sigma}_{11}\,(E) &= 2 \end{aligned}\right\} \tag{48}$$

Table 1 shows the analytical values of these quantities together with the numerical results obtained by this work (BCM) as well as by the BEM (Chandra and

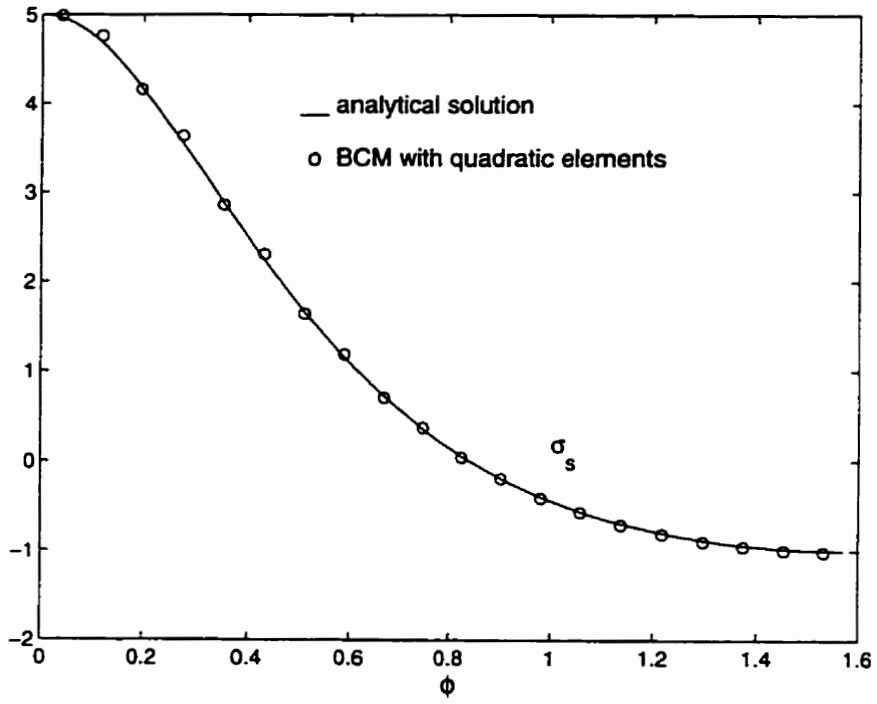

Figure 12: "Skin" stress σ_s on the arc EA (see Fig. 11).

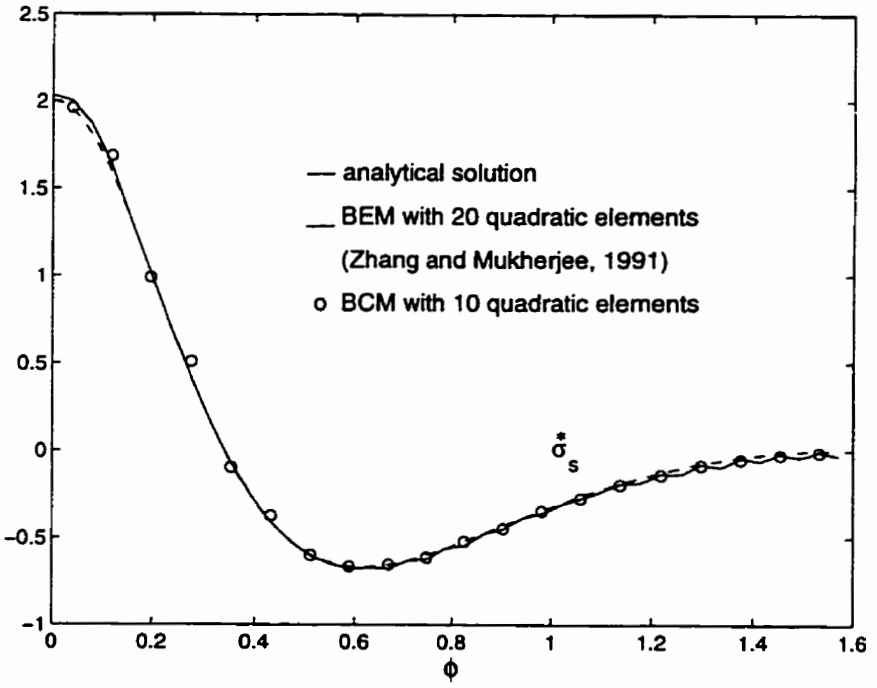

Figure 13: "Skin" stress sensitivity $\overset{*}{\sigma}_s$ on the arc EA (see Fig. 11).

Mukherjee, 1997). It should be noted that in the BCM, numerical results for stresses (and thus, stress sensitivities) are discontinuous at endpoint nodes. Although this is a minor drawback, it makes the modeling of corners trivial. At endpoint nodes on which the stresses from the analytical solution are continuous, the discontinuity magnitudes produced by the BCM are minor. Hence, it is reasonable to use the average values as final outputs. This kind of output is shown in the Table 1 as the numerical results from the BCM. Again, these results are in excellent agreement with the anlytical ones, and the performance of the BCM in design sensitivity analysis appears to be much superior to the BEM in this exemple.

Table 1: Stress sensitivities at A and E (Fig. 11) for different values of β.

	$a\,\dot{\sigma}_{22}\,(A)$			$a\,\dot{\sigma}_{11}\,(E)$		
β	Analytical	BCM	BEM	Analytical	BCM	BEM
0.5	-6	-5.996	-6.158	2	1.992	2.247
0.75	-2.667	-2.662	-2.983	2	1.992	2.339
1	-1.5	-1.506	-1.828	2	1.994	2.540

5. CONCLUSIONS

A formulation for design sensitivity analysis by the BCM for 2-D linear elasticity is presented in this paper. An implementation is carried out with quadratic boundary elements.

The present formulation deals with the calculation of DSCs throughout the domain of interest, i.e. on the boundary ∂B as well as inside the body B. Since global displacement and stress shape functions are used in the BCM, the nodal stress sensitivities can be recovered in a straightforward manner from these functions and from the results obtained after solving the system (27). For evaluating displacement and stress sensitivities in the domain B^*, direct formulas are developed from the corresponding nonsingular expressions for displacements and stresses in this domain given in Phan *et al.* (1997-a).

It is quite remarkable that the accuracy of numerical results for illustrative problems is seen to be very high. It is felt that the primary reason for this is the complete absence of numerical integration in the BCM for 2-D problems. Another possible reason is that the global displacement shape functions satisfy, a priori, the Navier-Cauchy equilibrium equations (Phan *et al.*, 1997-a). Accuracy and efficiency in design sensitivity analyses are crucial since they lead to faster convergence of iterative procedures in shape optimization.

The DDA developed in this work is advantageous for optimal shape design problems with few design variables and a large number of constraints. For problems involving many design variables and fewer constraints, the ASA is more suitable. The ASA, based on the BCM, is an important subject for future research.

Acknowledgement

Anh-Vũ Phan acknowledges the financial support from the Quebec Ministry of Education through the "Programme québécois de bourses d'excellence".

REFERENCES

Aithal, R., Saigal, S. and Mukherjee, S. (1991). Three dimensional boundary element implicit differentiation formulation for design sensitivity analysis. *Math. Comput. Modelling* **15,** 1.

Banerjee, P.K. (1994). *The Boundary Element Methods in Engineering.* McGraw-Hill, Maidenhead, Berkshire, UK.

Barone, M.R. and Yang, R.J. (1988). Boundary integral equations for recovery of design sensitivities in shape optimization. *AIAA Journal* **26,** 589.

Bonnet, M. (1995). Regularized BIE formulations for first- and second-order shape sensitivity of elastic fields. *Computers & Structures* **56,** 799.

Bui, H.D. and Bonnet, M. (1995). Unknown or variable domains, inverse problems. *Engng Anal. with Boundary Elements* **15** (special issue).

Chandra, A. and Mukherjee, S. (1997). *Boundary Element Methods in Manufacturing.* Oxford University Press, Oxford.

Haug, E.J., Choi, K.K. and Komkov, V. (1986). *Design Sensitivity Analysis of Structural Systems.* Academic Press, New York.

Kane, J.H. and Saigal, S. (1988). Design sensitivity analysis of solids using BEM. *Journal of Engineering Mechanics* **114,** 1703.

Kane, J.H., Zhao, G., Wang, H. and Guru Prasad, K. (1992). Boundary formulations for three-dimensional continuum structural shape sensitivity analysis. *ASME J. Appl. Mech.* **59,** 827.

Mellings, S.C. and Aliabadi, M.H. (1995). Flaw identification using the boundary element method. *Int. J. Numer. Meth. Engng* **38,** 399.

Mukherjee, S. (1982). *Boundary Element Methods in Creep and Fracture.* Elsevier Applied Science, London.

Mukherjee, S. and Chandra, A. (1991). A boundary element formulation for design sensitivities in problems involving both geometric and material nonlinearities. *Math. Comput. Modelling* **15,** 245.

Mukherjee, S. and Mukherjee, Y.X. (1977-a). The hypersingular boundary contour method for three-dimensional linear elasticity - Part I: General theory (submitted for publication).

Mukherjee, S. and Mukherjee, Y.X. (1977-b). The hypersingular boundary contour method for three-dimensional linear elasticity - Part II: Special cases and numerical examples (submitted for publication).

Nagarajan, A., Lutz, E.D. and Mukherjee, S. (1994). A novel boundary element method for linear elasticity with no numerical integration for two-dimensional and line integrals for three-dimensional problems. *ASME J. Appl. Mech.* **61,** 264.

Nagarajan, A., Lutz, E.D. and Mukherjee, S. (1996). The boundary contour method for three-dimensional linear elasticity. *ASME J. Appl. Mech.* **63,** 278.

Phan A.V., Mukherjee, S. and Mayer, J.R.R. (1997-a). The boundary contour method for two-dimensional linear elasticity with quadratic boundary elements. *Comput. Mech.* (in press).

Phan A.V., Mukherjee, S. and Mayer, J.R.R. (1997-b). The hypersingular boundary contour method for two-dimensional linear elasticity (submitted for publication).

Rice, J.R. and Mukherjee, S. (1990). Design sensitivity coefficients for axisymmetric elasticity problems by boundary element methods. *Engng Anal. with Boundary Elements* **7,** 13.

Rizzo, F.J. (1967). An integral equation approach to boundary value problems of classical elastostatics. *Quarterly of Applied Mathematics* **25,** 83.

Saigal, S., Borggaard, J.T. and Kane, J.H. (1989). Boundary element implicit differentiation equations for design sensitivities of axisymmetric structures. *Int. J. Solids Struct.* **25,** 527.

Sokolowski, J. and Zolesio, J.P. (1992). *Introduction to shape optimization. Shape sensitivity analysis.* Springer series in Computational Mathematics (vol. 16), Springer-Verlag.

Timoshenko, S.P. and Goodier, J.N. (1970). *Theory of Elasticity.* McGraw-Hill, New York.

Zhang, Q. and Mukherjee, S. (1991). Design sensitivity coefficients for linear elastic bodies with zones and corners by the derivative boundary element method. *Int. J. Solids Struct.* **27,** 983.

APPENDIX IV

Stresses, stress sensitivities and shape optimization in two-dimensional linear elasticity by the boundary contour method.

STRESSES, STRESS SENSITIVITIES AND SHAPE OPTIMIZATION IN TWO-DIMENSIONAL LINEAR ELASTICITY BY THE BOUNDARY CONTOUR METHOD

(submitted to *International Journal for Numerical Methods in Engineering*)

Anh-Vũ Phan
Graduate Student
Department of Mechanical Engineering
Ecole Polytechnique
Montréal, Québec
Canada H3C 3A7

Subrata Mukherjee
Professor
Department of Theoretical and Applied Mechanics
Cornell University
Ithaca, NY 14853
USA

J.R. René Mayer
Assistant Professor
Department of Mechanical Engineering
Ecole Polytechnique
Montréal, Québec
Canada H3C 3A7

SUMMARY

This paper presents new formulations for computing stresses as well as their sensitivities in two-dimensional (2-D) linear elasticity by the *boundary contour method* (BCM). The formulations are established directly from the boundary contour version of the *hypersingular boundary intergral equation* (HBIE) which can provide accurate numerical results and is very efficient with regard to numerical implementation as well as computational time. The *design sensitivity coefficients* (DSCs) computed from the above formulations or from the primary analysis of the BCM (as done earlier in Reference 1) can then be coupled with a mathematical programming method such as the Successive Quadratic Programming (SQP) algorithm in order to solve shape optimization problems. Numerical examples are presented to demonstrate the validity of the new formulations for calculation of stresses and their sensitivities. Also, shape optimization examples using the BCM are presented here for the first time.

KEY WORDS: boundary contour method; boundary element method; stress analysis; design sensitivity analysis; shape optimization

1. INTRODUCTION

1.1. The boundary contour method

The conventional *boundary element method* (BEM) for linear elasticity requires the numerical evaluation of line integrals for two-dimensional (2-D) problems and surface integrals for three-dimensional (3-D) ones (see, e.g., Reference 2). By observing that the integrand vector of the *boundary integral equations* (BIE) without body forces is divergence free, Nagarajan *et al.*[3,4] have proposed a novel approach, called the BCM, that achieves a further reduction in dimension. The divergence free property allows, for 3-D problems, the use of Stokes' theorem to transform surface integrals on the usual boundary elements into line integrals on the bounding contours of

these elements. For 2-D problems, a similar transformation eliminates numerical integration altogether. The above transformations are quite general and apply to boundary elements of arbitrary shape. Thus, the BCM reduces the dimensionality of analysis problems by two: the method requires only numerical evaluation of 1-D line integrals for 3-D problems and simply the evaluation of functions (called potential functions) at points on the boundary of a body for 2-D cases.

For 3-D elasticity problems, the BCM with quadratic boundary elements has been presented in the literature by Nagarajan *et al.*[4] and by Mukherjee *et al.*[5] The BCM for 2-D linear elasticity is the subject of Nagarajan *et al.*[3] and Phan *et al.*[6] A numerical implementation with linear boundary elements is carried out in the former paper whereas a full development with quadratic boundary element implementation is performed in the latter one. In Reference 6, stresses inside a body and at non-endpoint nodes on its boundary are computed from the boundary contour version of the standard BIE. The advantage of this approach is that it does not require the determination of potential functions because these functions can be derived directly from the Kelvin kernel tensors. The above approach is then employed in Reference 1 to develop a design sensitivity formulation by the BCM.

1.2. Hypersingular formulations for stress and stress sensitivity analysis

The present work also deals with boundary contour formulations for calculation of stresses and their sensitivities by the BCM in 2-D linear elasticity (as in References 6 and 1), but the starting point is a gradient form of the standard BIE which is called the HBIE because this equation is hypersingular if it is collocated at any point on the boundary. Although the potential functions have to be derived for this purpose, it can be seen that the formulations and thus, their numerical implementations, are simpler than those addressed in References 6 and 1. Once these potential functions are published through this paper, they are ready for users.

There are three approaches for design sensitivity analysis (see, e.g., Reference 7), namely, the *finite difference approach* (FDA), the *adjoint structure approach* (ASA) and the *direct differentiation approach* (DDA). In this paper, stress sensitivities are

obtained by direct differentiation of the hypersingular formulation aformentioned, i.e. by using the DDA. In the context of the BEM for elastostatics, the DDA has been used by several researchers for 2-D,[8–10] axisymmetric,[11,12] 3-D[13–15] and 2-D nonlinear problems.[16–18]

It is noted that stresses and stress sensitivities, formulated in this study, are those in the domain B^* (the whole body except the endpoint nodes on its boundary elements). The computations of physical quantities (displacements and stresses), as well as their sensitivities at endpoint nodes, have been addressed before in References 6 and 1.

1.3. Shape optimization using the BCM

Shape optimization refers to the optimal design of the shape of structural components and is of great importance in current mechanical engineering design. Most shape optimization problems employ gradient based mathematical programming methods in which DSCs, which are defined as the rates of change of physical response quantities with respect to changes in the design variables, are required for determination of the optimum shape of a body.

Unlike the well-known *finite element method* (FEM), the BEM only requires discretization on the boundary of a body. Hence, mesh generation and remeshing procedures, required at each new iterative step in a numerical optimization procedure, are much more straightforward and inexpensive than in the FEM. Furthermore, the BEM often provides accurate boundary physical responses (displacements, tractions, stresses). This explains why several researchers have used the BEM to develop efficient approaches for computing DSCs required in solving optimal shape design problems.

Research papers in shape optimization using the BEM have been published by, for example, Choi and Kwak,[19] Sandgren and Wu,[20] Yang,[21] Saigal and Kane,[22] Wei *et al.*,[18] Yamazaki *et al.*[23] and Tafreshi and Fenner.[24]

Besides having the same advantage in mesh generation as for the conventional

BEM, the BCM offers a further reduction in dimension, and especially, a nonsingular formulation for computing boundary stresses at regular points inside a boundary element. One of these formulations for stress evaluation has been addressed in Reference 6 and a second one is presented in this paper. Moreover, the stresses at boundary nodes can be recovered easily and exactly from the global displacement shape functions expressed in Cartesian coordinates. These advantages of the BCM are expected to make it very competitive in optimal shape design.

In this paper, a mathematical programming method called the SQP algorithm[25] (available as an IMSL library subroutine) is employed to solve practical shape optimization problems. The BCM and design sensitivity codes are coupled with the IMSL library subroutine to solve these problems. In order to demonstrate the performance of the BCM in 2-D optimal shape design, the above strategy is used to solve two shape optimization problems and the numerical results are compared against those obtained from the BEM. The DSCs required by these examples are those at boundary nodes of a body. Therefore, it is most convenient to calculate them from the primary BCM sensitivity algorithm presented before in Reference 1. This has been done in this work.

2. 2-D BCM FORMULATIONS

The information presented in this section is summarized from Reference 6 where more details can be found.

2.1. Basic formulation

The idea of dimensional reduction starts from the standard Boundary Integral Equation[26] (BIE) without body forces

$$c_{ik}(P)u_i(P) = \int_{\partial B} [U_{ik}(P,Q)\sigma_{ij}(Q) - \Sigma_{ijk}(P,Q)u_i(Q)]\,\mathbf{e}_j \cdot d\mathbf{S} \qquad (1)$$

where c_{ik} is the corner tensor, P, Q, u_i and σ_{ij} are the source point, field point, displacement vector and stress tensor respectively, U_{ik} and Σ_{ijk} are the Kelvin kernel

tensors,[26] and $\mathbf{e}_j$ are global Cartesian unit vectors. In 2-D problems, ∂B is the boundary of a body B, and $d\mathbf{S}$ is an infinitesimal boundary length vector.

Let

$$\mathbf{F}_k = [U_{ik}(P,Q)\sigma_{ij}(Q) - \Sigma_{ijk}(P,Q)u_i(Q)]\,\mathbf{e}_j \tag{2}$$

By discretizing the boundary ∂B into n elements, the BIE (1) becomes

$$c_{ik}(P)u_i(P) = \int_{\partial B} \mathbf{F}_k \cdot d\mathbf{S} = \sum_{\ell=1}^{n} \int_{E_{\ell 1}}^{E_{\ell 2}} \mathbf{F}_k \cdot d\mathbf{S} = 0 \tag{3}$$

where $E_{\ell 1}$ and $E_{\ell 2}$ are the endpoint nodes of element (ℓ).

Since the divergence of $\mathbf{F}_k$ at a field point Q is zero,[3] i.e.

$$\nabla_Q \cdot \mathbf{F}_k = 0 \tag{4}$$

everywhere except at the source point P, so for non-singular elements (elements that do not contain the source point P), functions Φ_k can be found by solving the following identity that satisfies equation (4)

$$\mathbf{F}_k = \frac{\partial \Phi_k}{\partial y}\mathbf{e}_1 - \frac{\partial \Phi_k}{\partial x}\mathbf{e}_2 \tag{5}$$

Hence, for a non-singular element (ℓ), substitution of (5) into (3) yields:

$$\int_{E_{\ell 1}}^{E_{\ell 2}} \mathbf{F}_k \cdot d\mathbf{S} = \Phi_k^{(\ell)}(E_{\ell 2}) - \Phi_k^{(\ell)}(E_{\ell 1}) \tag{6}$$

In view of the above identity, Φ_k are called global potential functions. A numerical implementation of equation (6) does not require any numerical integration!

It is noted that the evaluation of boundary integrals on singular elements (elements containing the source point P) can be avoided by using the rigid body motion technique as it is often performed in the standard BEM. A formulation using this technique explicitly is addressed in the next section.

2.2. Formulation using the rigid body motion technique

In order to regularize the Cauchy singular integrals in the BIE (1), a rigid body motion solution is applied to this equation to produce a new equation

$$\int_{\partial B} \{U_{ik}(P,Q)\sigma_{ij}(Q) - \Sigma_{ijk}(P,Q)\,[u_i(Q) - u_i(P)]\}\,\mathbf{e}_j \cdot d\mathbf{S} = 0 \tag{7}$$

As a result, it can be seen that potentially singular integrals in (7) only need to be evaluated on non-singular boundary elements.

Let the new (regularized) integrand vector

$$\mathbf{G}_k = \{U_{ik}(P,Q)\sigma_{ij}(Q) - \Sigma_{ijk}(P,Q)[u_i(Q) - u_i(P)]\}\mathbf{e}_j \tag{8}$$

The vector $\mathbf{G}_k$ is still divergence free (everywhere except at P). With a procedure anologous to that described in the previous section, one gets:

$$\int_{E_{\ell 1}}^{E_{\ell 2}} \mathbf{G}_k \cdot d\mathbf{S} = \Psi_k^{(\ell)}(E_{\ell 2}) - \Psi_k^{(\ell)}(E_{\ell 1}) \tag{9}$$

where Ψ_k is determined by solving the following identity

$$\mathbf{G}_k = \frac{\partial \Psi_k}{\partial y}\mathbf{e}_1 - \frac{\partial \Psi_k}{\partial x}\mathbf{e}_2 \tag{10}$$

2.3. Implementation with quadratic boundary elements

$\mathbf{G}_k$ contains the unknown fields u_i and σ_{ij}. In order for the divergence free property of $\mathbf{F}_k$ and $\mathbf{G}_k$ to hold, the displacement shape functions u_i must satisfy, a priori, the Navier-Cauchy equations:

$$\nabla^2 \mathbf{u} + \frac{1}{1-2\nu}\nabla(\nabla \cdot \mathbf{u}) = \mathbf{0} \tag{11}$$

and the stress shape functions σ_{ij} must be derived from those of u_i using Hooke's law,

$$\sigma_{ij} = \lambda \delta_{ij} u_{k,k} + \mu(u_{i,j} + u_{j,i}) \tag{12}$$

where λ and μ are Lamé constants of the material, δ_{ij} is the Kronecker delta ($\equiv 1$ for $i = j$ and $\equiv 0$ for $i \neq j$).

Quadratic shape functions that ensure the divergence free property of $\mathbf{F}_k$ and $\mathbf{G}_k$ are given by

$$\begin{Bmatrix} u_1 \\ u_2 \end{Bmatrix} = \beta_1 \begin{Bmatrix} 1 \\ 0 \end{Bmatrix} + \beta_2 \begin{Bmatrix} x \\ 0 \end{Bmatrix} + \beta_3 \begin{Bmatrix} y \\ 0 \end{Bmatrix} + \beta_4 \begin{Bmatrix} 0 \\ 1 \end{Bmatrix} + \beta_5 \begin{Bmatrix} 0 \\ x \end{Bmatrix} + \beta_6 \begin{Bmatrix} 0 \\ y \end{Bmatrix}$$
$$+ \beta_7 \begin{Bmatrix} x^2 \\ k_2 xy \end{Bmatrix} + \beta_8 \begin{Bmatrix} y^2 \\ k_1 xy \end{Bmatrix} + \beta_9 \begin{Bmatrix} k_1 xy \\ x^2 \end{Bmatrix} + \beta_{10} \begin{Bmatrix} k_2 xy \\ y^2 \end{Bmatrix} \tag{13}$$

where $k_1 = -2(1-2\nu)$, $k_2 = -4(1-\nu)$ and ν is the Poisson's ratio.

Equation (13) can also be written for element (ℓ) as

$$\left\{ \begin{array}{c} u_1 \\ u_2 \end{array} \right\}^{(\ell)} = \sum_{h=1}^{10} \beta_h^{(\ell)} \left\{ \begin{array}{c} \overline{u}_{1h}(x,y) \\ \overline{u}_{2h}(x,y) \end{array} \right\}^{(\ell)} \tag{14}$$

or in matrix form,

$$\left\{u^{(\ell)}\right\} = [T_u^{(\ell)}(x,y)]\{\beta^{(\ell)}\} \tag{15}$$

where $\{\beta^{(\ell)}\} = \langle \beta_1^{(\ell)} \ \beta_2^{(\ell)} \ \ldots \ \beta_{10}^{(\ell)} \rangle^T$.

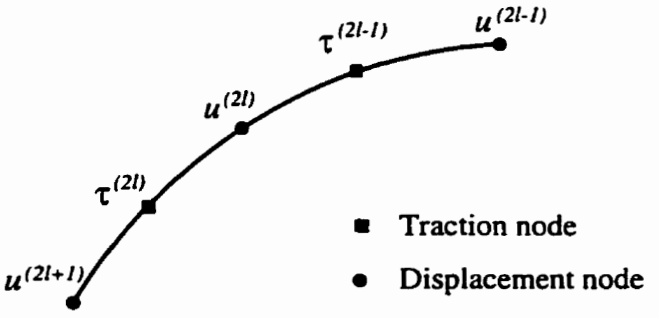

Figure 1: Quadratic boundary element (ℓ).

The configuration of a chosen quadratic boundary element is shown in Figure 1. The relationship between the physical variable vector $\left\{p^{(\ell)}\right\}$ and the artificial variable vector $\left\{\beta^{(\ell)}\right\}$ of boundary element (ℓ) is

$$\begin{aligned} \{p^{(\ell)}\} &= \left\langle u_1^{(2\ell-1)} \ u_2^{(2\ell-1)} \ \tau_1^{(2\ell-1)} \ \tau_2^{(2\ell-1)} \ u_1^{(2\ell)} \ u_2^{(2\ell)} \ \tau_1^{(2\ell)} \ \tau_2^{(2\ell)} \ u_1^{(2\ell+1)} \ u_2^{(2\ell+1)} \right\rangle^T \\ &= [T^{(\ell)}(x,y)]\{\beta^{(\ell)}\} \end{aligned} \tag{16}$$

where $\{\beta^{(\ell)}\} = \langle \beta_1^{(\ell)} \ \ldots \ \beta_{10}^{(\ell)} \rangle^T$.

A new coordinate system (ξ, η) centered at each source point is introduced. Equations (14) and (15) become respectively,

$$\left\{ \begin{array}{c} u_1 \\ u_2 \end{array} \right\}^{(\ell)} = \sum_{h=1}^{10} \hat{\beta}_h^{(\ell)} \left\{ \begin{array}{c} \overline{u}_{1h}(\xi,\eta) \\ \overline{u}_{2h}(\xi,\eta) \end{array} \right\}^{(\ell)} \tag{17}$$

$$\left\{u^{(\ell)}\right\} = [T_u^{(\ell)}(\xi,\eta)]\{\hat{\beta}^{(\ell)}\} \tag{18}$$

In equation (18),

$$\{\hat{\beta}^{(\ell)}\} = \langle \hat{\beta}_1^{(\ell)} \ \ldots \ \hat{\beta}_{10}^{(\ell)} \rangle^T = [B_j]\{\beta^{(\ell)}\} \tag{19}$$

where $\hat{\beta}_h^{(\ell)} = \beta_h^{(\ell)}$ for $h = 7, \ldots, 10$, and $[B_j]$ is a matrix depending only on the coordinates of the source point j (since it arises from a coordinate transformation from the global system (x, y) to a system (ξ, η) centered at j).

Since the coordinates of a source point P are always $(0, 0)$, the displacement field used in equation (7) can easily be found from equation (17) as

$$\left\{ \begin{array}{l} u_1(Q) - u_1(P) \\ u_2(Q) - u_2(P) \end{array} \right\}^{(\ell)} = \sum_{h=1}^{10} \tilde{\beta}_h^{(\ell)} \left\{ \begin{array}{l} \overline{u}_{1h}(\xi, \eta) \\ \overline{u}_{2h}(\xi, \eta) \end{array} \right\}^{(\ell)} \tag{20}$$

in which, with (q) the element containing the source point, i.e., the singular element,

$$\left. \begin{array}{ll} \tilde{\beta}_h^{(\ell)} = \hat{\beta}_h^{(\ell)} - \hat{\beta}_h^{(q)} & \text{if} \quad h = 1, 4 \\ \tilde{\beta}_h^{(\ell)} = \beta_h^{(\ell)} & \text{if} \quad h = 7, \ldots, 10 \\ \tilde{\beta}_h^{(\ell)} = \hat{\beta}_h^{(\ell)} & \text{otherwise} \end{array} \right\} \tag{21}$$

It can be seen that the displacement shape vectors in equations (14) and (20) are the same. Thus, by substituting each of these ten displacement shape vectors and its corresponding stress shape vector (using (12)) into equations (2) and (8), one obtains

$$\mathbf{F}_{kh} = \mathbf{G}_{kh} = [U_{ik}\overline{\sigma}_{ijh}(\xi, \eta) - \Sigma_{ijk}\overline{u}_{ih}(\xi, \eta)]\, \mathbf{e}_j \tag{22}$$

Equations (5) and (10) in this case take the following form

$$\mathbf{F}_{kh} = \mathbf{G}_{kh} = \frac{\partial \phi_z}{\partial \eta}\mathbf{e}_1 - \frac{\partial \phi_z}{\partial \xi}\mathbf{e}_2 \tag{23}$$

where $z = h + 10(k - 1)$; $h = 1, 2, \ldots, 10$ and $k = 1, 2$.

Equation (23) implies that the BIE (1) and its regularized form (7) have the same potential functions ϕ_z.

For a given value of h, the solution of (23) using (22) yields two potential functions ϕ_z associated with $k = 1, 2$. The 20 resulting potential functions (for

$h = 1,\ldots,10; k = 1,2$) are listed in the Appendix of Reference 6. It can be observed from this Appendix that only half of these 20 potential functions need to be determined.

By using these potential functions, equations (6) and (9) become respectively

$$\int_{E_{\ell 1}}^{E_{\ell 2}} \mathbf{F}_k \cdot d\mathbf{S} = \sum_{h=1}^{10} \hat{\beta}_h^{(\ell)} [\phi_z(E_{\ell 2}) - \phi_z(E_{\ell 1})] \tag{24}$$

$$\int_{E_{\ell 1}}^{E_{\ell 2}} \mathbf{G}_k \cdot d\mathbf{S} = \sum_{h=1}^{10} \tilde{\beta}_h^{(\ell)} [\phi_z(E_{\ell 2}) - \phi_z(E_{\ell 1})] \tag{25}$$

As shown in Reference 6, a development of (25) for all boundary elements leads to the following final BCM system of equations

$$[A]\{X\} = [B]\{Y\} \tag{26}$$

Or,

$$[A]\{X\} = \{Z\} \tag{27}$$

In equations (26) and (27), $[A]$ and $[B]$ are the BCM matrices which are associated with the potential functions ϕ_z; $\{X\}$ and $\{Y\}$ contain, respectively, the unknown and known (from boundary conditions) physical quantities. Thus, $\{Z\}$ is a known vector. Finally, system (27) can easily be solved to find the unknowns $\{X\}$.

3. STRESSES IN B*

3.1. Hypersingular boundary contour formulation

A method for computing stresses in B^*, starting from the HBIE, is presented here. This derivation is new and is different from that in Reference 6.

Stresses can be calculated using Hooke's law (12). To this end, the displacement gradient tensor used in (12) needs to be computed from the gradient form of the BIE (1) with respect to a source point P, i.e. from the following HBIE:

$$\gamma u_{k,M} = -\int_{\partial B} [U_{ik,m}(P,Q)\sigma_{ij}(Q) - \Sigma_{ijk,m}(P,Q)u_i(Q)]\,\mathbf{e}_j \cdot d\mathbf{S} \tag{28}$$

in which, the derivatives of the Kelvin kernels with respect to a source point P ($(\ )_{,M}$) have been converted to those with respect to a field point Q ($(\ )_{,m}$) by a sign change ($M = m = 1, 2$ in 2-D cases); and $\gamma = 0.5$ if the source point P (where stresses are to be computed) is on the boundary ∂B^* and $\gamma = 1$ if P is inside the body B.

In a (ξ, η) coordinate system centered at the source point P, the expressions for the gradients of Kelvin kernel tensors for plane strain problems are

$$\left.\begin{aligned} U_{ik,m} &= \frac{-1}{8\pi\mu(1-\nu)r}\left[(3-4\nu)\delta_{ik}r_{,m} - \delta_{in}r_{,k} - \delta_{nk}r_{,i} + 2r_{,i}r_{,m}r_{,k}\right] \\ \Sigma_{ijk,m} &= \frac{1}{4\pi(1-\nu)r^2}\left[8r_{,i}r_{,j}r_{,k}r_{,m} - 2(\delta_{in}r_{,j}r_{,k} + \delta_{jn}r_{,i}r_{,k} + \delta_{kn}r_{,i}r_{,j}) + (1-2\nu)\right. \\ &\left.(-\delta_{ik}\delta_{jn} - \delta_{jk}\delta_{in} + \delta_{ij}\delta_{kn}) + 2(1-2\nu)(\delta_{ik}r_{,j}r_{,m} + \delta_{jk}r_{,i}r_{,m} - \delta_{ij}r_{,k}r_{,m})\right] \end{aligned}\right\} \tag{29}$$

where $\mu = G$ is the shear modulus, δ_{ij} is the Kronecker delta and $r = \sqrt{\xi^2 + \eta^2}$.

It is noted that the integrand vector of equation (28)

$$\mathbf{H}_{km} = \left[U_{ik,m}(P,Q)\sigma_{ij}(Q) - \Sigma_{ijk,m}(P,Q)u_i(Q)\right]\mathbf{e}_j \tag{30}$$

is divergence free (everywhere except at P). This is true because the divergence is taken with respect to a field point Q whereas $\mathbf{H}_{km}$ is, initially, the gradient of $\mathbf{F}_k$ (which is itself divergence free[3]) with respect to a source point P .

Therefore, equation (28) can now be converted into the following BCM version

$$\gamma u_{k,M} = -\sum_{\ell=1}^{n}\left[\Lambda_{km}^{(\ell)}(E_{\ell 2}) - \Lambda_{km}^{(\ell)}(E_{\ell 1})\right] \tag{31}$$

where the global potential functions Λ_{km} are determined by solving the identity

$$\mathbf{H}_{km} = \frac{\partial \Lambda_{km}}{\partial \eta}\mathbf{e}_1 - \frac{\partial \Lambda_{km}}{\partial \xi}\mathbf{e}_2 \tag{32}$$

3.2. Numerical implementation

As usual, each of the ten displacement shape vectors in (17) (see also equation (13)) and its corresponding stress shape vector (using (12)) are employed in equation (30)

to give

$$\mathbf{H}_{kmh} = [U_{ik,m}\overline{\sigma}_{ijh}(\xi,\eta) - \Sigma_{ijk,m}\overline{u}_{ih}(\xi,\eta)]\,\mathbf{e}_j \tag{33}$$

Equation (32) in this case takes the following form

$$\mathbf{H}_{kmh} = \frac{\partial \lambda_w}{\partial \eta}\mathbf{e}_1 - \frac{\partial \lambda_w}{\partial \xi}\mathbf{e}_2 \tag{34}$$

where $w = h + 10(k-1) + 20(m-1)$; $h = 1, 2, \ldots, 10$; $k = 1, 2$ and $m = 1, 2$.

For a given value of h, the solution of (34) using (33) yields four potential functions λ_w (corresponding to $k = 1, 2$ and $m = 1, 2$). The 40 resulting potential functions (for $h = 1, \ldots, 10$) are listed in the Appendix where only half of them need to be determined.

With the origin of the coordinate system (ξ, η) is centered at P, a numerical implementation of (31) leads to

$$\gamma u_{k,M} = \sum_{\ell=1}^{n}\sum_{h=1}^{10} \lambda_w^{P\ell}\hat{\beta}_h^{(\ell)} \tag{35}$$

where $\lambda_w^{P\ell} = \lambda_w(\xi_{\ell 1}, \eta_{\ell 1}) - \lambda_w(\xi_{\ell 2}, \eta_{\ell 2}) - k_\lambda$, with $k_\lambda = 0.5$ if P is a regular point on ∂B and $w = 2, 16, 23$ or 35 (see Reference 6 and the Appendix of this paper). At regular boundary points on ∂B with other values of w, as well as at points inside the body, $k_\lambda = 0$.

In matrix form,

$$\gamma\,\{u_{k,M}\} = \sum_{\ell=1}^{n}\left[\Lambda^{(P\ell)}\right][B_P]\{\beta^{(\ell)}\} \tag{36}$$

where $[\Lambda_M^{(P\ell)}]$ is the matrix associated with the potential functions λ_w and it is noted that $\{\beta^{(\ell)}\}$ is known at this stage from the solution of the primary problem (27).

4. SENSITIVITY ANALYSIS

4.1. DSCs for the primary BCM problem

This section recapitulates results from Reference 1 where further details are available.

The DSCs under consideration can be found by differentiating equation (26) with respect to a design variable b, which is a typical component of a shape design vector b. The result is,

$$\dot{[A]}\,\{X\}+[B]\,\{Y\}+[A]\,\{\dot{X}\}+[B]\,\{\dot{Y}\}=\{0\} \tag{37}$$

where $\dot{(\ )}$ denotes the total derivative with respect to b, i.e. $\dot{(\ )}= d(\ )/db$ and generally,

$$\dot{(\ )}=(\ )_{,b}+v_i(\ )_{,i} \tag{38}$$

It is noted here that in order to avoid any ambiguities that might result from the use of the above notation for the total derivative of a long expresion, the alternative notation $(\ )^{\cdot}$ is used in such cases.

In equation (38), the quantities $v_i = dx_i/db$ are the components of the design velocity field. For 2-D cases, $x_1 \equiv x$ and $x_2 \equiv y$, thus equation (38) can be expanded to

$$\dot{(\ )}=(\ )_{,b}+(\ )_{,x}\,\dot{x}+(\ )_{,y}\,\dot{y} \tag{39}$$

This total derivative is totally analogous to the concept of the material derivative (often taken with respect to time) in continuum mechanics.

In equation (37), $\{X\}$ is known at this stage from the solution of the BCM system (27). Furthermore, it is assumed that the boundary conditions are kept fixed during the change of the design variables, so that $\{\dot{Y}\}=\{0\}$. By shifting the known terms to the right hand side, equation (37) becomes

$$[A]\,\{\dot{X}\}=-\dot{[B]}\,\{Y\}-\dot{[A]}\,\{X\} \tag{40}$$

or,

$$[A]\,\{\dot{X}\}=\{W\} \tag{41}$$

This final linear system is very similar to the BCM system (27). The matrix $[A]$ is identical in both equations. Also, it is generally overdetermined but always consistent and therefore, the rectangular system solving algorithm used to solve the usual BCM equations (27), can be reused here.

4.2. Stress sensitivities in B*

This section presents a new method for calculating stress sensitivities in B^*. The starting point here is equation (36) in section 3.2.

The stress sensitivities can be determined from Hooke's law (12) as

$$\dot{\sigma}_{ij} = \lambda \delta_{ij} (u_{k,k})^* + \mu \left[(u_{i,j})^* + (u_{j,i})^* \right] \tag{42}$$

The sensitivity of the displacement gradient tensor required in equation (42) is derived from (36) to give

$$\begin{aligned} \gamma \left\{ u_{k,M}(\mathbf{b}, P) \right\}^* &= \sum_{\ell=1}^{n} \left\{ \left[\dot{\Lambda}^{(P\ell)} \right] [B_P] \left\{ \beta^{(\ell)} \right\} + \left[\Lambda^{(P\ell)} \right] [\dot{B}_P] \left\{ \beta^{(\ell)} \right\} \right. \\ &+ \left. \left[\Lambda^{(P\ell)} \right] [B_P] \left\{ \dot{\beta}^{(\ell)} \right\} \right\} \end{aligned} \tag{43}$$

The new terms in equation (43) are computed as follows,

- The components of the matrix $\left[\dot{\Lambda}^{(P\ell)} \right]$ are given by

$$\dot{\lambda}_w^{(P\ell)} = \dot{\lambda}_w (\xi_{\ell 1}, \eta_{\ell 1}) - \dot{\lambda}_w (\xi_{\ell 2}, \eta_{\ell 2}) \tag{44}$$

  where,

$$\begin{aligned} \dot{\lambda}_w (\xi_\ell, \eta_\ell) &= \frac{\partial \lambda_w(\xi_\ell, \eta_\ell)}{\partial \xi} \left[\dot{x} (x_\ell, y_\ell) - \dot{x} (x_P, y_P) \right] \\ &+ \frac{\partial \lambda_w(\xi_\ell, \eta_\ell)}{\partial \eta} \left[\dot{y} (x_\ell, y_\ell) - \dot{y} (x_P, y_P) \right] \end{aligned} \tag{45}$$

  Although $\partial \lambda_w / \partial \xi$ and $\partial \lambda_w / \partial \eta$ are singular when $Q(x_\ell, y_\ell) \rightarrow P(x_P, y_P)$, i.e. when $(\xi, \eta) \rightarrow (0,0)$, but at the same time $\left[\dot{x} (x_\ell, y_\ell) - \dot{x} (x_P, y_P) \right] = \left[\dot{y} (x_\ell, y_\ell) - \dot{y} (x_P, y_P) \right] \sim O(r)$, therefore, unlike $\left[\Lambda^{(P\ell)} \right]$, the matrix $\left[\dot{\Lambda}^{(P\ell)} \right]$ is completely regular.

- The sensitivity of $[B_P]$ is

$$[\dot{B}_P] = [B_P]_{,x} \dot{x} (x_P, y_P) + [B_P]_{,y} \dot{y} (x_P, y_P) \tag{46}$$

- By taking the sensitivity of equation (16), we have

$$\left\{\dot{\beta}^{(\ell)}\right\}=\left[\left[T^{(\ell)}\right]^{-1}\right]^{\cdot}\left\{p^{(\ell)}\right\}+\left[T^{(\ell)}\right]^{-1}\left\{\dot{p}^{(\ell)}\right\} \tag{47}$$

where,

$$\left[\left[T^{(\ell)}\right]^{-1}\right]^{\cdot}=-\left[T^{(\ell)}\right]^{-1}\left[\dot{T}^{(\ell)}\right]\left[T^{(\ell)}\right]^{-1} \tag{48}$$

Although equation (45) requires the partial derivatives of the potential function λ_w, it is interesting to note that these derivatives do not need to be determined from λ_w. In fact, it can be seen from equation (34) that these partial derivatives are the components of the integrand $\mathbf{H}_{kMh}$, and these components can be found from (33) as

$$\left.\begin{aligned}\frac{\partial\lambda_w(\xi_\ell,\eta_\ell)}{\partial\xi} &= -U_{ik,m}\overline{\sigma}_{i2h}(\xi,\eta)+\Sigma_{i2k,m}\overline{u}_{ih}(\xi,\eta)\\ \frac{\partial\lambda_w(\xi_\ell,\eta_\ell)}{\partial\eta} &= U_{ik,m}\overline{\sigma}_{i1h}(\xi,\eta)-\Sigma_{i1k,m}\overline{u}_{ih}(\xi,\eta)\end{aligned}\right\} \tag{49}$$

in which, $\overline{u}_{ih}$ is the i^{th} component of the h^{th} displacement shape vector in (17), and $\overline{\sigma}_{i1h}$, $\overline{\sigma}_{i2h}$ are the stress components determined from $\overline{u}_{ih}$ by Hooke's law (12).

Finally, it can be observed that the process of evaluation of equation (36) and its sensitivity form (43) is simpler than use of the equivalent ones (equations (38) and (39) in Reference 1).

5. SHAPE OPTIMIZATION

5.1. Formulation of an optimal design problem

An optimal shape design problem can be stated as a minimization problem under certain constraints whose general form can be formulated as follows

$$\text{Minimize} \quad f(\mathbf{b}) \tag{50}$$

$$\text{Subject to} \quad g_i(\mathbf{b}) \geq 0 \qquad i=1,\ldots,N_g \tag{51}$$

$$h_j(\mathbf{b}) = 0 \qquad j=1,\ldots,N_h \tag{52}$$

$$b_k^l \leq b_k \leq b_k^u \qquad k=1,\ldots,N \tag{53}$$

in which, $\mathbf{b} = \langle b_1, b_2, \ldots, b_N \rangle^T$ are the design variables, $f(\mathbf{b})$ is called the objective function, and $g_i(\mathbf{b})$ and $h_j(\mathbf{b})$ are called inequality and equality constraints, respectively.

The fact that the optimization problem is stated as a minimization is not restrictive since it is always possible to maximize an objective function by minimizing its negative value.

The design variables $\mathbf{b}$ could be shape or sizing parameters that define a part or the whole boundary of a body.

The objective function could be:

- The weight of a 3-D body or the area of a 2-D domain. This is the most typical objective function in optimal shape design.
- The maximum effective stress over a region B_c where a stress concentration occurs. The effective stress can be principal, von Mises or Tresca stresses at a point in the region B_c. Such objective functions are often employed in stress concentration problems.
- The variance of the stresses over a boundary ∂B_c, which can be stated mathematically as

$$f(\mathbf{b}) = \frac{1}{L} \int_{\partial B_c} [\sigma(S) - \overline{\sigma}]^2 \, dS \tag{54}$$

  where $\overline{\sigma}$ is the mean value of σ which could be effective or tangential stresses on the boundary ∂B_c of length L. Minimization of this kind of objective function requires the effective stress to be as uniform as possible on the boundary ∂B_c.

The constraints (51) and (52) describe all the restrictions associated with the optimal problem under consideration. In shape optimization, the usual constraints are

- Effective stress in the body should not exceed the allowable stress.
- Displacements at given positions should be less than prescribed values.

- Stiffness or stability constraints in buckling problems.
- Frequency constraints in vibration problems.
- Technological or manufacturing constraints.

Expression (53) contains side constraints and is used to limit the region of search for the optimization problem. Here b_k^l and b_k^u denote lower and upper bounds, respectively, of the design variable b_k. The side constraints are introduced to prevent unreasonable or meaningless solutions. For example, the sizing dimensions of a structure must always be positive.

5.2. Shape modeling

An important issue in shape optimization is how to model the design boundary under given conditions while the number of design variables are kept as low as possible. In general, some nodes (called *control nodes*) on the part of boundary to be optimized are chosen as design variables. Then, fitting interpolations such as B-spline,[20] cubic spline,[19,24] using these control nodes, are employed to represent the design boundary.

In special cases, a boundary can be modelled by the following parametrized equations[18]

$$\left.\begin{aligned} x &= a(\cos\theta + \epsilon\cos 3\theta) \\ y &= a(\beta\sin\theta - \epsilon\cos 3\theta) \end{aligned}\right\} \tag{55}$$

where the parameters a, ϵ and β control, respectively, the size, shape and aspect ratio of the boundary. Thus, they can be chosen as design variables. By using appropriate values for these parameters, a variety of smooth curves such as circles, ellipses or rectangles with rounded corners can be generated.

Both aformentioned approaches are employed in the optimization examples of this work. The cubic spline fitting is used in the example of a fillet problem whereas the parametrized equations (55) are applied in the example of a plate with cutout.

5.3. Mathematical programming methods

In general, both objective function and constraints in shape optimization problems are nonlinear functions of the design variables and cannot be expressed analytically (in closed form). Therefore, numerical approaches such as mathematical programming methods must be employed to solve the optimal problem (50) - (53). The most common methods in the context of optimal shape design are *successive linear programming* (SLP) and *successive quadratic programming* (SQP) methods.

SLP is the most popular and simplest approach which approximates the objective function and the constraints of problem (50) - (53) by their first order Taylor series expansions about the design vector $\mathbf{b}$ obtained from the previous iterative step. The new linearized problem can then be solved easily by using the well-known simplex method or other standard optimization algorithms.

Due to the linearization of the SLP method, moving limits must be imposed here to prevent high errors of this approximation. Otherwise the problem may have unbounded or oscillatory solutions. If the moving limits can guarantee a good approximation for the linearized problem, its solution will be closer to the optimal one than that of the previous step. In general, the moving limits should be shrunk when the design solution approaches the optimum since the linear approximation needs to be more accurate at that time. The way to choose and the requirement to adjust moving limits are the main drawbacks of the SLP method.

In the SQP method, the optimization problem is approximated by expanding the objective function in a second order Taylor series about the current values of the design variables, and the contraints, in a first order Taylor series as follows,

$$\left.\begin{aligned}
&\text{Minimize} && f(\mathbf{b}^{(m)}) + \nabla^T f(\mathbf{b}^{(m)})\{\Delta\mathbf{b}\} + \frac{1}{2}\{\Delta\mathbf{b}\}^T[H]\{\Delta\mathbf{b}\} && \\
&\text{Subject to} && g_i(\mathbf{b}^{(m)}) + \nabla^T g_i(\mathbf{b}^{(m)})\{\Delta\mathbf{b}\} \geq 0 && i = 1, \ldots, N_g \\
& && h_j(\mathbf{b}^{(m)}) + \nabla^T h_j(\mathbf{b}^{(m)})\{\Delta\mathbf{b}\} = 0 && j = 1, \ldots, N_h \\
& && b_k^l - b_k^{(m)} \leq \Delta b_k \leq b_k^u - b_k^{(m)} && k = 1, \ldots, N
\end{aligned}\right\} \qquad (56)$$

where m denotes the previous optimization step, $\{\Delta \mathbf{b}\} = (\Delta b_1, \Delta b_2, \ldots, \Delta b_N)^T$ are the changes in the design variables, $[H]$, $\nabla f(\mathbf{b}^{(m)})$ and $\nabla g(\mathbf{b}^{(m)})$ are, respectively, the Hessian matrix, the gradients of the objective function and its contraints.

The SQP method is usually considered a powerful method in various optimization problems thanks to the use of quadratic programming that leads to faster convergence than the SLP and more accurate final solutions. This method is used in this paper to solve optimization examples.

Since Taylor series are employed in the SLP and SQP methods, it can be seen that DSCs are required by these methods in order to form the gradients of the objective functions and the contraints.

5.4. Shape optimization program

The C function "`f_min_con_nonlin`" from the IMSL library is coupled with the 2-D BCM analysis and sensitivity programs to solve shape optimization examples of this paper. The function is based on the FORTRAN subroutine NLPQL developed in Reference 25 where theoretical details of the algorithm are presented. "f_min_con_nonlin" uses the SQP method to solve the general nonlinear optimization problem (56) in which the Hessian is replaced by a positive definite approximation. Thus, the evaluation of second order DSCs for the objective function is avoided.

6. NUMERICAL EXAMPLES

Four examples are studied in this section. For the first three examples, the following material data are used: Young's modulus $E = 2.5$ (in consistent units) and Poisson's ratio $\nu = 0.3$. The first example is concerned with stress analysis in a narrow cantilever and the second with stress sensitivity analysis in a hollow cylinder (Lamé's problem). In these two examples, stresses and their sensitivities are computed by the new approach (sections 3 and 4.2). The last two examples deal with shape optimization. In these cases, stress sensitivites at boundary nodes are obtained from the primary BCM design sensitivity analysis developed in Reference 1 and summarized in section 4.1.

6.1. Bending of a narrow cantilever - stress analysis

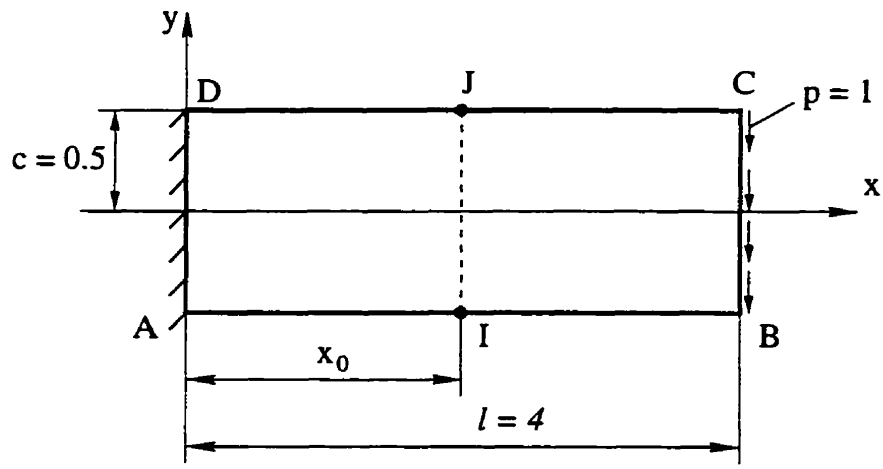

Figure 2: Modeling of the narrow cantilever problem.

Consider a cantilever of narrow rectangular cross section as shown in Figure 2. The structure is subjected to a distributed shearing force p along its free end and the resultant load is equal to P. The stresses in section IJ are computed using the formulas presented in section 3. The cantilever boundary is discretized by 18 quadratic elements: four and five elements are equally spaced along each of the vertical and horizontal edges, respectively. Due to the narrow rectangular cross section of the cantilever compared with its depth $2c$, this example can be considered to be in a state of plane stress.

By virtue of Saint-Venant's principle, the following elementary solution can represent the stress distribution for cross sections at a considerable distance from the ends[27]

$$\left.\begin{aligned} \sigma_x &= \frac{P(l-x)y}{I} \\ \sigma_y &= 0 \\ \sigma_{xy} &= -\frac{P}{2I}\left(c^2 - y^2\right) \end{aligned}\right\} \tag{57}$$

where $I = 2c^3/3$ is the moment of inertia of the cross section of the cantilever, $P = 2pc$ is the resultant end load.

The above analytical solution for the stresses in section IJ with $x = x_0 = l/2$

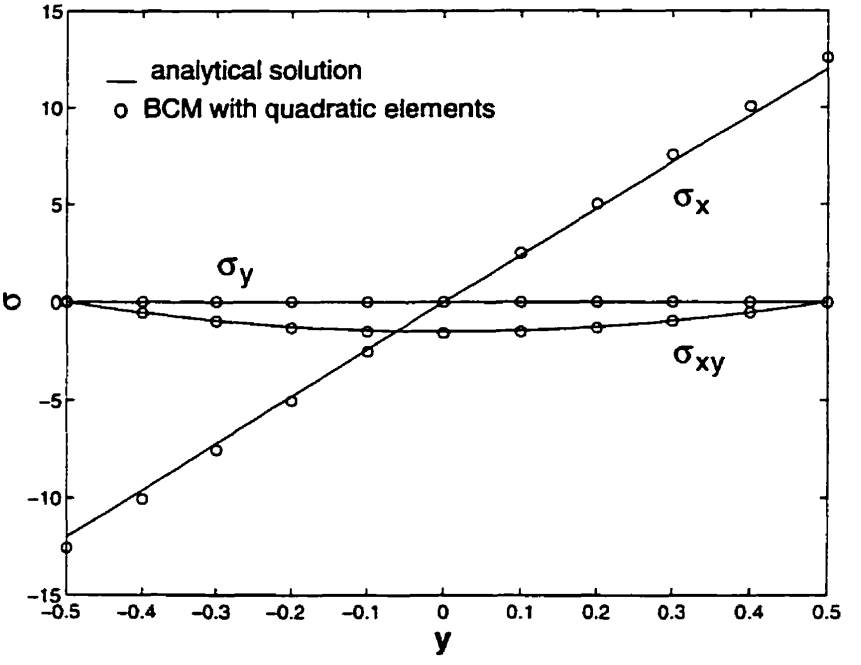

Figure 3: Stress components along the line IJ (see Figure 2).

and the BCM numerical results are plotted in Figure 3 where good agreement is observed.

6.2. Lamé's problem - stress sensitivity analysis

The second example deals with the calculation of stress sensitivities for Lamé's problem. Consider a thick cylinder subjected to uniform pressures p_i and p_o on the inner and outer surfaces, respectively. Let a and b be the inner and outer radii of the cylinder where a is chosen as the design variable.

The analytical expressions in polar coordinates (r, θ), for the stress fields of Lamé's problem, are given by[27]

$$\sigma_{r/\theta} = \pm \frac{a^2 b^2 (p_o - p_i)}{(b^2 - a^2) r^2} + \frac{p_i a^2 - p_o b^2}{b^2 - a^2} \tag{58}$$

in which, the expressions for σ_r and σ_θ correspond to the upper and lower signs, respectively.

By assuming that the geometry changes linearly with changes of the design

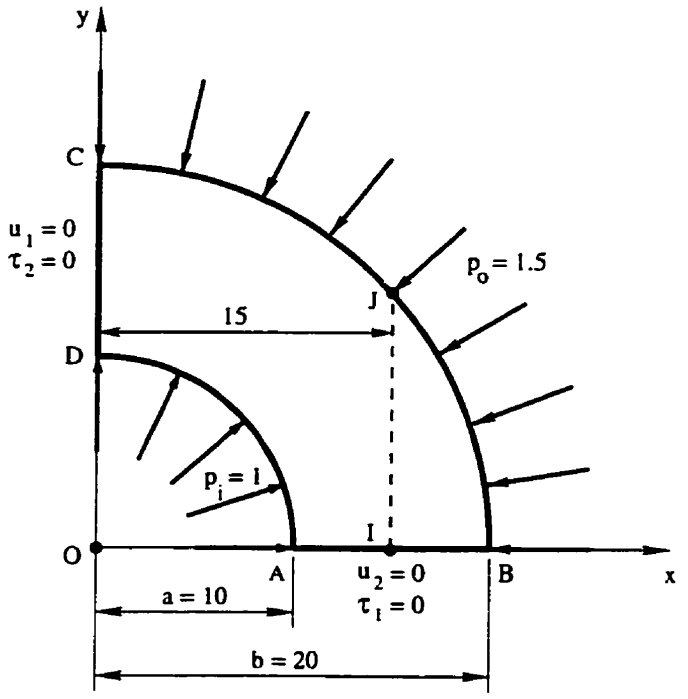

Figure 4: Modeling of Lamé's problem.

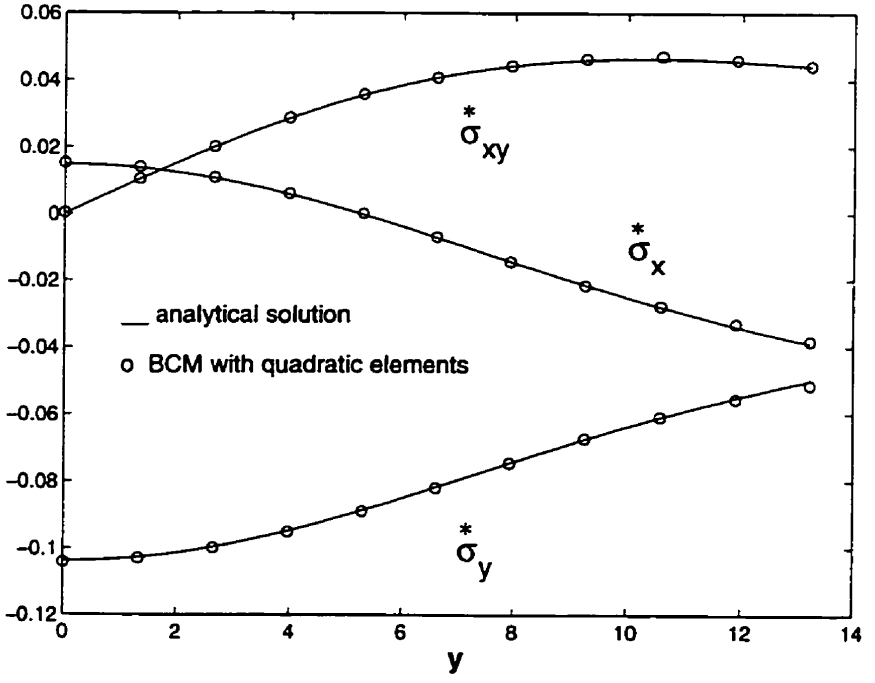

Figure 5: Stress sensitivities along the line IJ (see Figure 4).

variable a, it is easy to get

$$\dot{r} = \frac{b-r}{b-a} \tag{59}$$

Therefore, the analytical sensitivity fields are found by taking the total derivative of equation (58) with respect to the design variable a (using equation (38) written in polar coordinates) to give

$$\dot{\sigma}_{r/\theta} = \frac{2ab^2\left(p_i - p_o\right)\left[r\left(r^2 \mp b^2\right) \pm a(b-r)(b+a)\right]}{\left(b^2-a^2\right)^2 r^3} \tag{60}$$

Due to symmetry, only a quarter of the structure needs to be modeled as shown in Figure 4. The mesh consists of equal numbers of quadratic boundary elements on each segment of the boundary. Also, all the elements on a given segment are of equal length. This example is solved by using a total of 20 quadratic elements. The formulas in section 4.2 are used to compute the stress sensitivities (Figure 5) on the line segment IJ (see Figure 4). Excellent agreement is achieved between the analytical and numerical solutions.

6.3. Shape optimization of a plate with cutout

A square plate with a central cutout, subjected to uniform biaxial tensile loads, is shown in Figure 6. Because of symmetry, only a quarter of the plate is considered. The model is set up with 42 quadratic elements, 10 at equal eccentric angles on EA, 4 at equal distance along each of BC and CD, and 12 at unequal distance along each of AB and DE. Due to stress concentration at A and E, the mesh density is increased from B to A and from D to E.

The objective here is to design the cutout shape EA so that the variance of tangential stress σ_s on this cutout is minimized. Therefore, the objective function has the form of equation (54) with, $\sigma \equiv \sigma_s$. Based on this equation, the sensitivity of the objective function, required by the SQP algorithm, is given by[18]

$$\dot{f} = -\frac{\dot{L}}{L} f + \frac{2}{L}\int_A^E \left(\sigma_s - \overline{\sigma}_s\right)\left(\dot{\sigma}_s - \dot{\overline{\sigma}}_s\right) dS + \frac{1}{L}\int_A^E \left(\sigma_s - \overline{\sigma}_s\right)^2 \left(\dot{dS}\right) \tag{61}$$

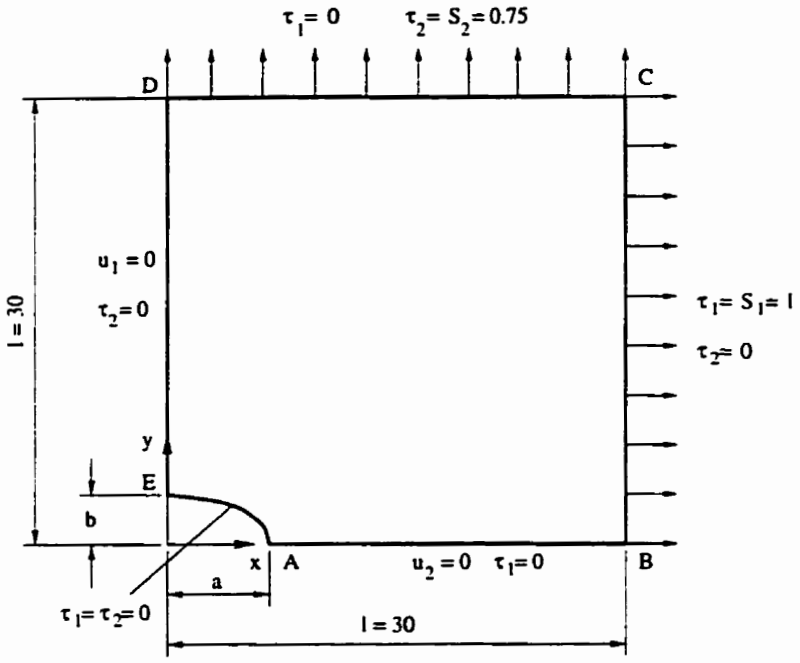

Figure 6: Modeling of the plate with cutout.

in which,

$$\left.\begin{aligned} L &= \int_A^E dS \;; \quad \dot{L} = \int_A^E (\dot{dS}) \\ \overline{\sigma}_s &= \frac{1}{L}\int_A^E \sigma_s dS \\ \dot{\overline{\sigma}}_s &= -\frac{\dot{L}}{L}\overline{\sigma}_s + \frac{1}{L}\int_A^E \dot{\sigma}_s\, dS + \frac{1}{L}\int_A^E \sigma_s\, (\dot{dS}) \end{aligned}\right\} \tag{62}$$

In this example, the design cutout is modeled using equation (55) with $\epsilon = 0$, i.e.,

$$\left.\begin{aligned} x &= a\cos\theta \\ y &= a\beta\sin\theta \end{aligned}\right\} \tag{63}$$

where θ, a and $a\beta = b$ are, respectively, eccentric angle, semi-major and semi-minor axes of the cutout. Here, β is chosen as the design variable. The constraint imposed in this case is

$$0.3 \leq \beta \leq 1 \tag{64}$$

Hence,

$$\left.\begin{aligned} dS &= a\sqrt{\sin^2\theta + \beta^2\cos^2\theta}\,d\theta \\ (\dot{dS}) &= \frac{a\beta\cos^2\theta}{\sqrt{\sin^2\theta + \beta^2\cos^2\theta}}\,d\theta \end{aligned}\right\} \tag{65}$$

A linear assumption is used to determine the geometry changes (design velocity field) of the cutout.

It has been proved[28] that the analytical solution for this kind of problem is

$$\beta = \frac{b}{a} = \frac{S_2}{S_1} = 0.75 \tag{66}$$

Table 1 displays the history of the iterative optimization process for this problem. The final solution $\beta = 0.7501$ is obtained after 6 steps, using a CPU time of 36.78 s on an IBM RS/6000. This result is very close to the analytical solution and more accurate than that obtained from the BEM by Wei *et al.*[28] ($\beta = 0.756$ obtained after 5 steps, with a CPU time of 29.78 s on an IBM 3090 supercomputer).

Table 1: History of iterative optimization process for the plate with cutout problem.

Number of iterations	$\beta = b/a$	f
1	1.0000	0.126108
2	0.8307	0.015546
3	0.7942	0.004843
4	0.7712	0.001140
5	0.7485	0.000007
6	0.7501	0.000001

6.4. Shape optimization of a fillet

The last example involves optimizing the shape of a fillet in a tension bar whose area is selected as the objective function. An optimal shape is sought that minimizes the area without causing yielding anywhere in the bar. The result will be compared

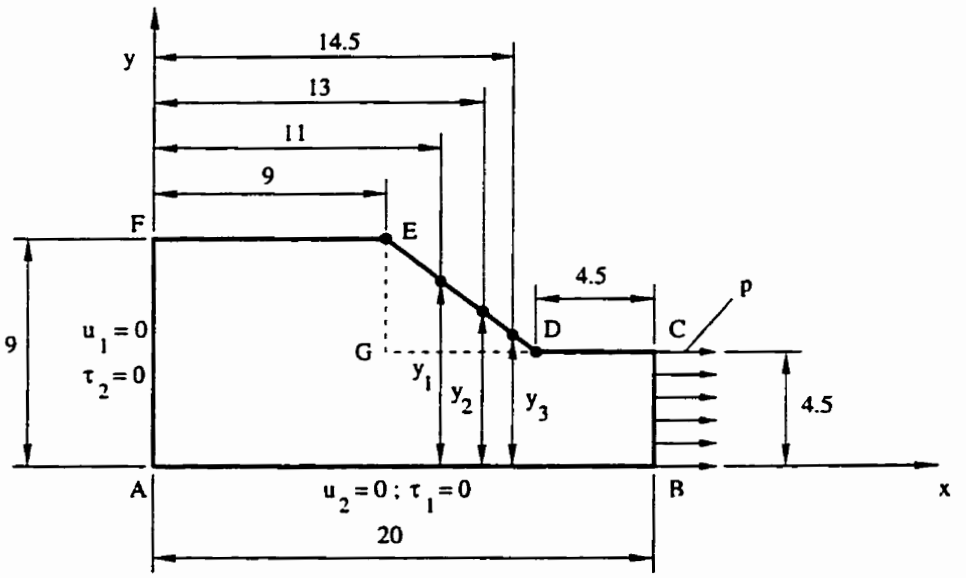

Figure 7: Modeling of the fillet problem.

against those obtained in Reference 21 where shape design sensitivity analysis has been used with the BEM.

Because of symmetry, only the upper half of the bar is modeled as displayed in Figure 7. Young's modulus, Poisson's ratio and allowable von Mises stress are $E = 3.10^7\ psi$, $\nu = 0.3$ and $[\sigma_{VM}] = 150\ psi$, respectively. The design boundary DE is to be varied while points D and E are fixed. A total of 13 quadratic elements is meshed on the boundary: 3 elements on the edge AB, 1 on BC, 2 on CD, 4 on the fillet DE, 2 on EF and 1 on FA. This mesh is densified around D which is a point of stress concentration. The ordinates y_1, y_2 and y_3 of three endpoint nodes inside the fillet DE (control nodes) are chosen as the design variables.

The first task is to model the design boundary DE based on the coordinates of the 5 endpoint nodes on this boundary. A cubic spline interpolation is used to build the design curve $y_{DE}(y_1, y_2, y_3, x)$. In this case, the objective function can be evaluated via the area bound by DE, two vertical lines through D and E, and the x axis as follows:

$$f(y_1, y_2, y_3) = \int_{x_E}^{x_D} y_{DE}(y_1, y_2, y_3, x)dx \tag{67}$$

The constraints associated with the above objective function are described as

$$[\sigma_{VM}] - \sigma_{VMi}(y_1, y_2, y_3) \geq 0 \qquad 1 \leq i \leq 8 \tag{68}$$

$$4.5 \leq y_1 \leq 7.61 \tag{69}$$

$$4.5 \leq y_2 \leq 6.23 \tag{70}$$

$$4.5 \leq y_3 \leq 5.19 \tag{71}$$

where $\sigma_{VMi}(y_1, y_2)$ are the von Mises stresses at nodes i on DE, and the last two expressions are the side constraints that force the design boundary DE to lie within the triangle EGD.

The von Mises stress and its sensitivity are:

$$\left.\begin{aligned} \sigma_{VM} &= \sqrt{\sigma_{11}^2 + \sigma_{22}^2 + 3\sigma_{12}^2 - \sigma_{11}\sigma_{22}} \\ \dot{\sigma}_{VM} &= \frac{(2\sigma_{11} - \sigma_{22})\,\dot{\sigma}_{11} + (2\sigma_{22} - \sigma_{11})\,\dot{\sigma}_{22} + 6\sigma_{12}\,\dot{\sigma}_{12}}{2\sigma_{VM}} \end{aligned}\right\} \tag{72}$$

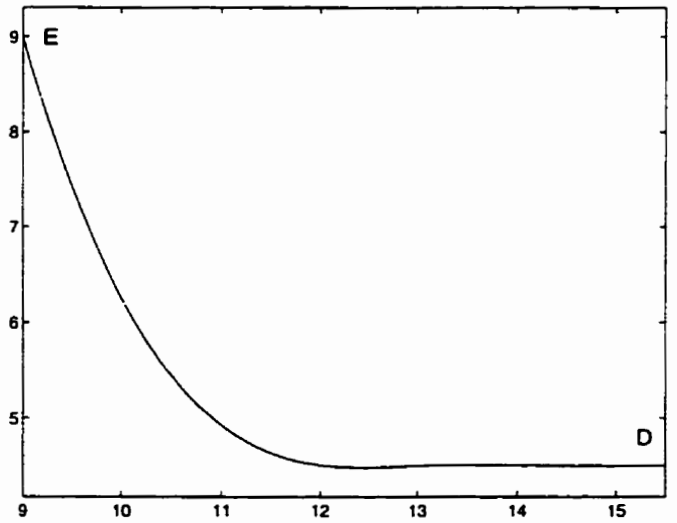

Figure 8: Optimal shape of the fillet.

The SQP (function "`f_min_con_nonlin`" from the IMSL library) is again employed to solve this problem. The final converged solution is reached with a CPU time of 40.4 s on an IBM RS/6000. The optimal shape of the fillet is shown in

Figure 8. The area of the structure is reduced from the initial value of 145.125 in^2 with stress violation around point D to the final value of 134.64 in^2 without yielding on the boundary. This result is in good agreement with that obtained in Reference 21 (134.29 in^2) where the CPU time was not shown. However, it is useful to point out that only three design variables and 13 quadratic boundary elements are used here as opposed to five design variables and 15 quadratic elements employed in the work of Yang.[21]

7. CONCLUSIONS AND DISCUSSION

This paper contains two primary contributions.

The first is the development of new formulations, based on the HBIE, for computing stresses and their sensitivities in 2-D linear elastic solid bodies. This approach is valid at all points inside and on the boundary of a body, except at the ends of boundary elements. The formulations are shown to be very efficient with respect to ease of numerical implementation and computational effort. Results for two numerical examples are seen to be uniformly accurate. It is felt that the primary reason for this is that numerical integration is completely avoided in the 2-D BCM. Only function evaluations are necessary.

The second contribution is the development and execution of a shape optimization algorithm with DSCs calculated from the BCM. Again, the optimal solutions are obtained very efficiently and accurately, demonstrating that the BCM has great potential for engineering design problems.

Acknowledgement

Anh-Vũ Phan gratefully acknowledges the support from the Quebec Ministry of Education through the "Programme québécois de bourses d'excellence".

REFERENCES

1. A.V. Phan, S. Mukherjee and J.R.R. Mayer, 'A boundary contour formulation for design sensitivity analysis in two-dimensional linear elasticity', *Int. J. Solids Struct.*, in press.

2. S. Mukherjee, *Boundary Element Methods in Creep and Fracture*, Elsevier Applied Science, London, 1982.

3. A. Nagarajan, E.D. Lutz and S. Mukherjee, 'A novel boundary element method for linear elasticity with no numerical integration for two-dimensional and line integrals for three-dimensional problems', *J. Appl. Mech. ASME*, **61,** 264-289 (1994).

4. A. Nagarajan, S. Mukherjee and E.D. Lutz, 'The boundary contour method for three-dimensional linear elasticity', *J. Appl. Mech. ASME*, **63,** 278-286 (1996).

5. Y.X. Mukherjee, S. Mukherjee, X. Shi and A. Nagarajan, 'The boundary contour method for three-dimensional linear elasticity with a new quadratic boundary element', *Eng. Anal. Boundary Elements*, in press.

6. A.V. Phan, S. Mukherjee and J.R.R. Mayer, 'The boundary contour method for two-dimensional linear elasticity with quadratic boundary elements', *Compt. Mech.*, in press.

7. E.J. Haug, K.K. Choi and V. Komkov, *Design Sensitivity Analysis of Structural Systems*, Academic Press, New York, 1986.

8. M.R. Barone and R.J. Yang, 'Boundary integral equations for recovery of design sensitivities in shape optimization', *AIAA J.*, **26,** 589-594 (1988).

9. J.H. Kane and S. Saigal, 'Design sensitivity analysis of solids using BEM', *J. Eng. Mech.*, **114,** 1703-1722 (1988).

10. Q. Zhang and S. Mukherjee, 'Design sensitivity coefficients for linear elastic bodies with zones and corners by the derivative boundary element method', *Int. J. Solids Struct.*, **27**, 983-998 (1991).

11. S. Saigal, J.T. Borggaard and J.H. Kane, 'Boundary element implicit differentiation equations for design sensitivities of axisymmetric structures', *Int. J. Solids Struct.*, **25**, 527-538 (1989).

12. J.R. Rice and S. Mukherjee, 'Design sensitivity coefficients for axisymmetric elasticity problems by boundary element methods', *Eng. Anal. Boundary Elements*, **7**, 13-20 (1990).

13. R. Aithal, S. Saigal and S. Mukherjee, 'Three dimensional boundary element implicit differentiation formulation for design sensitivity analysis', *Math. Comput. Modelling*, **15**, 1-10 (1991).

14. J.H. Kane, G. Zhao, H. Wang and K. Guru Prasad, 'Boundary formulations for three-dimensional continuum structural shape sensitivity analysis', *J. Appl. Mech. ASME*, **59**, 827-834 (1992).

15. M. Bonnet, 'Regularized BIE formulations for first- and second-order shape sensitivity of elastic fields', *Comput. Struct.*, **56**, 799-811 (1995).

16. S. Mukherjee and A. Chandra, 'A boundary element formulation for design sensitivities in materially nonlinear problems', *Acta Mechanica*, **78**, 243-253 (1989).

17. S. Mukherjee and A. Chandra, 'A boundary element formulation for design sensitivities in problems involving both geometric and material nonlinearities', *Math. Comput. Modelling*, **15**, 245-255 (1991).

18. X. Wei, A. Chandra, L.J. Leu and S. Mukherjee, 'Shape optimization in elasticity and elasto-viscoplasticity by the boundary element method', *Int. J. Solids Struct.*, **31**, 533-550 (1994).

19. J.H. Choi and B.M. Kwak, 'Boundary integral equation method for shape optimization of elastic structures', *Int. j. mumer. methods eng.*, **26,** 1579-1595 (1988).

20. E. Sandgren and S.J. Wu, 'Shape optimization using the boundary element method with substructuring', *Int. j. mumer. methods eng.*, **26,** 1913-1924 (1988).

21. R.J. Yang, 'Component shape optimization using BEM', *Comput. Struct.*, **37,** 561-568 (1990).

22. S. Saigal and J.H. Kane, 'Boundary-element shape optimization system for aircraft structural components', *AIAA J.*, **28,** 1203-1204 (1990).

23. K. Yamazaki, J. Sakamoto and M. Kitano, 'Three-dimensional shape optimization using the boundary element method', *AIAA J.*, **32,** 1295-1301 (1994).

24. A. Tafreshi and R.T. Fenner, 'General-purpose computer program for shape optimization of engineering structures using the boundary element method', *Comput. Struct.*, **56,** 713-720 (1995).

25. K. Schittkowski, 'NLPQL: A FORTRAN subroutine solving constrained nonlinear programming problems', in Clyde L. Monma (eds.), *Annals of Operations Research*, **5,** 485-500 (1986).

26. F.J. Rizzo, 'An integral equation approach to boundary value problems of classical elastostatics', *Q. Appl. Math.*, **25,** 83-95 (1967).

27. S.P. Timoshenko and J.N. Goodier, *Theory of Elasticity*, McGraw-Hill, New York, 1970.

28. N.V. Banichuk, *Problems and Methods of Optimal Structural Design*, Plenum Press, New York, 1983.

APPENDIX

POTENTIAL FUNCTIONS

$$
\begin{aligned}
\lambda_1(\xi,\eta) &= -\frac{k\eta}{r^2}\left(\frac{2\xi^2}{r^2}+1-2\nu\right)\\
\lambda_2(\xi,\eta) &= k\left[\frac{\xi\eta}{r^2}\left(\frac{4\nu^2-5\nu+2}{2\nu-1}-\frac{2\xi^2}{r^2}\right)-2(1-\nu)\arctan\left(\frac{\eta}{\xi}\right)\right]\\
\lambda_3(\xi,\eta) &= k\left[\frac{\xi^2}{r^2}\left(\frac{2\xi^2}{r^2}-2\nu-\frac{3}{2}\right)+\left(\frac{3}{2}-2\nu\right)\ln r\right]\\
\lambda_4(\xi,\eta) &= \frac{k\xi}{r^2}\left(\frac{2\xi^2}{r^2}-1-2\nu\right)\\
\lambda_5(\xi,\eta) &= k\left[\frac{\xi^2}{r^2}\left(\frac{2\xi^2}{r^2}-2\nu-\frac{1}{2}\right)+\frac{1}{2}\ln r\right]\\
\lambda_6(\xi,\eta) &= \frac{k\xi\eta}{r^2}\left(\frac{4\nu^2+\nu-2}{1-2\nu}+\frac{2\xi^2}{r^2}\right)\\
\lambda_7(\xi,\eta) &= k\eta\left\{2(\nu-1)+\frac{\xi^2}{r^2}\left[3+6\nu-8\nu^2+\frac{2\xi^2}{r^2}(4\nu-5)\right]\right\}\\
\lambda_8(\xi,\eta) &= k\eta\left\{1+\frac{\xi^2}{r^2}\left[1-2\nu-8\nu^2+\frac{2\xi^2}{r^2}(4\nu-1)\right]\right\}\\
\lambda_9(\xi,\eta) &= k\xi\left\{-8\nu^2+8\nu-1+\frac{\eta^2}{r^2}\left[8\nu^2-14\nu+3+\frac{2\eta^2}{r^2}(4\nu-1)\right]\right\}\\
\lambda_{10}(\xi,\eta) &= k\xi\left\{-8\nu^2+14\nu-6+\frac{\eta^2}{r^2}\left[8\nu^2-22\nu+13+\frac{2\eta^2}{r^2}(4\nu-5)\right]\right\}\\
\lambda_{11}(\xi,\eta) &= -\lambda_4(\eta,\xi)\\
\lambda_{12}(\xi,\eta) &= -\lambda_6(\eta,\xi)\\
\lambda_{13}(\xi,\eta) &= -\lambda_5(\eta,\xi)\\
\lambda_{14}(\xi,\eta) &= -\lambda_1(\eta,\xi)\\
\lambda_{15}(\xi,\eta) &= -\lambda_3(\eta,\xi)\\
\lambda_{16}(\xi,\eta) &= -\lambda_2(\eta,\xi)\\
\lambda_{17}(\xi,\eta) &= -\lambda_{10}(\eta,\xi)\\
\lambda_{18}(\xi,\eta) &= -\lambda_9(\eta,\xi)\\
\lambda_{19}(\xi,\eta) &= -\lambda_8(\eta,\xi)\\
\lambda_{20}(\xi,\eta) &= -\lambda_7(\eta,\xi)
\end{aligned}
$$

$$
\begin{aligned}
\lambda_{21}(\xi,\eta) &= \frac{k\xi}{r^2}\left(\frac{2\xi^2}{r^2}+1-2\nu\right)\\
\lambda_{22}(\xi,\eta) &= k\left[\frac{\xi^2}{r^2}\left(\frac{4\nu^2-5\nu+2}{1-2\nu}+\frac{2\xi^2}{r^2}\right)-\left(\frac{4\nu^2-7\nu+3}{1-2\nu}\right)\ln r\right]\\
\lambda_{23}(\xi,\eta) &= k\left[\frac{\xi\eta}{r^2}\left(\frac{1}{2}-2\nu-\frac{2\xi^2}{r^2}\right)-2(1-\nu)\arctan\left(\frac{\eta}{\xi}\right)\right]\\
\lambda_{24}(\xi,\eta) &= \frac{k\eta}{r^2}\left(\frac{2\xi^2}{r^2}+1-2\nu\right)\\
\lambda_{25}(\xi,\eta) &= \frac{k\xi\eta}{r^2}\left(\frac{2\xi^2}{r^2}+\frac{3}{2}-2\nu\right)\\
\lambda_{26}(\xi,\eta) &= k\left[\frac{\xi^2}{r^2}\left(\frac{4\nu^2+\nu-2}{2\nu-1}-\frac{2\xi^2}{r^2}\right)-\left(\frac{\nu-1}{2\nu-1}\right)\ln r\right]\\
\lambda_{27}(\xi,\eta) &= k\xi\left\{1+\frac{\eta^2}{r^2}\left[-8\nu^2+22\nu-17+\frac{2\eta^2}{r^2}(5-4\nu)\right]\right\}\\
\lambda_{28}(\xi,\eta) &= k\xi\left\{2(1-\nu)+\frac{\eta^2}{r^2}\left[-8\nu^2+14\nu-3+\frac{2\eta^2}{r^2}(1-4\nu)\right]\right\}\\
\lambda_{29}(\xi,\eta) &= k\eta\left\{8\nu^2-14\nu+6+\frac{\xi^2}{r^2}\left[-8\nu^2+6\nu-1+\frac{2\xi^2}{r^2}(4\nu-1)\right]\right\}\\
\lambda_{30}(\xi,\eta) &= k\eta\left\{8\nu^2-20\nu+11+\frac{\xi^2}{r^2}\left[-8\nu^2+14\nu-3+\frac{2\xi^2}{r^2}(4\nu-5)\right]\right\}\\
\lambda_{31}(\xi,\eta) &= -\lambda_{24}(\eta,\xi)\\
\lambda_{32}(\xi,\eta) &= -\lambda_{26}(\eta,\xi)\\
\lambda_{33}(\xi,\eta) &= -\lambda_{25}(\eta,\xi)\\
\lambda_{34}(\xi,\eta) &= -\lambda_{21}(\eta,\xi)\\
\lambda_{35}(\xi,\eta) &= -\lambda_{23}(\eta,\xi)\\
\lambda_{36}(\xi,\eta) &= -\lambda_{22}(\eta,\xi)\\
\lambda_{37}(\xi,\eta) &= -\lambda_{30}(\eta,\xi)\\
\lambda_{38}(\xi,\eta) &= -\lambda_{29}(\eta,\xi)\\
\lambda_{39}(\xi,\eta) &= -\lambda_{28}(\eta,\xi)\\
\lambda_{40}(\xi,\eta) &= -\lambda_{27}(\eta,\xi)
\end{aligned}
$$

where,

$$k=\frac{1}{4\pi(1-\nu)} \quad \& \quad r^2=\xi^2+\eta^2$$

IMAGE EVALUATION
TEST TARGET (QA-3)

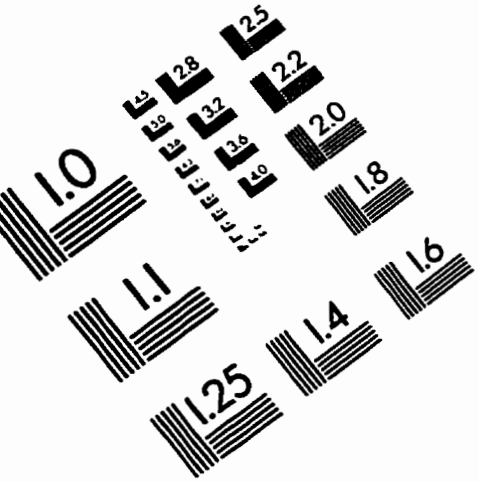

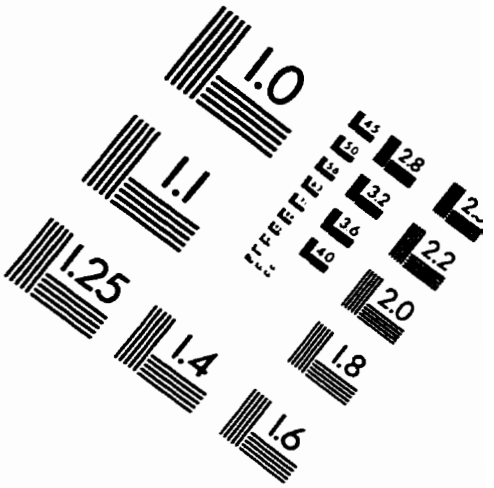

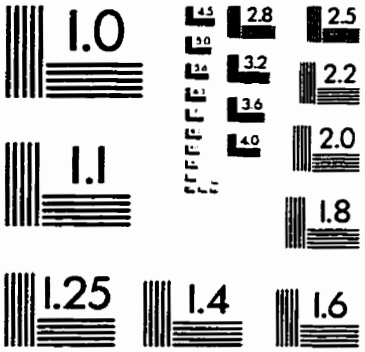

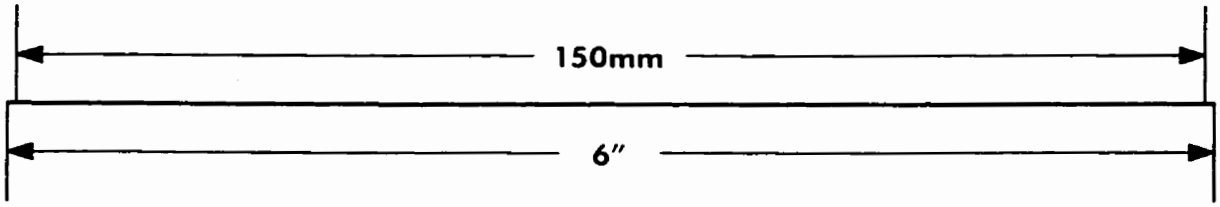

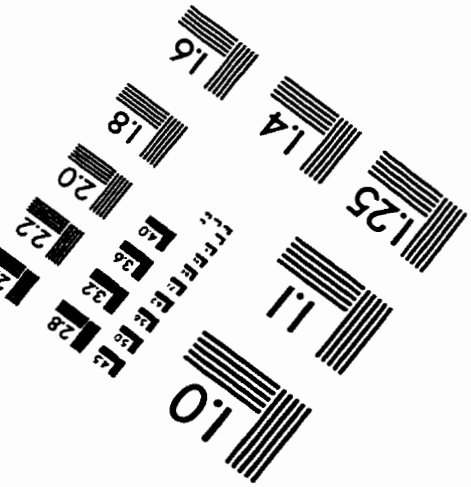

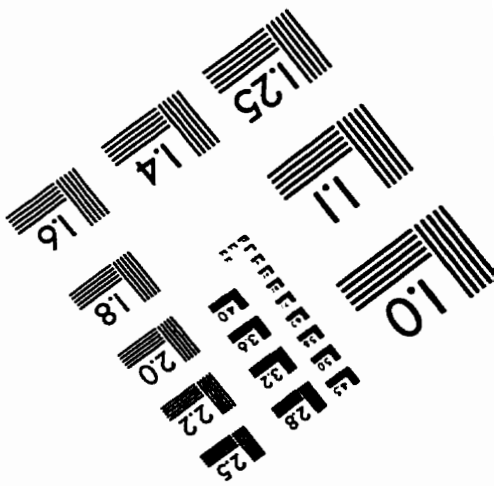

APPLIED IMAGE, Inc
1653 East Main Street
Rochester, NY 14609 USA
Phone: 716/482-0300
Fax: 716/288-5989